Optical Neural Network based on Laser Diode Longitudinal Modes

Evert Mos

Optical Neural Network based on Laser Diode Longitudinal Modes

PROEFSCHRIFT

ter verkrijging van de graad van doctor
aan de Technische Universiteit Eindhoven,
op gezag van de Rector Magnificus, prof.dr. M. Rem,
voor een commissie aangewezen door
het College voor Promoties
in het openbaar te verdedigen
op dinsdag 7 september 1999 om 16.00 uur

door

Evert C. Mos

geboren te Arnhem

Dit proefschrift is goedgekeurd door de promotoren:

prof.ir. G. D. Khoe
en
prof.dr.ir. W. M. G. van Bokhoven

Copromotor:
dr. J. J. H. B. Schleipen

Aan mijn ouders,
aan Liseth

Dankwoord

Voor u ligt mijn proefschrift, het resultaat van 4 jaar promotieonderzoek uitgevoerd op het Philips Natuurkundig Laboratorium. Hoewel alleen mijn naam als auteur op de kaft prijkt, heb ik het onderzoek dat in dit proefschrift beschreven wordt niet in mijn eentje gedaan. Vele mensen hebben mij geholpen, bijgestaan, gesteund, aangemoedigd, gemotiveerd, of hebben zelfs meegeschreven aan dit proefschrift. Voor u verder leest wil ik van de gelegenheid gebruik maken om deze mensen te bedanken.

Jean Schleipen, die mij op plezierige wijze wegwijs heeft gemaakt in het vakgebied van de experimentele optica, de wereld van het technisch-wetenschappelijk onderzoek en op het Nat.Lab. Hij was bovendien een groot motivator (niet alleen als de dingen een beetje tegen zaten) en heeft met zijn inhoudelijke inbreng en talloze suggesties sterk bijgedragen aan het welslagen van het onderzoek.

Jurgen Hoppenbrouwers en Martijn Blüm die tijdens hun afstudeerproject een alternatief optisch neuron hebben onderzocht. Ook Martin Hill wil ik danken voor zijn bijdrage in dit onderzoek (Thanks mate!). Zonder hun bijdrage zou het alternatieve optische neuron, beschreven in Hoofdstuk 6, ongetwijfeld niet verwezenlijkt zijn.

Djan Khoe van de vakgroep Telecommunicatie Technologie en Electromagnetisme aan de Technische Universiteit Eindhoven, die mij als promotor de mogelijkheid heeft gegeven om dit onderzoek te doen en vele suggesties heeft aangedragen voor verbeteringen aan dit proefschrift. Ook Huug de Waardt dank ik voor zijn suggesties voor en bijdragen aan het onderzoek. Verder alle anderen op de Technische Universiteit Eindhoven die mij, ook al was ik niet zo vaak op de TU, op allerlei manieren hebben geholpen.

Mijn collega's bij Philips Research: Gert 't Hooft, Egbert Lenderink, Sel Colak, Rob Hendriks, Teus Tukker en Martin van der Mark die mij een zeer aangename en leerzame tijd hebben bezorgd tijdens mijn promotieonderzoek op het Nat.Lab. en er zo mede voor gezorgd hebben dat ik met veel plezier het onderzoek heb voltooid.

De groepsleiders van de groepen op het Nat.Lab. waarbij ik het onderzoek heb uitgevoerd, Henk van Houten en Evert van Loenen, voor hun gastvrijheid die zij namens Philips Research hebben verleend.

Alle andere mensen bij Philips Research die mij op talloze manieren hebben geholpen, in het bijzonder dank ik Anton Verhulst, Hans de Vrieze (Uniphase) en Guido van Tartwijk (Uniphase) voor hun bijdragen aan de verwezenlijking van het onderzoek. Verder natuurlijk de Electronica Ontwerp Groep en de Mechanische Werkplaats van het Nat.Lab. die de experimenten mogelijk maakten.

Contents

1

Introduction

In this chapter we provide some background information on the subjects of the thesis. We start with a brief introduction on neural networks. The basic operation of neural networks is explained and their main features are discussed. The advantages of implementing neural networks in the optical domain are introduced. In contemporary optical neural networks the threshold function, needed for neural operation, is often in the electrical domain. For applications in all-optical signal processing, it is preferable to have all-optical neural operation. An example of such an application in the area of optical telecommunication is presented in this chapter. We conclude the chapter by describing the organization and contents of this thesis.

1.1   Neural Networks

Many of the inventions of scientists and engineers are inspired by nature. This is certainly
the case for the concept of artificial neural networks that was inspired by the operation of
the human brain about half a century ago. The starting point of the field of artificial neural
networks is generally believed to be 1943. In that year McCulloch and Pitts [1] proposed
to use a model of the biological neuron as a circuit component to perform computational
tasks. Since 1943 the field has gradually matured and much insight has been gained on
the theory and the operating principles of neural networks. Many applications of neural
networks have been presented. Today half a dozen dedicated scientific journals is devoted
to the subject and many textbooks (See e.g. Refs. [2]–[5]) have been published.

1.1.1   Bio-Inspired Computing

Artificial neural networks consist of a (preferably large) number of simple computing ele-
ments called neurons, that are modeled after the human nerve cell. Each neuron receives a
number of input signals and performs a simple operation on this set of inputs. The output
of each neuron is fanned out to the inputs of other neurons.

(a)   (b)
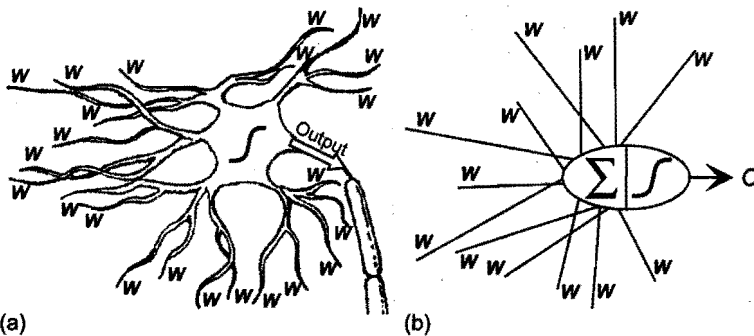
Figure 1.1 Human nerve cell (a) and its model (b). Weighted (w) input signals are added.
The resulting sum is compared to a threshold as is depicted with the nonlinear, S-shaped
neural response function in the cell body.

In Fig. 1.1 a human nerve cell, or neuron, (a) and its artificial equivalent (b) are sketched.
The neuron receives a set of input signals via a number of tentacles or *dendrites*. At the
tip of each dendrite the input signal is weighted with a factor w, that can be positive or
negative. All the signals from the dendrites are added in the cell body to contribute to
a weighted sum of inputs of the neuron. If a weight is positive the corresponding input
will have an excitatory influence on the weighted sum. With a negative weight, an input
decreases the weighted sum and is inhibitory.

In the cell body the weighted sum of inputs is compared to a threshold value. If the
weighted sum is above this threshold, the neuron sends a signal via its output to all con-
nected neurons. The threshold operation is essentially a nonlinear response function as is
indicated in the figure with an S-shaped, sigmoid, curve.

The function of a neuron can be described in mathematical form with:

$$O = \mathcal{F}\left(\sum_i w_i \cdot I_i\right) \tag{1.1}$$

where O is the output signal of the neuron and I_i are the input signals to the neuron, weighted with a factor w_i. $\mathcal{F}$ is some nonlinear function representing the threshold operation on the weighted sum of inputs.

I_b	I_0	I_1	$\sum_i w_i I_i$	O
1	0	0	-0.5	0
1	0	1	-0.2	0
1	1	0	-0.2	0
1	1	1	0.1	1
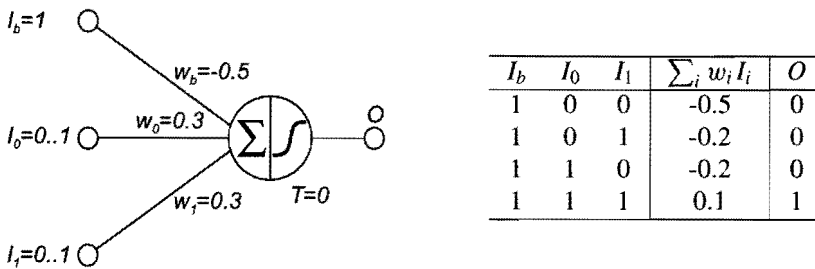
Figure 1.2 A neural implementation of a logical AND function and the corresponding truth table including weighted sum of inputs of the neuron.

The input-output function that is implemented by a neuron depends on the values of the weights and on the level of the threshold. As an example, the neuron presented in Fig. 1.2 can be used to implement a logical function on two digital input signals. With the weights set to the values indicated in the figure, the neuron performs a logical AND function as is explained in the accompanying truth table. Only if both input signals are active ($I_i = 1, i = 1, 2$) the weighted sum of inputs will be higher than the threshold level T. Note that the threshold level of the neuron in this example is shifted to 0.5 by use of a *bias* input signal with a constant level 1 and a corresponding bias weight w_b that is set to -0.5. By treating the threshold as an extra weight value, the implemented function of a neuron is defined by its weights. Setting the weights of the neuron in Fig. 1.2 to, for example, $\{w_b, w_0, w_1\} = \{0.5, -0.7, -0.6\}$ would define a logical NOR operation.

1.1.2 Parallel Distributed Processing

The input-output function of a single neuron is of limited complexity. A number of these neurons, however, can be connected to form a neural network as shown in Fig. 1.3. Such a neural network receives an input vector, or pattern, that consists of a set of input signals. The collection of neurons that form the network process an input pattern in a highly parallel, distributed fashion and can perform a complicated computational task.

Because the computational task is distributed over all neurons of the network, malfunction of one of the neurons will only have a small influence on the performance of the network. The same holds for a defective connection between two neurons. Because of this immunity to small defects neural networks are robust systems.
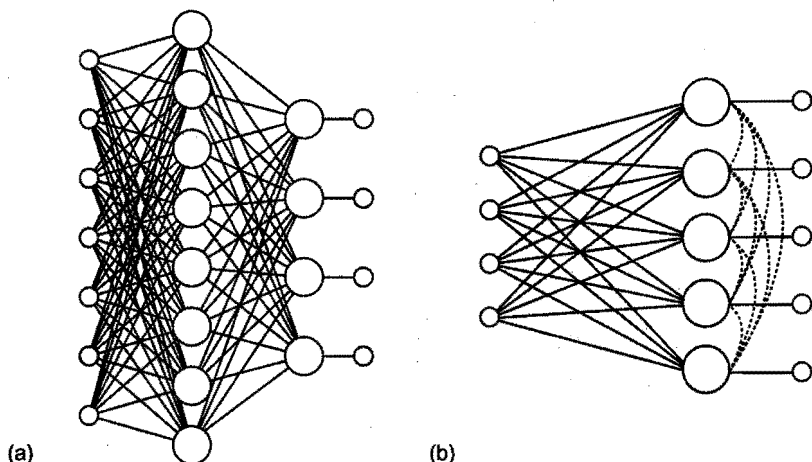
Figure 1.3 Two small neural networks. Circles represent neurons, lines represent weighted connections. Small circles denote input signals and output signals. (a) A two layer feedforward neural network, each layer of neurons receives signals from a previous layer. (b) A recurrent neural network. The dotted lines represent connections from the output of each neuron to the inputs of all other neurons.

The high degree of parallelism that is maintained throughout the network enables neural networks to solve problems such as pattern recognition where data is presented in a parallel way. As all data is processed simultaneously, neural networks can have a higher operation speed as compared to sequential computers.

1.1.3 Learning from Examples

Another feature of neural networks is their ability to learn from examples. Because the computational task of a neural network is determined by the weight values of the interconnections between the neurons, the task can be adapted simply by changing the weight values. The process of adapting the weights to perform a given task is called the *training phase* of the neural network.

One of the strategies of training is to use a supervised learning algorithm. In this type of learning algorithm a set of input-output vector pairs, the training set, is needed that represents the task to be trained. During each iteration of the learning algorithm, a training supervisor shows all the example input patterns to the network and records the corresponding output patterns. The recorded output patterns are compared to the output patterns of the training set and an error value is computed based on this comparison. Iteratively, the weights of the network are changed until the error measure is below a predefined minimum value and the learning algorithm stops. After the training phase, the neural network performs the computational task defined by the input-output pairs of the training set.

1.1.4 Why Optics

In most cases the artificial neurons are just pieces of code on a sequential computer and the parallelism is only emulated. Applications of these neural networks are numerous. Typical applications are in areas where the problem to be solved is of parallel nature and examples of input-output patterns are abundant. Some of these application areas are process control, data series analysis, stock market prediction, optical character recognition (OCR), speech recognition etc... Neural network based software is now commercially available. Examples are OCR software (*OmniPage* package by Caere) and credit card fraud detection, which is a special case of data series analysis (*Falcon* system by HNC Software Inc.).

Although software implementations of neural networks have proven to be successful, neural networks are essentially degraded to just another computing tool in this approach. A clear disadvantage of software implementation is the severe slowdown of operation speed. This is due to the fact that the microprocessor of the computer on which the neural network program runs calculates the neuron states one by one. Considerable acceleration can be achieved by implementing neural networks in dedicated, parallel hardware. Recently a number of products in OCR (*OCR-on-chip* by Ligature) and speech recognition applications (*Interactive Speech* chip by Sensory) have become available.

As the connections in software are virtual, only existing in a computer program, any number of connections is possible. When implementing a neural network on a chip, however, the number of connections between the neurons will be physically limited. This limitation is essentially due to the fact that connections cannot cross each other within the same layer on a chip, and consequently they need to be separated in one dimension. Because the number of layers on a chip is limited, the number of crossing connections also is limited.

Optics can help to solve this connectivity problem in two ways. As photons only interact with matter and not with each other, the light beams that form the connections in an optical neural network can cross each other without problems. Furthermore the rays of light do not need to be guided in free space. As a consequence no predefined paths or wires are necessary in an optical neural network. This means that all three dimensions in space can be used without "soldering".

For these reasons much effort is put in optical neural networks since the mid 1980's. For an overview of optical neural networks see e.g. Refs. [6]–[8], a collection of papers is given in Ref. [9].

Optical Threshold

In most of these optical neural networks, the threshold operation is in the electrical or opto-electrical domain [8]. In these hybrid neural networks optics is used for its massive parallelism and input and output data are defined in the electronic domain.

In application areas where input and output data are defined in the optical domain it is beneficial if the threshold function also operates in the optical domain. The delays arising from the conversions between the optical and electrical domain can be avoided in this way. An example of an application area where data is represented in the optical domain

is the field of optical telecommunications. In optical telecommunication systems, data is send through optical fibers in a digital fashion where a logical 1 is represented with a certain amount of optical power. Thus the input signals to a processing unit in an optical telecommunication system are in the optical domain.

An Application Example

An example of a signal processing task in an optical telecommunication network is the recognition and routing of a data packet in a packet switched network. Figure 1.4 provides a schematic view of a packet switched telecommunication network. The figure shows a number of connected network routers. Data packets arrive at one of the routers, separated in time.
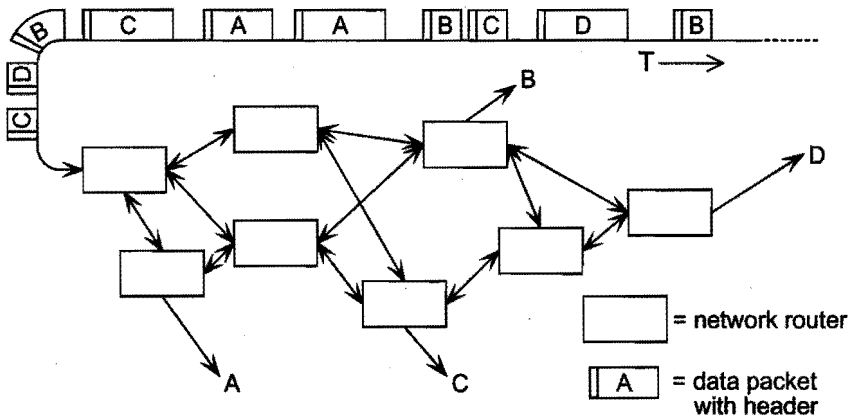
Figure 1.4 A packet switched telecommunication network. In each network router data packets are routed according to their destination address.

Each packet contains data for a certain destination A, B, C or D. In a header, at the beginning of a data packet, this destination is encoded in a bit sequence. The beginning of a header is marked with a header detect sequence for synchronization purposes.

The task of the network routers in this network is to detect the arrival of a packet by detecting the header detect sequence and to route a packet according to its destination information. This means that the routers in the network should perform a pattern detection task on the header detect sequence and classify the packets by their destination address.

The tasks of pattern detection and destination classification are typical neural network tasks. As the information is in the optical domain, an all-optical neural network is desirable for this type of application.

1.2   This Thesis

In this thesis an all-optical neural network is investigated. All key neural functions, weighted summation, connections and threshold operation are implemented in the op-

tical domain. The proposed optical neural network uses the longitudinal modes of a laser diode as neurons. The outputs of this Laser Neural Network (LNN) correspond to the light intensity contained in the longitudinal modes of the laser diode. The inputs to the neural network are implemented by providing controlled optical feedback to the laser diode for each of the longitudinal modes. For this purpose, the laser diode is coupled to an external cavity in which inputs and weights are implemented by use of a transmission matrix and a number of optical components. The inputs of this LNN are in the optical transmission domain.

The advantages of the LNN will be further investigated for use in all-optical signal processing for the application area of optical telecommunications [10].

1.2.1 Thesis Objectives and Outline

The main objectives of this Thesis are:

- to explain the principles of operation of the proposed optical neural network,

- to demonstrate the operation principle of the optical neural network experimentally,

- to show the functional capabilities of the optical neural network concept in relation to the envisioned application area,

- to investigate the operation speed of the optical neural network and

- to provide an alternative all-optical neuron with inputs in the optical power domain.

The operation principles of a laser neural network that uses optical feedback to provide weighted inputs are explained in Chapter 2. The threshold operation is explained using a multimode rate-equation model of the laser diode. Also the weighting of inputs, for which an optical vector-matrix multiplier is used, is discussed.

In Chapter 3 experiments are described that demonstrate the operation principles of the laser neural network. An experimental setup and a learning algorithm are presented. Simple functions are trained to the network to prove the LNN concept.

We describe an advanced experimental laser neural network in Chapter 4. A more sophisticated external-cavity configuration and a different transmission matrix are used in this setup. The training speed and the network complexity are enhanced. A new learning algorithm is used to train the network. Trained functions are chosen towards the application area of optical telecommunication data switching.

Chapter 5 deals with the operation speed of the laser neural network. The transient behavior of longitudinal mode switching in an external-cavity laser diode is investigated. A model is used to simulate this behavior numerically. The mode switching behavior is analyzed experimentally in a two wavelength, double external-cavity laser diode. Both theoretical and experimental results are related to the laser neural network of Chapters 2–4 and the application area of optical telecommunications. The simulated and experimental results are extrapolated for a LNN that is implemented in integrated optics.

An alternative all-optical neuron is presented in Chapter 6. The neuron consists of a laser diode with external optical feedback that receives injected light as inputs. The

external optical feedback is used to control the shape of the threshold function. With this neuron we aim at implementing inputs in the optical power domain.

As all the experimental optical neural networks described in this thesis use an external-cavity laser diode with some kind of wavelength selective optical feedback, Chapter 7 is devoted to some anomalous effects that can occur in such a setup. Self-pulsating behavior and cross-modulation between the output power at two wavelengths are presented. It is explained that these effects are probably caused by the carrier and thermal induced refractive index changes of the laser diode material. The effects are related to anomalous behavior of the LNN which is reported in Chapter 4.

References

[1]   W. S. McCulloch and W. Pitts, "A logical calculus of the ideas immanent in nervous activity," *Bulletin of Mathematical Biophysics* **5**, 115–133, 1943.

[2]   J. Hertz, A. Krogh, and R. Palmer, *Introduction to the theory of neural computation*, (Addison-Wesley, Redwood City, CA, 1991).

[3]   R. Hecht-Nielsen, *Neurocomputing*, (Addison-Wesley, Amsterdam, The Netherlands, 1990).

[4]   C. M. Bishop, *Neural networks for pattern recognition*, (Oxford University Press, Oxford, 1995).

[5]   B. D. Ripley, *Pattern recognition and neural networks*, (Cambridge University Press, Cambridge, 1996).

[6]   F. T. S. Yu, "Optical neural networks: architecture, design and models," in *Progress in Optics*, E. Wolf Ed., (North Holland, Amsterdam, 1993), Vol. 32, pp. 61–144.

[7]   H. J. Caulfield, J. Kinser, and S. K. Rogers, "Optical neural networks," *Proc. IEEE* **77**, 1573–1583, 1989.

[8]   S. Jutamulia and F. T. S. Yu, "Overview of hybrid optical neural networks," *Opt. Laser Technol.* **28**, 59–72, 1996.

[9]   S. Jutamulia Ed., "Selected papers on optical neural networks," *SPIE Milestone Series* Vol. MS-96, 1994.

[10] J. H. Wolter, G. D. Khoe, and M. K. Smit, "Photonics in communication technologies," COBRA-NWO-NRC-Programme proposal (Granted), 1998.

2

Laser Neural Network

In the previous Chapter 1 we introduced the necessary ingredients to build a neural network. In the major part of this thesis the neural operation is implemented by providing controlled optical feedback to a laser diode. In this chapter we explain the principles of operation of this approach starting from an introduction on laser diode theory. We introduce the experimental concepts used to build the optical neural network.

2.1   Laser Diodes

A laser diode basically consists of an active layer that is sandwiched between p-type and n-type material. The electrons and holes that contribute to the current through the diode recombine in the active region.

2.1.1   Optical Gain and Loss and Longitudinal Modes

The recombination of electrons and holes can result in emission of radiation. As shown in Fig. 2.1 this emission of a photon can be either spontaneous (a) or stimulated (b), which means that it is initiated by another photon. In the latter case the new photon is exactly in phase with the incoming photon and coherent amplification of light results.

Apart from this recombination induced optical gain, a photon in the active region also experiences optical losses. The optical losses in the active region are caused by absorption and scattering of light by the laser diode material

In the Fabry-Perot type laser diode of Fig. 2.1 two cleaved facets act as mirrors. The mirrors reflect a portion of the spontaneous and amplified light generated in the active layer and form a resonator.
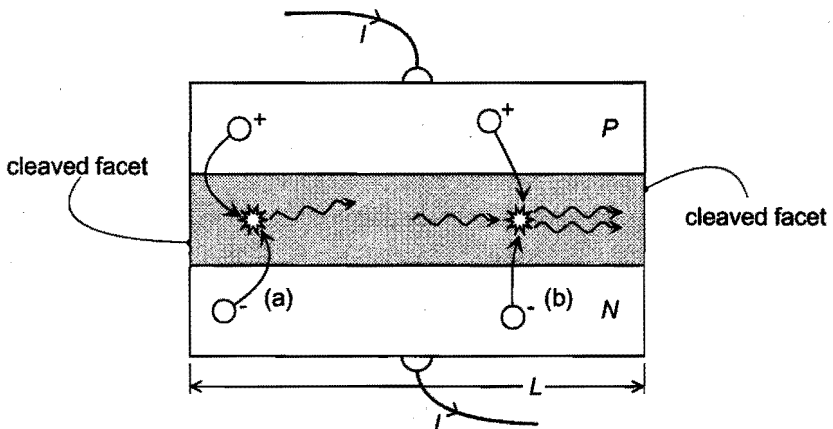
Figure 2.1 A laser diode of length L with two cleaved facets and driving current I. In the active layer (gray area), between n-type and p-type material, electrons (-) and holes (+) recombine. This can result in spontaneous (a) or stimulated (b) emission of a photon.

As spontaneous and stimulated emission results from the recombination of electrons and holes, the amount of emitted photons is proportional to the amount of charge carriers in the active layer and thus to the current through the laser I. If the current is sufficiently high, the optical gain will compensate the optical losses of the laser material and the mirrors. Now, the round-trip optical gain of a light wave traveling inside the active region will be unity. When a photon is generated in the active layer, the laser can start to emit coherent radiation if the wavelength of the generated photon fits inside the resonator. For this it is necessary that an integer multiple of the half wavelength is equal to the length
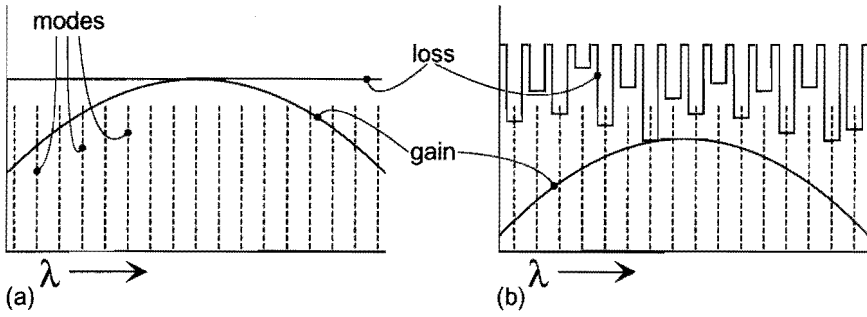
Figure 2.2 Optical gain and losses versus wavelength for a normal Fabry-Perot laser diode (a) and a Fabry-Perot laser diode with controlled optical losses (b). Longitudinal mode wavelengths are indicated with dashed lines.

of the resonator L. The wavelengths for which this condition is met correspond to the longitudinal modes of the laser diode.

In a normal Fabry-Perot laser diode, the optical losses γ of the mirrors and the laser material are practically independent of wavelength. The gain G is wavelength dependent as is shown in Fig. 2.2(a). This means that for one of the longitudinal mode wavelengths the net optical gain is maximal and the round trip gain of this mode will reach unity first when the current is increased. This will be the wavelength at which the laser will oscillate.

The operation of the optical neural network presented in this thesis is based on the control of the optical losses of a laser diode by applying external optical feedback. The amount of optical feedback is controlled for each longitudinal mode individually. As shown schematically in Fig. 2.2(b) this will result in a different level of optical losses for the individual longitudinal modes of the laser diode. Thus the oscillation wavelength of the laser diode will depend on the spectrum of the light that is reflected back into the laser diode.

2.1.2 Multi Mode Rate-Equations

To explain the principles of operation of the optical neural network presented in this thesis, let us introduce a model of the laser diode in which we can incorporate the controlled optical losses for each longitudinal mode. For this purpose, a set of rate-equations [1],[2] can be used for the photon and carrier density in the active layer of the laser diode.

The equations describe the time-derivative of the photon density S_m for longitudinal mode m, and the carrier density N. For the photon density of mode m we can write:

$$\dot{S}_m = (G_m - \gamma_m)\, S_m + R_{sp} \tag{2.1}$$

where the optical gain and losses are labeled m to express the fact that they are different for each mode. Although Eq. 2.1 originates from a field propagation model of an optical field inside the active layer [1],[2], the equation can also be understood intuitively. The change in the photon density of a mode is equal to the net optical gain $(G_m - \gamma_m)$ of the mode times the photon density of the mode plus the number of photons that are spontaneously generated and contribute to the mode per unit of time R_{sp}.

The optical losses γ_m for each mode are a function of the power reflectivity R_m of the cleaved facets for wavelength m via

$$\gamma_m = v_g \left(\alpha_{int} - \frac{1}{L} \ln(R_m) \right) \tag{2.2}$$

where α_{int} accounts for the internal scattering and absorption losses of the laser material and v_g is the group velocity. The optical losses of the laser diode facets are distributed over the length of the active layer with the logarithm and the factor $1/L$.

As discussed earlier, both the gain G and the spontaneous emission rate for each mode R_{sp} are proportional to the number of charge carriers inside the active region. For the purpose of explaining the operating principle of the optical neural network we assume this dependency to be linear.

The time derivative of the charge carrier density N can be described by:

$$\dot{N} = I/qV - \gamma_e N - \sum_m G_m S_m \tag{2.3}$$

where I/qV is the density of charge carriers with charge q entering the active region with volume V, per unit of time. Of these injected charge carriers, an amount of $\gamma_e N$ recombines spontaneously per unit of time and volume. The rightmost part of Eq. 2.3 accounts for the stimulated carrier recombination.

2.2 An Optical Neural Network

As the operating principle of the optical neural network described in this thesis is based on varying the optical losses via external optical feedback for a number of modes, let us see what happens in a two mode laser diode. Without loss of generality we assume that the two longitudinal modes have approximately the same wavelength and we can write $G_m = G$. We introduce the controlled optical feedback for the two modes via the facet reflectivities R_1 and R_2 of the modes that are labeled 1 and 2. We examine the behavior of the laser diode as a function of varying R_m.

2.2.1 Threshold Operation

To explain the origin of the threshold function we use the steady state solution of the rate-equations of Section 2.1.2. We will use a fixed mirror reflectivity for one mode and we will vary the reflectivity for the other mode around this value.

Neglecting Spontaneous Emission

For clarity, let us first neglect the spontaneous emission R_{sp}. In a two mode system in steady state this yields:

$$(G - \gamma_1) S_1 = 0 \tag{2.4}$$

$$(G - \gamma_2) S_2 = 0 \tag{2.5}$$

$$I/qV - \gamma_e N - G(S_1 + S_2) = 0 \tag{2.6}$$

It can easily be seen that the equations for the photon densities (Eqs. 2.4–2.5) only have solutions $\{G = \gamma_1, S_2 = 0\}$ and $\{G = \gamma_2, S_1 = 0\}$ for $\gamma_1 \neq \gamma_2$. This means that the laser is either lasing in mode 1 or mode 2, depending on the optical losses for these two modes. The mode with the lowest amount of optical losses will be lasing.

The photon density of the lasing mode and the carrier density can be found analytically by substituting the above solutions in Eq. 2.6 using the linear relation between G and N.
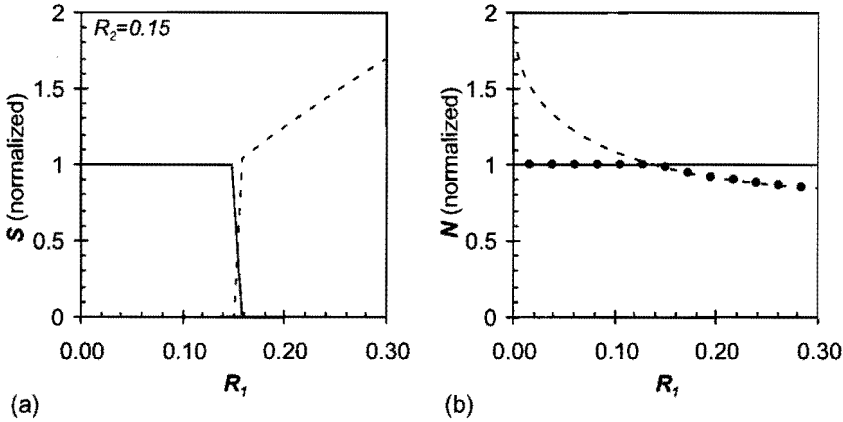
Figure 2.3 Normalized photon S (a) and carrier density N (b) versus mode 1 facet reflectivity R_1. In Fig. (a) S_1 and S_2 are plotted with a dashed and a drawn line respectively. The dashed line in Fig. (b) corresponds to the solution for $S_1 \neq 0$, the drawn line to the solution for $S_2 \neq 0$. The actual solution for N, corresponding to Fig. (a) is marked with dots.

With parameters from Ref. [2] and the reflectivity for mode 2, $R_2 = 0.15$, set arbitrary to half the reflectivity of a normal laser diode facet, we can solve Eqs. 2.4–2.6 for the photon densities S_1 and S_2 as a function of R_1. The results, normalized to the value for S_2 when this mode is lasing are presented in Fig. 2.3(a). The normalized photon density for mode 1 is represented with a dashed line, that of mode 2 with a drawn line.

The laser emits at the wavelength with the lowest optical losses. If $R_1 < R_2$, mode 2 is the mode with the highest reflectivity and therefore the lowest optical losses. When $R_1 > R_2$, mode 1 experiences the lowest optical losses and will lase. This results in a sharp threshold in the photon densities of the modes at $R_1 = R_2$.

The normalized carrier density is plotted in Fig. 2.3(b). The solution for N corresponding to $\{G = \gamma_1, S_2 = 0\}$ is plotted with a dashed line, the drawn line corresponds to $\{G = \gamma_2, S_1 = 0\}$. The solutions are normalized to the value for N for $\{G = \gamma_2, S_1 = 0\}$ which is independent of R_1. As expected we see that the lower of the two solutions for N corresponds to the actual solution that is marked with dots. From the figure it follows that the switching from mode 2 to mode 1 at $R_1 = R_2$ can be explained by the reduction in N resulting from the decreasing optical losses of mode 1. This reduction in N will result in a decrease of the optical gain G. For mode 2 this means that $G = \gamma_2$ is no longer valid and therefore $S_2 = 0$.

From the preceding we can conclude that the threshold operation of Fig. 2.3 is essentially caused by the coupling between the modes via the carrier density and the dependency of the gain on the carrier density.

Including Spontaneous Emission

The solution to Eqs. 2.4–2.6 including the spontaneous emission can be obtained in a similar fashion. Now either mode 1 is lasing and mode 2 only contains (amplified) spontaneous emission or vise versa. The exact solution can be found analytically by solving the third order polynomial equation in N that results from substituting the equations for S_1 and S_2 in the equation for N. Using the same procedure and parameter set that was used to produce Fig. 2.3 we obtain Fig. 2.4.

Figure 2.4(a) shows a softer threshold than Fig. 2.3(a). This softer threshold is caused by amplified spontaneous emission that occurs when the gain is only slightly lower than the optical losses for a mode. This happens near the point where $R_1 = R_2$.

A third solution for N that can be observed in Fig. 2.4 corresponds to the situation when none of the two modes would be lasing. This situation will never occur as it would cause the optical gain, that is proportional to the carrier density to be much higher then any of the optical losses. As a consequence, the mode with the lowest optical losses would immediately start lasing.

The above analysis for two longitudinal modes is also valid for any number of modes. The mode with the highest net gain $(G_m - \gamma_m)$ will be the one that lases. A threshold operation is associated with the controlled amount of optical feedback and the photon density for each mode. Making the controlled optical feedback for each mode individually proportional to a weighted sum of inputs will result in neural-like operation for each of the modes.

(a)   (b)
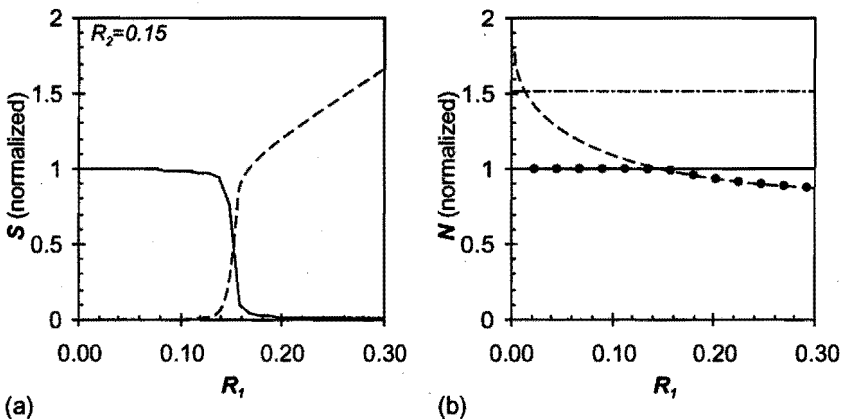
Figure 2.4 Same as Fig. 2.3 but including spontaneous emission. The spontaneous emission results in a softer threshold for the photon densities. A third solution for N can be observed (dashed-dotted line) corresponding to the situation where modes 1 and 2 only exhibit spontaneous emission. Again the actual solution of N is marked with dots.

Thus a neural network can be formed with as many neurons as there are longitudinal cavity modes in the laser diode. The output of the network is the emission spectrum of the laser diode and is in the optical power domain. The inputs and weights are applied via the controlled optical feedback.

The coupling between the modes via the carrier density can directly be translated to connections between the neurons of the optical neural network. Just like in Fig. 1.3(b), the output of each neuron influences the activity of all other neurons. As the influence is negative, these connections are inhibitory. As discussed above this coupling results in a situation where only one mode, or one neuron, will be active. In neural network literature such a neural network is generally called a *winner-take-all* network or *maxnet* [3].

2.2.2   Weighted Inputs

The controlled optical feedback is provided to one of the laser diode facets. This facet is antireflection coated to enhance the effect of the optical feedback. In order to control the amount of optical feedback for each of the longitudinal modes of the laser diode individually, first the laser beam exiting the diode at the antireflection coated facet is dispersed in space as shown schematically in Fig. 2.5.
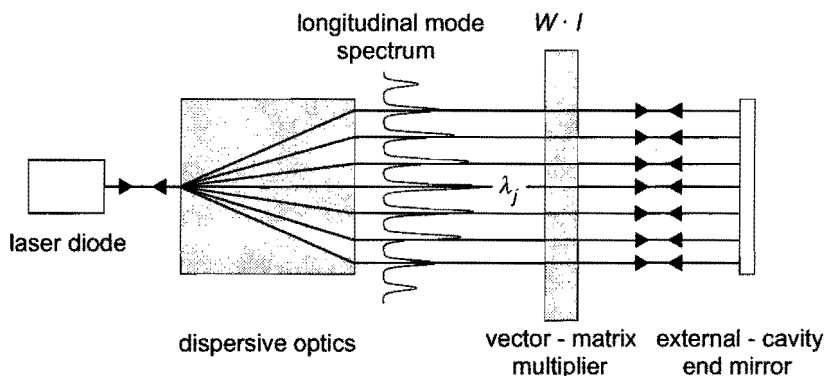
Figure 2.5 External optical feedback is provided to a laser diode to control the amount of optical losses for each longitudinal mode of the laser diode individually. A vector-matrix multiplier is used to make the amount of optical feedback proportional to a weighted sum of input signals.

This results in a light beam for each of the longitudinal mode wavelengths λ_j of the laser diode. Each light beam is attenuated by a controlled amount before it is reflected back into the laser diode by the external-cavity end mirror. The attenuation for each modal light beam is made proportional to a weighted sum of input signals by use of a vector-matrix multiplier [5].

The vector-matrix multiplier consists of two arrays of controllable transmission elements and some (cylindrical) lenses. A schematic representation, drawn without the lenses, is given in Fig. 2.6. A first set of two cylindrical lenses distribute the optical power $P_{j.in}$ contained in each light beam over the rows of a one-dimensional array of

transmission elements. With m rows, the amount of power incident on each transmission element is $P_{in,j}/m$ for each light beam j. After an element of the transmission matrix is passed, the amount of optical power is attenuated with a factor I_i that represents input signal i.

The resulting optical power in each of the m light beams in each column is $P_{j,in}I_i/m$. The light beams are further attenuated by a two-dimensional array of transmission elements. Each of these transmission elements is set to a transmission value $w_{i,j}$ that corresponds to the weight factor for wavelength j and input i. A second pair of cylindrical lenses recombines the optical power of the m light beams of each column. The resulting output power of each light beam $P_{j,out}$ is $\frac{P_{j,in}}{m} \sum_i w_{i,j} I_i$
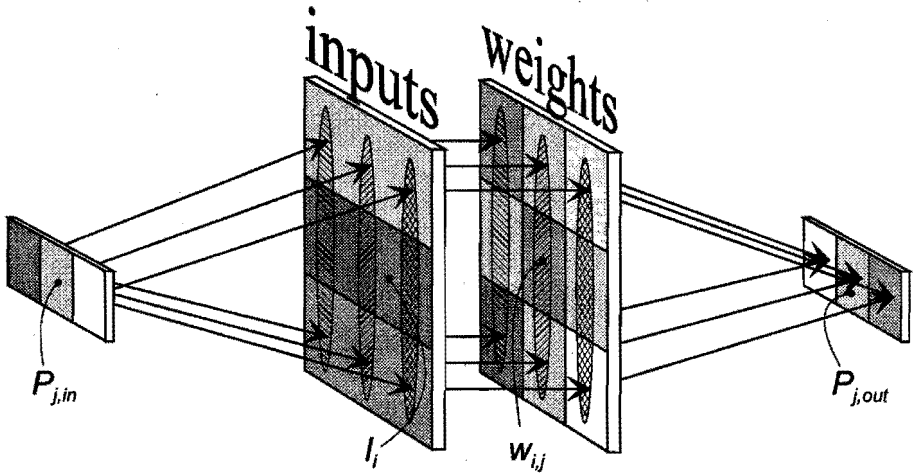
Figure 2.6 Optical vector-matrix multiplier. The optical power at each wavelength $P_{j,in}$ is distributed over a column of a transmission matrix consisting of line elements. The light is attenuated by a factor proportional to an input signal I_i in each line i of the transmission matrix. For each wavelength j and each input signal i the light is further attenuated by a weight factor $w_{i,j}$ in a second transmission matrix. The light from one column is combined resulting in $P_{j,out} \propto P_{j,in} \sum_i w_{i,j} I_i$.

As shown in Fig. 2.5, the optical vector-matrix multiplier is placed in an external-cavity setup. Thus the portion of optical power returning to the laser diode for each wavelength j can be found by comparing $P_{j,in}$ and $P_{j,out}$. As the vector-matrix multiplier is also passed in the return path, each light beam experiences the same attenuation factor twice. This results in an effective external power reflection R_j according to:

$$R_j = \left(\frac{P_{j,in}}{P_{j,out}} \right)^2 = \left(\frac{1}{m} \sum_i w_{i,j} I_i \right)^2 \tag{2.7}$$

Thus R_j is made proportional to the square of a weighted sum of input signals. From the preceding it is clear that the resulting optical neural network has its inputs and weights in the optical transmission domain. The outputs are represented in the optical power domain.

2.2.3 Learning

In order to train the network (See Chapter 1) we need a training supervisor that provides input patterns to the network and is able to read the neuron output states. The supervisor should also be capable of controlling the weight matrix. Furthermore the supervisor needs a learning algorithm to adjust the weight matrix iteratively during the learning phase. The supervisor in this thesis is a personal computer (PC).

Because the weight matrix and the input mask are implemented with a transmission matrix they can be combined in a single matrix. The inputs and weights can be superimposed in the PC. In the experimental optical neural network presented in this thesis we use a liquid crystal display as a variable transmission matrix.

To read the output pattern of the optical neural network, the PC should be able to monitor the output spectrum of the laser diode. For this purpose we use an optical spectrum analyzer that is connected to the PC.

To train the network, a learning algorithm is implemented on the supervisor PC. In the following Chapters 3 and 4 we describe two different experimental implementations of the conceptual optical neural network. The two experimental implementations differ in the used transmission matrix, the external-cavity configuration and the learning algorithm. Both implementations use the concepts presented in this chapter.

References

[1]   K. Petermann, "Laser diode modulation and noise," in *Advances in Optoelectronics*, T. Okoshi Ed., (Kluwer Academic, Dordrecht, The Netherlands, 1991).

[2]   G. P. Agrawal and N. K. Dutta, *Long-wavelength semiconductor lasers*, (van Nostrand Reinhold, New York, 1986).

[3]   F. T. S. Yu, "Optical neural networks: architecture, design and models," in *Progress in Optics*, E. Wolf Ed., (North Holland, Amsterdam, 1993), Vol. 32, pp. 61–144.

[5]   J. W. Goodman, A. R. Dias, and L. M. Woody, "Fully parallel, high-speed incoherent optical method for performing discrete Fourier transforms," *Opt. Lett.* **2**, 1–3, 1978.

3

Optical-Mode Neural Network by use of the Nonlinear Response of a Laser Diode to External Optical Feedback

We present an intelligent all-optical neural network using a single laser diode that is provided with controlled external feedback. The outputs of the laser neural network (LNN) are represented in the optical domain by the longitudinal cavity modes of the laser diode. The inputs to the LNN are applied by means of adjusting the external feedback of each longitudinal mode through an optical vector-matrix multiplier. Supervised training of some basic input-output mappings is demonstrated by means of a stochastic learning algorithm. The stability and reproducibility of the LNN setup is examined.

19

3.1 Introduction

One of the main characteristics of neural networks is their intrinsically parallel operation. Software has played an important role in the development of artificial neural networks; however, classical (sequential) computers use the parallelism of computation only as a concept. The use of dedicated neural hardware would therefore lead to an increase in computational speed. This is the main reason why various neural circuits have been realized on silicon (in Ref. [1] an overview of a number of neural chips is given).

An even more suitable candidate for implementing neural networks is the optical domain. First, light beams cross each other in free space without interacting. Second, all three dimensions can be used, which reduces the problem of interconnectivity and allows for larger and more complex networks. Third, optical systems are potentially much faster. Weighting and summation in the optical domain can be done very quickly, while speed limitations caused by charge buildup, as in electronic systems, are not present. These advantages of using optics for processing data are illustrated by the numerous optical neural network and optical computing experiments that have been performed in the past 5 to 10 years [2]-[7].

In these systems the neural action, which is the nonlinear response of a neuron to its weighted inputs, is usually realized in the electro-optical domain. In this chapter we present the results of an optical neural network experiment in which a single laser diode under external optical feedback is used to provide a set of neurons. The longitudinal modes of the laser represent the neuron signals. The optical powers contained in the modes respond nonlinearly to the degree of optical feedback.

In Section 3.2 we explain the basic principles of the laser neural network (LNN). Section 3.3 describes the experimental setup. In Section 3.4 we demonstrate its neural activity. Some real-time learning experiments are presented in Section 3.5. Possible areas of application considered are optical data storage or optical communication. We therefore restrict ourselves to training digital input-output mappings to the LNN. In Section 3.6 we discuss the performance and some features of our neural network. Finally, in Section 3.7 we give conclusions and an outlook toward future experiments.

3.2 Laser Neural Network Operation Principles

An artificial neuron is a simplified model of a biological neuron—it has a number of inputs and one output and it performs some simple arithmetic operations. The inputs to the neuron are weighted and summed. This weighted sum is compared with a threshold, and, depending on the result, the output of the neuron will be either high or low. Usually the threshold is a soft threshold, and the relation between output signal and weighted sum is a nonlinear S-shaped (or sigmoid) function. A network consisting of a number of neurons can be trained to perform an input-to-output vector function by the proper setting of the weight values of all neurons. This process of adjusting the neural weights is called the learning phase.

The LNN is described in Chapter 2 and in Refs. [8] and [9] in which a detailed theoretical description [8] of the LNN and some preliminary experimental results [9] are given.

In our LNN the complete network is formed by a single laser diode and some additional optics. The response of the laser diode to external optical feedback applied to one mirror is used to provide neural action. Sensitivity to external feedback is an unwanted effect in most laser diode applications, such as in optical data storage and optical communications, but in our neural network this nonlinear effect is very useful. The reflectivity of the laser diode mirror at the feedback side is reduced by means of a coating to maximize the effect of the external optical feedback. The amount of external optical feedback in our setup is, however, not sufficient to obtain single-mode external-cavity operation. The spectral distribution of the lasing external-cavity modes is similar to that of a single longitudinal mode of the diode cavity. The mode-spacing of the laser diode in our experimental setup is therefore determined by the diode cavity length (300 μm).

In the external cavity the laser beam is separated into several beams by means of dispersive optics. This results in one light beam for each of the longitudinal cavity modes. Each of these beams is attenuated individually before being reflected back into the laser diode by the end mirror of the external cavity. The amount of attenuation for each beam, and thus for each longitudinal cavity mode, is made proportional to a weighted sum of inputs. The weighting of inputs is implemented by use of an optical vector-matrix multiplier. A schematic drawing showing this concept is presented in Fig. 3.1.
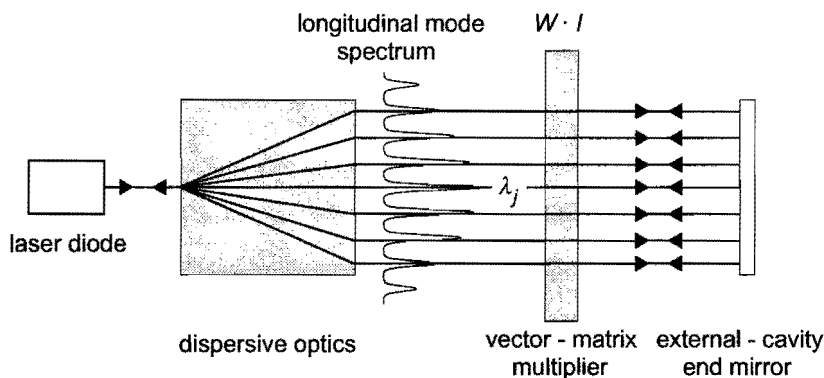
Figure 3.1 Schematic drawing of a laser diode with an external cavity to provide external optical feedback. Dispersive optics is used to separate the light beams of the longitudinal modes spatially . A vector-matrix multiplier ($W \cdot I$) is used to make the optical feedback for each wavelength λ_j proportional to a sum of weighted inputs for each of the longitudinal modes. In this drawing, W represents the weight matrix and I represents the input vector.

A small amount of external optical feedback is sufficient to modify the longitudinal mode spectrum of the laser diode [10]. The optical output power of the modes of the laser will vary nonlinearly with the amount of external optical feedback applied [11]. Controlling the feedback of each of the longitudinal modes separately results in the optical power contained in each mode exhibiting neural behavior. In this manner a set of neurons is formed in which the optical powers of the longitudinal cavity modes of the laser provide the outputs. Because of the longitudinal mode competition commonly found in multimode

lasers [12], connections between the neurons arise. These connections are inhibitory; an increase in the optical power contained in one mode will cause a decrease in the optical powers of the other modes. In Fig. 3.2 the resulting neural network architecture is shown schematically.
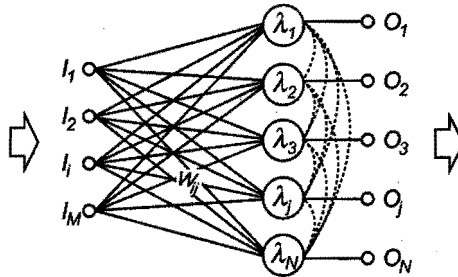
Figure 3.2 Schematic architecture of an M-input, N-output LNN. The solid lines denote weighted connections $W_{i,j}$, the dashed curves denote inhibitory connections caused by mode competition, and the open circles circles represent neurons with the corresponding longitudinal mode wavelength λ_j. The information flow is from left to right.

The potential speed of this optical neural network is expected to be very high, because the response of a laser diode to a change in external optical feedback is primarily governed by the intra-band relaxation time of the charge carriers inside the laser diode, which is of the order of 10^{-12} s [13]. For a more detailed theoretical description of the LNN and its response time we refer the reader to Ref. [8]. The response time will be investigated in more detail in Chapter 5.

3.3 Experiment

3.3.1 Optical System

The laser used in our experiment is a multiple-quantum-well laser diode (Philips Opto-electronics Centre, CQL806 series) with a high-quality ($R < 0.1\%$) antireflection coating applied to the facet at the external-cavity side. The laser diode is temperature stabilized to prevent thermal drift of the longitudinal mode wavelengths. A dc current with a super-imposed ac current ($I_{peak} = 30$–40 mA) is fed to the laser. For permitting well-controlled external optical feedback, the period of this ac current corresponds to the photon round-trip time of the external cavity (ac frequency of $\sim$90 MHz, cavity length of $\sim$3.3 m). In this manner the current through the laser is synchronized with the optical pulse traveling in the external cavity.

The experimental setup is shown in Fig. 3.3. The lenses L1 (f = 4.4 mm, NA = 0.5, aspherical) and L2 (f = 200 mm) are used to form a sharp image of the active area of the laser chip on the external-cavity mirror M in order to obtain maximum feedback. Two gratings G1 and G2 (both are 1200 g/mm; the distance between G1 and G2 is 2.18 m) provide the dispersion needed to resolve the longitudinal modes of the laser diode spa-

tially. The spatial separation between two adjacent modes matches the spacing of the attenuation elements (0.88 mm) of the optical vector-matrix multiplier. The vector-matrix multiplier, a sketch of which is given in the inset of Fig. 3.3, is formed by the two cylinder lenses L3 (f = 25.4) and L4 (f = 50.0) and a passive-matrix liquid-crystal display (LCD) that is used in transmission. A polarizer, that is needed for proper operation of the LCD, is not shown in the figure.
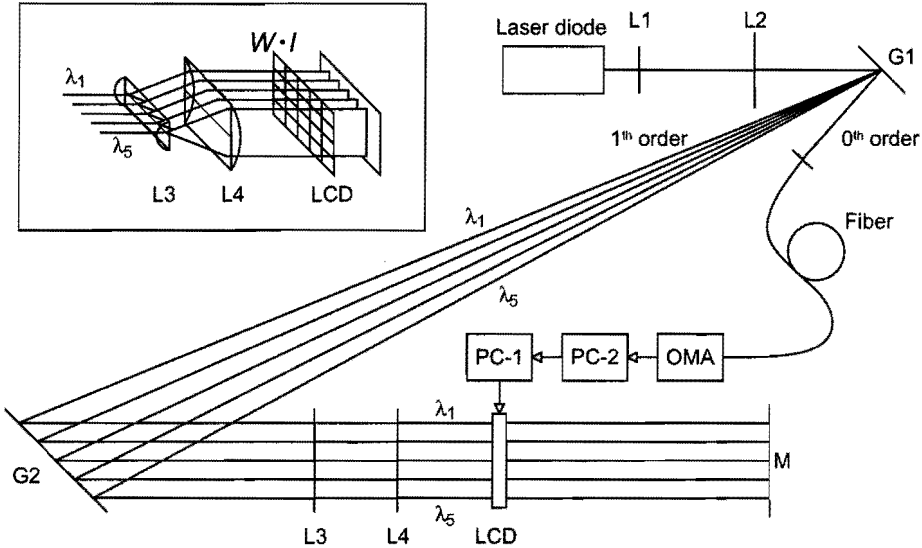
Figure 3.3 Schematic drawing of experimental LNN setup: Two lenses L1 and L2 form an image of the laser diode exit facet on mirror M. Two gratings G1 and G2 are used to disperse the longitudinal cavity modes ($\lambda_1 \ldots \lambda_5$) of the laser diode. An optical vector-matrix multiplier is inserted in the external cavity thus formed. A three-dimensional drawing of the vector-matrix multiplier is shown in the inset at the upper left-hand side. The cylinder lenses L3 and L4 serve to distribute the optical power of all light beams over the rows of the LCD. Each row corresponds to an input of the LNN. The weight matrix W and the input vector I are superimposed in PC-1, and the resulting image is fed to the LCD. In this manner the external optical feedback of the diode laser is made proportional to a weighted sum of inputs for each longitudinal mode individually. Also shown is the training system of the LNN. The optical power of the zeroth 0th order of grating G1 is coupled into a fiber and analyzed by the OMA. PC-1 receives the output values of the LNN by means of PC-2, which is connected to the OMA.

On the LCD an image of four rows and five columns is formed, in which each of the pixels can be set to one of 31 discrete gray levels. The LCD contains standard twisted nematic liquid-crystal material, limiting the switching speed of the display to $\sim$200 ms in this experiment. We use the LCD to adapt the neural weights as well as to provide the inputs to the network. For this purpose the input pattern of horizontal lines and the weight mask, a matrix of transmission elements, are superimposed. The resulting pattern is displayed on the LCD. The number of rows and columns of our LCD limits the number of

inputs and neurons to four and five, respectively. For measuring the neural outputs, which are contained in the longitudinal mode pattern of the laser, the optical power reflected in the zeroth order of grating G1 is coupled into a fiber and fed to an optical multichannel analyzer (OMA). The OMA measures the spectral distribution of the longitudinal cavity modes that are used as neurons in the experiment.

3.3.2 Training System

A supervised learning algorithm is used to train the LNN to produce a specified output at a given input. With such algorithms the supervisor feeds sample input patterns to the network and simultaneously monitors the output of the network. The weight matrix of the network is changed by means of an algorithm until the supervisor receives the desired output pattern for each applied input pattern.

For such a learning scheme to be applicable in our experiment a supervisor must be able to set the inputs and weights of the LNN and measure its output vector. In our setup a first personal computer (PC-1) is the learning supervisor and controls the addressing of the LCD via its parallel port (See Fig. 3.3). PC-1 provides the network with the four input gray levels and the 4×5 gray level matrix of neural weights.

Monitoring the output is done by means of a second PC (PC-2), which receives the neural outputs from the OMA in integer counts proportional to the optical power in the longitudinal cavity modes. During each learning trial the outputs are read by PC-2 and subsequently sent to the supervisor PC-1, on which a stochastic learning algorithm is implemented. In this type of algorithm the weights of the network are changed randomly until the difference between the actual and the desired output vectors is below a preset level for all input patterns. We chose to use a stochastic algorithm instead of the well-known backpropagation algorithm [14] because the latter uses the known response of the neurons to calculate an estimate of the weight changes. In our case the behavior of the neurons is not known exactly and depends on various physical parameters. In addition, connections between the neurons exist in our LNN, whereas the backpropagation method is designed for feed-forward neural networks without such connections. Finally, it is believed that stochastic algorithms will need less computational power [15],[16] and will therefore be easier to implement in hardware.

Our learning algorithm uses a Cauchy-distributed random disturbance vector [17]. As occurs in simulated annealing [18], the amplitude of this vector is controlled by an artificial temperature that slowly decays. In this way the neural network is forced to look in increasingly smaller neighborhoods of the last-found optimum. Although our algorithm does not use an artificial temperature in exactly the same way that it is used in simulated annealing, the term is used throughout this text. To test the algorithm before actual learning we performed experiments in which the LNN was simulated in software. The use of heuristic learning rules, as suggested in Refs. [19] and [20], did not improve the algorithm substantially during these simulations, and they were therefore not implemented in the experiments. The algorithm is described in the flowchart of Fig. 3.4.

In this algorithm a trial matrix (W^{trial}) is shown to the network for all input vectors ($I_{\text{tr},s}$) during each iteration. The trial matrix is calculated by use of the best matrix so far (W) and a random matrix (W^{rand}), which is scaled by an artificial temperature T that slowly decays

Initialize:
T   Artificial temperature
η Temperature-decay rate
$I_{tr,s}$ Input training patterns
$O_{tr,s}$ Output training patterns
W   Weight matrix

Generate W^{rand} :
$$W_{i,j}^{rand} = T \tan\left[-0.5\pi + Random(\pi)\right], \forall i, j$$

Show $W^{trial} = W + W^{rand}$ to LNN
for all input patterns $I_{tr,s}$

Read outputs from the LNN: O_s
calculate error:
$$error = \sum_{all\ s} \|O_s - O_{tr,s}\|$$

ERROR<BESTERROR?   **Yes**

No

Show $W^{trial} = W - W^{rand}$ to LNN
for all input patterns $I_{tr,s}$

Read outputs from the LNN: O_s
calculate error:
$$error = \sum_{all\ s} \|O_s - O_{tr,s}\|$$

ERROR<BESTERROR?   **Yes**   BESTERROR:=ERROR
                                    W:=W^{trial}

No

$T := \eta T$

No

BESTERROR=0 ?

end

Figure 3.4 Flowchart of the stochastic learning algorithm: The algorithm searches for a weight matrix W for which the LNN input-output mapping is correct. Disturbing W with a random matrix W^{rand} is the process used to accomplish this. The disturbance matrix is scaled with an artificial temperature T that slowly decays. In this manner the algorithm searches in smaller and smaller neighborhoods of the last-found optimum.

with a factor η in each iteration. The optimization criterion (ERROR, BESTERROR) is the sum of the differences between desired output vector (O_{tr}, s) and the actual output vector (O_s) for the complete training set. This error $\| O_s - O_{tr.s} \|$ is defined as 0 if the actual output value of the neuron is above the ON or below the OFF value in the case of a desired digital 1 or 0 respectively. In other cases this error is equal to the absolute difference between the actual output value and the corresponding, desired ON or OFF value. The algorithm is said to converge if the optimization criterion equals 0.

3.4 Laser Sigmoid and Neural Activity

The neural activity of our setup can be demonstrated by the measurement of the relation between the sum of weighted inputs and the output levels of a set of neurons. In the LNN the sum of weighted inputs for a specific neuron corresponds to the total transmission of its LCD column, whereas the output levels of the neurons are represented by the optical powers contained in the cavity modes.

The transmission of a LCD pixel varies nonlinearly with the gray level assigned to it by PC-1. To correct this we used a subset of all possible gray levels by means of a lookup table. The resulting transmission, that is presented scaled to the maximum value in Fig. 3.5, shows an almost linear relation with the applied gray level.
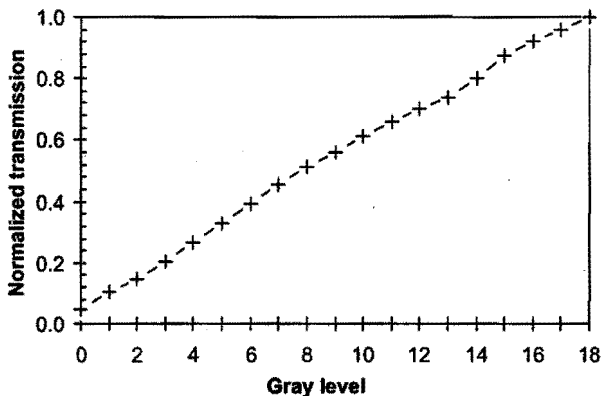
Figure 3.5 Normalized measured LCD response as a function of applied gray level. The accuracy of the measurements is within 10% of the difference between succeeding transmission values.

With the LCD calibrated in this manner, the sum of weighted inputs for two neurons is varied linearly by the adjustment of the gray levels of the two corresponding LCD columns. The output of the two neurons is monitored by measuring the optical power contained in the corresponding longitudinal cavity modes. In Fig. 3.6 the results of these measurements are given. The optical powers of modes 1 and 2 are plotted versus the gray-level of column 2 (g_2) in Figs. 3.6(a) and 3.6(b), respectively. During the measurements

g_1, the gray level of column 1, is used as a parameter: $g_1 = 0, 4, 8, 12, 16$, as indicated in the figure.
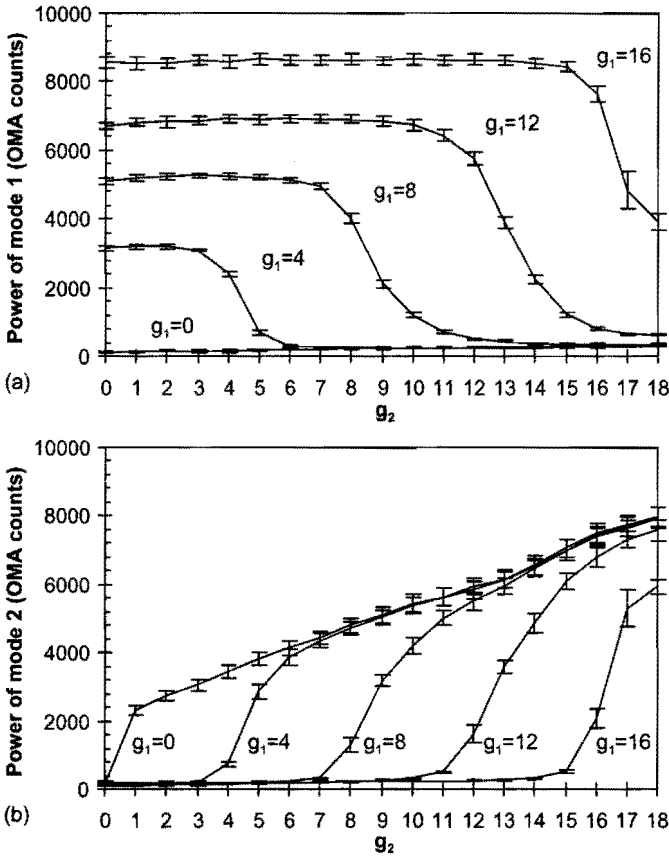
Figure 3.6 Optical power contained in two longitudinal cavity modes: (a) mode 1 and (b) mode 2, as a function of gray level of the corresponding columns g_1 and g_2. In these measurements g_1 is set to 0, 4, 8, 12, and 16, while g_2 is varied from 0 to 18. The error bars indicate the variance of a series of 20 measurements. The figures show a sigmoidal response for both longitudinal cavity modes.

Figure 3.6(a) shows that the output level of neuron 1 drops dramatically when neuron 2 starts lasing, demonstrating the mode competition of the two corresponding cavity modes. As can be seen from Fig. 3.6(b), the output level of neuron 2 varies nonlinearly with its applied sum of weighted inputs for all values of g_1. Figure 3.6 also shows a change in the threshold value for neuron 2 when the total sum of inputs for neuron 1 (g_1) is set to a different value. Again, this is a result of the mode competition between the two longitudinal cavity modes. When the optical power contained in one mode increases, the amount of population inversion will decrease. This results in a decreased optical gain for

all other modes. Thus, a larger amount of optical feedback will be needed by these modes
to reach the threshold condition for lasing.

3.5   Training Examples

3.5.1   Real-Time Learning

With the setup described in Section 3.3 a neural network with up to four inputs and five
outputs can be constructed. One of the rows of the input mask is used as a bias, i.e., it is
always fully transmitting. The corresponding bias weights serve to control the threshold
values of the neurons as discussed in Chapter 1 (See also Ref. [21]). The stochastic
learning algorithm described in Section 3.3 was used to make this network perform some
(digital) input-output functions of up to three inputs and five outputs. We discuss one of
the training examples that is based on the NOR–XOR–AND function. In this example the
task of the network is to provide the input-output mapping of Table 3.1.

Table 3.1 NOR–XOR–AND (Outputs O_1, O_2, O_3, respectively) truth table.

Input		Output		
I_1	I_1	O_1	O_2	O_3
0	0	1	0	0
0	1	0	1	0
1	0	0	1	0
1	1	0	0	1

In the learning algorithm the logical ON and OFF levels are preset to 1000 and 4000
OMA counts respectively, for all wavelengths corresponding to the three selected modes.
The error measure BESTERROR and the artificial temperature T of this training-session
example are plotted as a function of the iteration count in Fig. 3.7 (See also the flowchart
of Fig. 3.4). After 142 iterations the algorithm converges to the solution for the weight
matrix that is presented in Fig. 3.8.

The input-to-output mapping reproduced by the network with this weight matrix is
shown in Fig. 3.9. From this figure it is clear that the network has indeed learned the
truth table from Table 3.1. The output of the network responds correctly to the set of
input patterns.

With the same procedure, some other functions are trained to the network, the truth
tables of which are presented in Table 3.2. The 1:4 (and 1:5) demultiplexing can be of use
in optical communications where an incoming packet of binary optical data needs to be
routed to one out of four (or five) output channels. The three-input parity function could
be used as a simple form of error detection. It detects odd or even parity on three input
bits and thus could be used as an error detection for a two-input plus parity digital signal.

In Table 3.3 the training results for these input-output mappings, as well as those for
some other functions, are listed with the number of inputs (number in) and outputs (num-
ber out) needed, the average number of iterations and the standard deviation on this av-
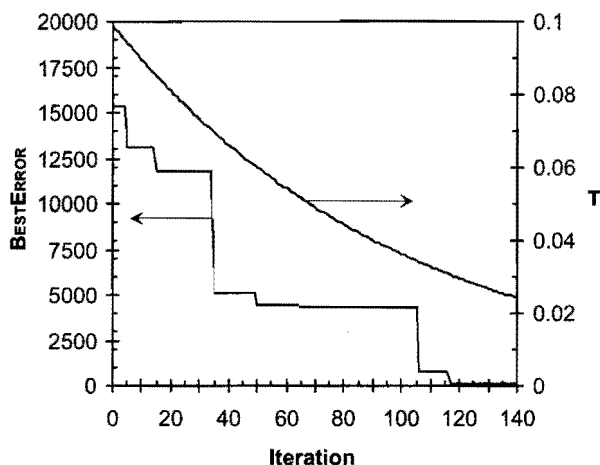
Figure 3.7 Error measure BESTERROR and artificial temperature T versus the iteration count of the NOR–XOR–AND training-session example.

0.98	0.60	0.97
0.10	0.85	0.79
0.38	0.50	0.79
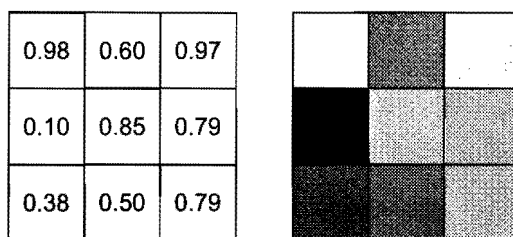
Figure 3.8 Weight matrix resulting from the example training session in normalized transmission value per pixel (left) and the gray shade representation of these transmission levels (right).

erage. All averages and standard deviations are calculated over 20 training sessions, with each training session being a completion of the algorithm shown in Fig. 3.4. The initial matrix for these experiments is $W_{i,j} = 0.5(\forall i, j)$. The initial temperature is in the range of 0.1 to 0.3 and the temperature-decay rate η is 0.99. In the training examples three-input AND–NAND and three-input parity, an initial matrix resulting from learning trials of a simulated LNN is used with a lowered initial temperature ($T = 0.01$) to force the network to search in a small neighborhood of this theoretical solution. The combination of a long-term stability drift of the setup resulting from the large external-cavity size and long training cycles caused by the relatively slow LCD inhibited the network from learning these examples without help from the simulations. With normal initialization these learning examples did not converge within 5000 iterations.
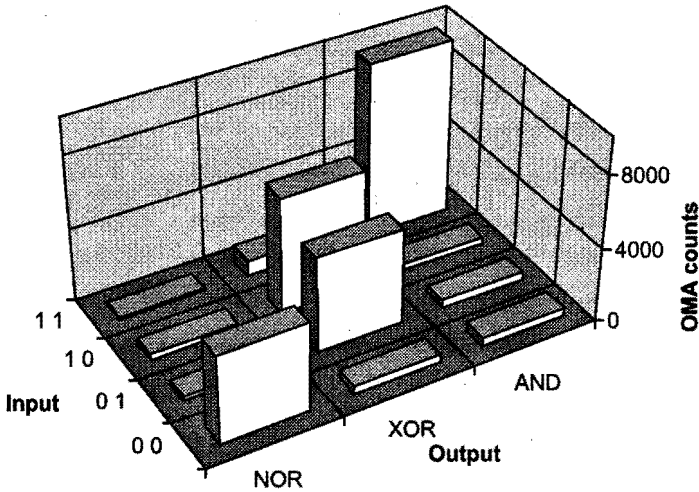
Figure 3.9 Output of the LNN after training of the NOR-XOR-AND example. The output of NOR, XOR and AND modes in counts of the OMA are plotted as a function of binary input patterns.

Table 3.2 Truth table for the functions 1:4 demultiplexing, 1:5 demultiplexing, and three-input parity training examples.

Input	Demultiplexing 1:4	Demultiplexing 1:5	Three-Input Parity [a]
000	1000	10000	1**0**000
001	0100	01000	0**1**000
010	0010	00100	0**1**000
011	0001	00010	0**0**100
100	DC[b]	00001	0**1**000
101	DC	DC	0**0**010
110	DC	DC	0**0**001
111	DC	DC	0**1**000

[a] The second (bold) neuron of the three-input parity mapping represents the actual output parity bit.
[b] DC denotes a don't care result: The corresponding input vector is not trained to the network

3.5.2   Noise Characteristics

In the setup of this chapter we use a rather long external cavity. Using a vector-matrix multiplier with a smaller spatial separation between the attenuation elements or with dis-

Table 3.3 Training results of the input-output mappings used in the LNN experiments.

Problem	Number In	Number Out	Average Iterations	Standard Deviation
Inverter	1	2	8	3
OR–NOR	2	2	13	8
AND–NAND	2	2	125	85
NOR–XOR–AND	2	3	196	128
1:4 Demultiplexing	2	4	390	157
3-Input OR–NOR	3	2	37	25
3-Input AND–NAND	3	2	71	71
1:5 Demultiplexing	3	5	326	91
3-Input Parity	3	5	369	283

persive elements with higher dispersion would reduce the length of this cavity. A small alignment mismatch in the long cavity of the setup can lead to errors in the operation of the LNN. For this reason some stability tests were performed on the trained LNN. After each of the 20 training sessions we tested the resulting weight matrix by showing all input patterns to the network and checking the resulting outputs. This was repeated 10 times for each of the resulting weight matrices.

The number of mistakes the network makes is a measure of the stability of the LNN. In only one of these test examples ($<0.1\%$) was the digital output pattern different from the training output: A binary 0 occurred where a 1 was expected. In less than 5% of all the tests the output of the network was not exact for one of the modes. The output of one mode, for example, was 1066 counts when a digital 0, and therefore a value below 1000 counts, was expected. The average deviation from the binary decision levels is 10% in these cases.

To get an estimate of the sensitivity of the LNN to changes in the input values, a weight matrix resulting from the learning algorithm (NOR–XOR–AND) is shown to the network. Instead of digital inputs, analog values between 0 and 1 are used as inputs. The resulting optical powers of the three selected modes are measured as a function of inputs I_1 and I_2. In Fig. 3.10(a) the results of these measurements are plotted for each of the modes. The gray shades correspond to the optical power; a white region denotes a fully lasing mode. In Fig. 3.10(b) regions are indicated where the optical power is below the level defined as OFF or above the level defined as ON in the learning algorithm. The sizes of these regions determine the so-called noise margins on the inputs. Figure 3.10(c) illustrates the same regions in input–output space for an optimal digital system with the same NOR–XOR–AND functionality. As can be seen from the figure the decision regions of the LNN are far from optimal. The output of the XOR mode [mode 2; see Fig. 3.10(b)], for instance, is 0 in a relatively small region near $I_1 = 0$.
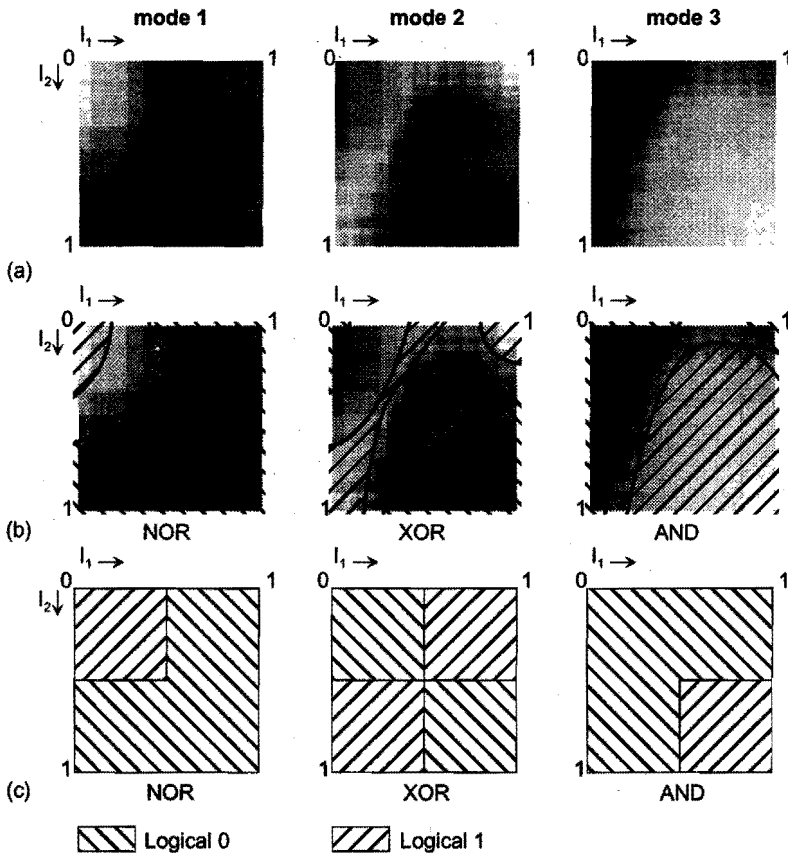
Figure 3.10 (a) Output of NOR, XOR, and AND modes versus analog inputs I_1 and I_2, for the trained LNN. The brightness is proportional to the optical power contained in a mode. (b) Same as (a) but with added decision regions for digital output values. The corners of these graphs correspond to the four 2-bit digital input patterns. The sizes of the logical 0 and 1 regions determine the noise margins on the digital inputs. (c) Depiction of optimal regions of the same problem as for (a) that maximize the input noise margins.

3.6 Discussion

3.6.1 Noise Margins

The noise margins of the network should be optimized when the LNN is to be used in a practical system. One way of doing this is to alter the training algorithm. In its present form the algorithm applies only digital input patterns to the network. This means that only the corners of Fig. 3.10 are probed. Adding some analog input training vectors and their corresponding output vectors to the training set allows some in-plane points to be included in the optimization. In this way the performance of the LNN should improve. Although analog input-output mappings (which can be used, for instance, in image processing) are

in principle possible with this network, the LNN preferably should be operated in a binary output mode because of the character of mode competition (See Section 3.6.3, below).

3.6.2 Speed

Note that just one LCD is used to display the inputs and weights. The weighting and summation of inputs are done in the optical domain, whereas we present the inputs to the LNN in software by setting the appropriate weights to zero. Adding, e.g., a second LCD with line elements will transfer the multiplication to the optical domain. The fastest LCD's, however, will still be slow when compared with conventional computers. A real gain in computational speed will be obtained when the inputs are applied to the network by means of a fast electro-optic effect or by use of optical switching techniques. Speed limitations caused by the photon round-trip time of the extended laser cavity need to be minimized in that case by a reduction of the length of the external cavity. Only in all-optical systems such as those used for optical telecommunication would the resulting neural network profit from its potential speed. In all other cases the interface between electronics and optics will severely limit the speed of operation.

3.6.3 Effects of Mode Competition

Although the inhibitory connections arising from mode competition (See Fig. 3.2) cannot be controlled easily, they do make the network more versatile. If these connections did not exist, it would be impossible to make the network perform the XOR function. One can understand this quite easily by looking at the amount of external optical feedback for one mode: It is always higher for the 11 input pattern than it is for the 01 or the 10 input pattern. This relation implies that an extra mechanism is needed to switch off the XOR lasing mode in the 11 input state. By looking at the feedback for two modes, the way mode competition provides this mechanism becomes clear. If, in the 01 and 10 input states, a mode (i.e., the XOR mode) is lasing, its external feedback will be higher than that for all other modes. Although the external feedback for this mode will be higher in the 11 input state, it is possible that another mode receives even more external feedback for this 11 input. This mode would then start lasing, forcing the XOR mode that was already lasing to switch off.

In the examples described in Section 3.4 only one mode of the laser lases at each instance. This is the result of the strong mode competition that arises when laser diodes are operated well above threshold [22]. For the system depicted in the schematic drawing of Fig. 3.2 this means that the lateral inhibition, represented by the dashed curves, that is due to mode-competition dominates the behaviour of our neural network. In neural network terms the LNN would be called a *winner-take-all* [21] network in this regime, since one neuron gains all the optical power.

A set of inequalities can be formulated for each input-output vector pair for this type of network: The sum of weighted inputs for the winning neuron is higher than that of all others. For all input-output combinations of a given training set, a set of inequalities results. This set of inequalities can be used to determine whether or not a given function can be trained to the network. If the inequalities conflict, the input-output mapping cannot

be trained to the network. If, on the other hand, the inequalities can be solved, a solution to the set of inequalities can be used as an initial weight matrix for the learning algorithm. This procedure is useful not only in our LNN but also in other types of *winner-take-all* neural networks.

3.7 Conclusions

We have demonstrated a learning neural network that performs some basic input-output mappings. In this neural network the longitudinal cavity modes of a diode laser are used as neurons. The inputs to the network are presented in an external cavity in which the external optical feedback for each longitudinal cavity mode is controlled, providing the nonlinear behavior needed for neural action. Not only trivial learning examples such as the inverter problem were trained to the network, but also relatively complicated tasks such as the three-input parity problem were trained to our one-layer network by use of a simple stochastic supervised learning algorithm.

Mode competition plays an important role in the operation of the LNN, and some trained functions depend on this mechanism. The training process is speeded up when a theoretically determined initial weight matrix is applied. The experiments show that the network can be trained with good reproducibility. The stability of the network is good, although a relatively long extended-cavity is used.

In future experiments we plan to train more complicated learning tasks to the network in order to examine the performance of the LNN in more practical applications such as pattern recognition. First, more inputs and outputs will be needed. This indicates one of the major shortcomings of the LNN setup described in this chapter, which is capable of handling only up to (4×5)- or (5×4)-dimensional input-output problems. The number of inputs and outputs can be raised by the introduction of a matrix with more rows and columns. The number of outputs will be eventually limited by the number of active laser modes. With the laser used in this chapter we were able to activate more than 100 longitudinal cavity modes. The limit on the number of inputs strongly depends on the quality of the matrix that is used, as well as on the sensitivity of the laser diode to external optical feedback. This limit will have to be determined experimentally.

In addition, the speed of the system described in this chapter is limited. This not only means that a training session takes a lot of time but also (and more importantly) that the rate at which inputs can be processed is limited. Finally, the input vector is controlled electronically rather then optically. Future investigations should therefore focus on using faster and larger matrices and optically addressed modulators. Furthermore, other learning algorithms, e.g. a modified backpropagation algorithm, should be examined.

References

[1]   D. Hammerstrom and S. Rehfuss, "Neurocomputing hardware: present and future," *Art. Intell. Rev.* **7**, 285–300, 1993.

[2]   A. Jennings, P. Horan, and J. Hegarty, "Optical neural network with quantum well devices," *Appl. Opt.* **33**, 1469–1476, 1994.

[3]   A. Hirose and R. Eckmiller, "Coherent optical neural networks that have optical frequency controlled behavior and generalization ability in the frequency domain," *Appl. Opt.* **35**, 836–843, 1996.

[4]   B. Javidi, J. Li, and Q. Tang, "Optical implementation of neural networks for face recognition by the use of nonlinear joint transform correlators," *Appl. Opt.* **34**, 3950–3962, 1995.

[5]   I. Saxena and E. Fiesler, "Adaptive multilayer optical neural network with optical thresholding," *Opt. Eng.* **34**, 2435–2440, 1995.

[6]   S. Juthamulia and F. T. S. Yu, "Overview of hybrid optical neural networks," *Opt. Laser Technol.* **28**, 59–72, 1996.

[7]   F. T. S. Yu, "Optical neural networks: architecture, design and models," in *Progress in Optics*, E. Wolf Ed., (North Holland, Amsterdam, 1993), Vol. 32, pp. 61–144.

[8]   S. B. Colak, J. J. H. B. Schleipen, and C. T. H. Liedenbaum, "Neural network using longitudinal modes of an injection laser with external feedback," *IEEE Trans. Neural Networks* **7**, 1389–1400, 1996.

[9]   J. J. H. B. Schleipen, S. B. Colak, E. C. Mos, and C. T. H. Liedenbaum, "An injection laser neural network," in *Fourth int. conf. on microelectronics for neural networks and fuzzy systems* (IEEE Computer Society Press, Los Alamitos, Calif, 1994), pp. 8–12.

[10] K. Petermann, "Laser diode modulation and noise," in *Advances in Optoelectronics*, T. Okoshi Ed., (Kluwer Academic, Dordrecht, The Netherlands, 1991).

[11] J. Sacher, W. Elsässer, and E. O. Göbel, "Nonlinear dynamics of semiconductor laser emission under variable feedback conditions," *IEEE J. Quantum Electron.* **27**, 373–379, 1991.

[12] A. E. Siegman, *Lasers*, (University Science Books, Mill Valley, Calif., 1986).

[13] G. P. Agrawal and N. K. Dutta, *Long wavelength semiconductor lasers*, (van Nostrand Reinhold, New York, 1986), Chap. 6.

[14] D. E. Rumelhart, G. E. Hinton, and R. J. Williams, "Learning internal representation by error propagation," in *Parallel distributed processing*, D. E Rumelhart and J. L. Mc Clelland Eds., (MIT Press, Cambridge, Mass., 1986), Vol. 1, pp. 318–362.

[15] Y. Maeda, H. Hirano, and Y. Kanata, "A learning rule of neural networks via simultaneous perturbation and its hardware implementation," *Neural Networks* **8**, 251–259, 1995.

[16] J. Alspector, R. B. Allen, V. Hu, and S. Satyanarayana, "Stochastic learning networks and their electronic implementation," in *Neural Information Processing Systems*, D. Z. Anderson Ed., (American Institute of Physics, Denver, Colo., 1988), pp. 9–21.

[17] H. Szu and R. Hartley, "Fast Simulated annealing," *Phys. Lett. A* **122**, 157–162, 1987.

[18] S. Geman and D. Geman, "Stochastic relaxation, Gibbs distribution and Baysian restoration of images," *IEEE Trans. Pattern Anal. and Machine Intell.* **6**, 721–741, 1984.

[19] J. Sun, W. I. Grosky, and H. Hassoun, "A fast algorithm for finding global minima of error functions in layered neural networks," in *Proceedings of the International Joint Conference on Neural Networks* (IEEE Neural Network Council, Ann Arbor, Mich., 1990), Vol. 1, pp. 715–720.

[20] N. Baba, "A new approach for finding the global minimum of error function of neural networks," *Neural Networks* **2**, 367–373, 1989.

[21] P. D. Wasserman, *Neural computing, theory and practice*, (van Nostrand Reinhold, New York, 1989).

[22] T. P. Lee, C. A. Burrus, J. A. Copeland, A. G. Dentai, and D. Marcuse, "Short cavity InGaAsP injection lasers: dependence of mode spectra and single-longitudinal-mode power on cavity length," *IEEE J. Quantum Electron.* **18**, 1101–1113, 1982.

4

Loop-Mirror Laser Neural Network using a Fast Liquid-Crystal Display

In our laser neural network (LNN) all-optical threshold action is obtained by application of controlled optical feedback to a laser diode. In this chapter an extended experimental LNN is presented with as many as 32 neurons and 12 inputs. In the setup we use a fast liquid-crystal display to implement an optical vector-matrix multiplier. The display, that is based on ferroelectric liquid-crystal material, enables us to present 125 training examples to the LNN per second. To maximize the optical feedback efficiency of the setup, a loop-mirror is introduced. We use a δ-rule learning algorithm to train the network to perform a number of functions toward the application area of telecommunication data switching.

4.1   Introduction

Since the resurgence of interest in the field of neural networks in the mid 1980's, many optical implementations have been presented in literature [1]–[3]. This can be explained by the highly parallel nature of neural networks and the ease of implementing highly parallel systems in (free-space) optics. As indicated by Jutamulia and Yu [3], the threshold function of the neurons in these optical neural networks is almost always in the electro-optical domain.

In our laser neural network (LNN) all key neural operations are realized in the optical domain. A liquid-crystal display (LCD) is used to provide a weighted sum of inputs to the network. The LCD is placed in an external-cavity laser diode setup. The threshold function is implemented by use of the sensitivity of a laser diode to external optical feedback. In this way we avoid the electro-optical interface and the inherent speed limitations of electronics that are due to charge buildup. With the LNN we aim to expand the application area of optical neural networks to high speed all-optical systems such as optical telecommunication networks.

In the previous Chapters 2 and 3 we presented a theoretical description of the LNN-concept (See also Ref. [4]) and we demonstrated the principle of operation experimentally (See also Refs. [5] and [6]). The trained functions had only up to four inputs and five outputs.

In this chapter we investigate the possible use of an optical neural network in the physical layer of a high-speed optical telecommunication system. Applications can, for example, be in the routing and switching of data or in the detection of a data packet header pattern, which is an inherently parallel problem.

To experimentally verify whether the LNN can perform functions of sufficient complexity for telecommunication applications, we designed an improved experimental setup to accommodate more inputs and outputs. The larger number of inputs and outputs is realized by use of a smaller-pitch LCD. Ferroelectric liquid-crystal material is used in the LCD to obtain a fast response time.

In addition to the use of a fast LCD, the experimental setup described in this chapter was designed to obtain a high level of optical feedback. For this reason the linear feedback arrangement described in the previous Chapter 3 is replaced with a loop-mirror.

In Section 4.2 the operation principles of our LNN are explained briefly. For a detailed description of the operation principles we refer the reader to Chapter 2 of this thesis and to Ref. [4]. In Section 4.3 we describe the experimental setup of our LNN. The training results of a number of functions related to the application area of telecommunications data switching are presented in Section 4.4. These results are discussed in Section 4.5. Finally, we conclude this chapter in Section 4.6 and discuss future research.

4.2   Principles of Operation

The principles of operation of the optical neural network described in this chapter are introduced. Laser diodes and their longitudinal modes are briefly explained.

4.2.1 Laser Diodes and Optical Feedback

A laser diode consists of an optical gain medium inside a resonator. The gain originates from the stimulated emission of photons at the diode junction. The two cleaved facets of the laser diode chip act as mirrors and form the resonator. When the optical gain compensates for the optical losses, which are caused by the mirrors and the diode material, a light wave can oscillate at wavelengths that correspond to the longitudinal cavity modes of the resonator.

The optical gain of a typical laser diode is a function of wavelength, as shown in Fig. 4.1. The longitudinal mode wavelengths are also shown in the figure. The losses can be considered independent of wavelength, whereas the gain shows a parabolic dependence on wavelength and is a function of the electrical current through the laser diode [7].
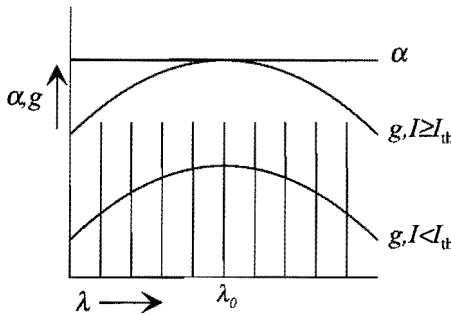
Figure 4.1 Gain, g, and optical losses, α, as a function of wavelength for a typical laser diode. The vertical lines represent wavelength values that match the laser resonator. When the electrical current reaches some threshold value, I_{th}, the gain will compensate the losses for the central wavelength λ_0 and the laser will start to lase. When the current is increased above I_{th}, the gain will clamp to its threshold value. Also, the shape of the gain curve will remain unchanged.

If the current through the laser is sufficiently high, $I = I_{th}$ in Fig. 4.1, the gain will compensate the optical losses for the central wavelength λ_0. As a result the laser will start to oscillate at the corresponding longitudinal cavity mode.

When the current is increased above its threshold value, the gain curve will not shift to higher values, since the gain cannot exceed the optical losses. All excess photon emission will result in an increase in optical output power. If the current is not too high above threshold, the laser exhibits homogenous line broadening [7] which means that the shape of the gain curve will not change.

In simple terms the threshold function, needed for neural operation, is obtained by control of the optical characteristics of the resonator. First, the optical losses of the laser diode resonator are raised by application of an antireflection coating to the exit facet of the laser diode, thus causing the laser to stop lasing. Then external optical feedback is introduced to reduce the optical losses in a controllable manner for each longitudinal cavity mode individually.

The gain- and loss curves for this configuration are plotted in Fig. 4.2, together with the
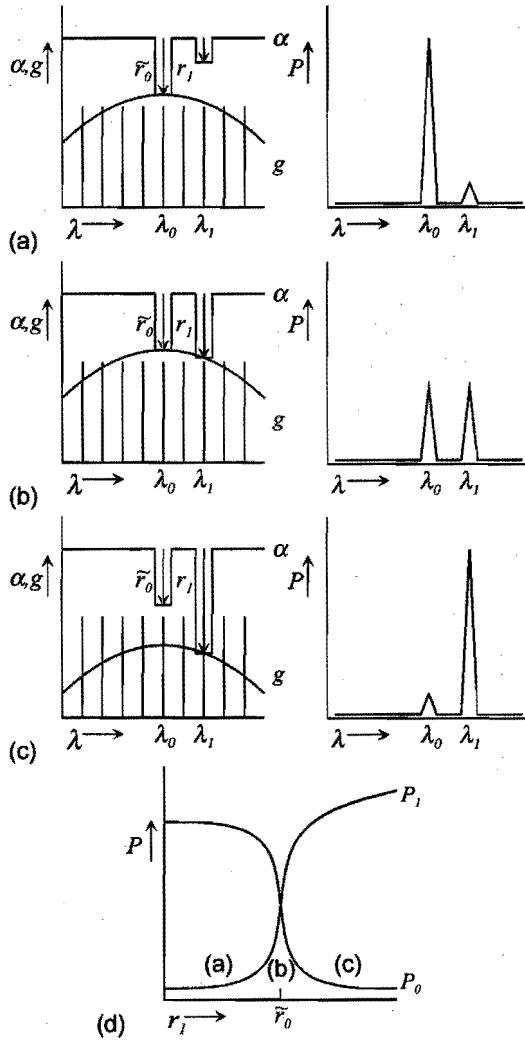
Figure 4.2 Same as Fig. 4.1 for an anti-reflection coated laser diode with optical feedback for two modes at wavelength λ_0 and λ_1. The left-hand part of Figs. (a)–(c) show the optical gain and loss spectra for various amounts of optical feedback for mode 1, r_1. In the right-hand part of Figs. (a)–(c) the resulting spectrum is indicated. The amount of optical feedback for λ_0 is fixed to $\tilde{r}_0$. (a) When r_1 is lower than $\tilde{r}_0$, the gain is clamped to the fixed amount of losses for λ_0 and does not compensate the losses for λ_1. The laser emits at λ_0. (b) When r_1 is increased, the condition for lasing is restored for λ_1 and the laser starts to emit at λ_1. (c) With further increase of r_1, the gain is clamped to the losses for λ_1. As a result the laser will only emit at λ_1. (d) By combining Figs. (a)–(c) we obtain a simple qualitative analysis of the output power at wavelengths λ_0 and λ_1, P_0 and P_1, as a function of r_1. The curves show threshold functions that are used to obtain neural operation in the LNN.

corresponding output spectra of the laser diode. In this example, feedback is applied to the laser diode for wavelengths λ_0 and λ_1 only. The feedback for λ_0 is kept at a constant level $\tilde{r}_0$, which is high enough to make the laser oscillate at λ_0. At first, reducing the losses by increasing r_1 has no effect as depicted in Fig. 4.2(a). The losses for λ_1 will still exceed the gain for λ_1, and the laser will continue to emit at wavelength λ_0. At a certain threshold level of r_1, near $\tilde{r}_0$, the conditions for lasing will be restored for mode λ_1 and the laser will start to emit at λ_1. This corresponds to Fig. 4.2(b). If r_1 is increased further, the gain curve will be clamped to the lower optical losses at λ_1. As a result, the gain for λ_0 will not be sufficient to compensate for the optical losses at λ_0 and the laser will emit light only at λ_1, as shown in Fig. 4.2(c). In Fig. 4.2(d) we have sketched the optical output power for the two modes as a function of the controlled feedback for λ_1, r_1.

4.2.2 Longitudinal Modes as Neurons

We can use the resulting S-shaped, or sigmoid, functions to construct a neural network by making the amount of optical feedback proportional to a weighted sum of inputs for each longitudinal cavity mode, as shown in the block diagram of Fig. 4.3. The inputs of the resulting neural network are in the optical transmission domain. The modes of the laser represent the neurons of a single layer neural network. The optical output power at the longitudinal mode wavelengths $(\lambda_1 \ldots \lambda_n)$ correspond to the neural outputs.
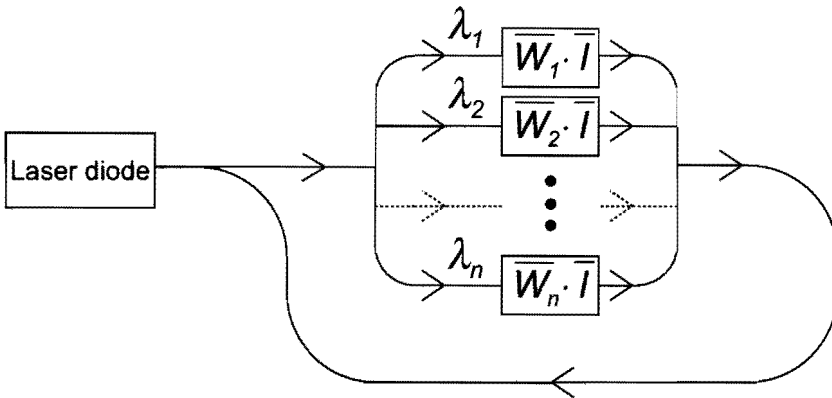
Figure 4.3 Operation principle of our LNN. Optical feedback is applied to a laser diode. For each of the longitudinal cavity modes of the laser resonator $(\lambda_j, j = 1 \ldots n)$, the amount of optical feedback is made proportional to a weighted sum of inputs $(\overline{W_j} \cdot \overline{I})$. For each mode the output power is a sigmoid function of this optical feedback, as shown in Fig. 4.2

Owing to the mode competition that results from gain clamping and homogeneous line broadening, only the mode with the highest amount of optical feedback will be active. For all other modes the optical losses will exceed the optical gain. For our neural network this means that only the neuron with the highest weighted sum of inputs will be active: A so-called *winner-take-all* neural network.

4.3 Experimental Setup

4.3.1 Overview

Our experimental setup, shown schematically in Fig. 4.4, is a straightforward implementation of the block diagram of Fig. 4.3. Figure 4.4 shows an antireflection coated laser diode coupled to a loop-mirror setup. The spectral components of the light are dispersed in the loop by means of grating G1. For each longitudinal cavity mode of the laser diode, the optical throughput of the LCD can be made proportional to a weighted sum of inputs. These attenuated spectral components are combined, and the resulting beam is directed back into the laser by means of some mirrors and polarizing beam splitter PBS. The optical power flow in the loop is managed by use of polarization control. Not shown in the figure are a supervising computer and measurement and control equipment needed to train and test the LNN.
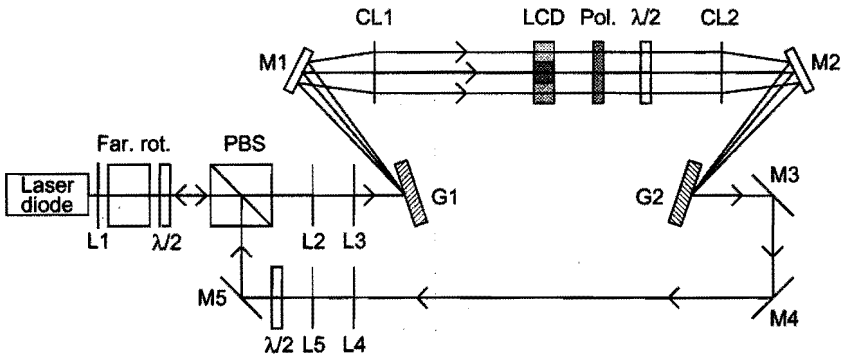
Figure 4.4 Schematic drawing of the LNN setup. Optical feedback is applied to a laser diode via a loop-mirror setup. In this loop-mirror, the optical power is attenuated proportionally to $\overline{W}_j \cdot \overline{I}$ for each mode j of the laser diode by use of a vector-matrix multiplier. This vector-matrix multiplier consists of lenses L2...L5, gratings G1 and G2, cylinder lenses, CL1 and CL2, and the LCD. Optical signal flow is indicated with arrows. The $\lambda/2$ plates, the polarizing beamsplitter PBS and the Faraday rotator Far. Rot. play a role in maintaining the direction of the optical signal flow (See also Fig. 4.6).

4.3.2 Detailed Description of our Setup

Laser Diode

The laser diode that is used in our setup is a standard Uniphase CQL-806 series multiple-quantum-well type laser diode with an emission wavelength of $\sim$675 nm. To enhance the sensitivity of the laser to optical feedback, an antireflection coating with a residual reflectivity of less than 0.1% is applied to its exit facet. Without this coating, the laser diode has a typical threshold current of 26 mA. In our setup the coated laser diode is operated at 70 mA. It is below threshold if the optical feedback path is blocked. The

laser diode is temperature stabilized to prevent thermal drift of the longitudinal mode wavelengths. The light emitted by the laser diode is collimated by lens L1.

Mode Dispersion

Grating G1 (2400 l/mm) is placed in the first focal plane of cylindrical lens CL1 (f = 300 mm). In this way the angular dispersion introduced by the grating is exactly compensated for by the cylindrical lens. In the second focal plane of CL1 line images of the diode facet are formed on the columns of the LCD for all modes of the laser. The distance between these line images, the mode pitch, is made equal to the column pitch of the LCD by adjustment of the angle of grating G1. On the other side of the LCD an identical grating G2 and cylindrical lens CL2 recombine the spectral components after attenuation by the LCD.

Liquid-Crystal Display

The LCD in our setup is used to implement both the inputs and the weights of the neural network. For each column of the LCD, and thus for each longitudinal mode of the laser diode, the total amount of optical throughput is made proportional to a weighted sum of inputs. In Fig. 4.5 this is illustrated schematically for a LNN with an m-element input vector and n output wavelengths.
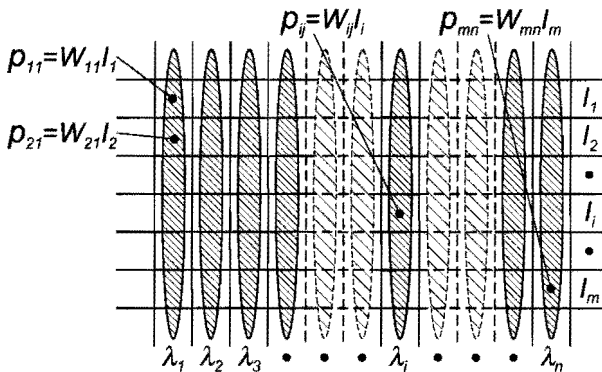
Figure 4.5 Line images on the LCD. Each longitudinal mode of the laser diode (λ_j, $j = 1 \ldots n$), is projected on a different column of the LCD. The transmission value p_{ij} of each pixel on row i and column j is set to $W_{ij} I_i$, with W_{ij} the weight corresponding to neuron wavelength j and input element I_i. The total transmission of a column is proportional to the weighted sum of inputs for the corresponding mode.

The figure shows line images on the transmission matrix that correspond to longitudinal mode wavelengths $\lambda_1 \ldots \lambda_n$ projected on the columns of the display. For each column j each pixel transmission value p_{ij} is set to the product of the neural weight value W_{ij} (corresponding to neuron j and input element i) and the input value I_i. The total amount of optical transmission for each longitudinal cavity mode is the sum of the optical trans-

mission of all the pixels that belong to the corresponding column. Thus this part of the setup implements an optical vector matrix multiplier [8] in which the columns of the LCD correspond to the neurons and the rows of the LCD to the input elements.

The number of illuminated rows, and thus the maximum number of inputs of our LNN, is determined by the height of the line images and by the row pitch of the LCD. The height of the line images depends on the magnification of the beam expanders, L2 + L3 and L4 + L5, and on the beam diameter after the collimator lens L1.

During the learning phase the weights of the network are updated iteratively. To speed up this learning phase the switching speed of the LCD needs to be maximized. This switching speed is primarily limited by the speed of the liquid-crystal material being used. In the LNN setup described in this chapter, the LCD is filled with deformed-helix ferroelectric liquid-crystal (DHFLC) material. This material has a typical switching speed of the order of microseconds. The LCD consists of 32 × 32 transmission elements; each of these pixels can be set to one out of 100 gray levels with a contrast ratio of ~1:30. The pixel pitch of the DHF-LCD is 0.24 mm. A detailed description of this DHF-LCD, intended for video display, can be found in Ref. [9].

A drawback of the fast DHFLC material as compared to the most commonly used twisted nematic liquid-crystal material is its lower transmission value. For the DHFLC material this value is typically 55% of that of twisted nematic liquid-crystal. The optical throughput of the device is further reduced by the thin-film electronic components needed to address each pixel. This results in a total maximum transmittance of the LCD of ~25%.

The setup presented in this chapter contains a loop-mirror instead of the linear extended cavity that was used in the setup described in Chapter 3 (See also Ref. [5]). In this loop-mirror setup the LCD is passed only once and thus the corresponding losses are reduced by a factor of 2.

Loop-Mirror by Polarization Control

The direction of optical power flow in the loop-mirror is controlled by use of polarization manipulation. This is explained by means of Fig. 4.6 in which the polarization state of the light beam is represented by an arrow inside a circle. A horizontal arrow indicates light that is horizontally polarized with respect to the plane of the setup; a vertical arrow denotes vertically polarized light.

The light emitted by the laser diode is vertically polarized. The Faraday rotator rotates the polarization state by 45° in a clockwise direction with respect to a space-fixed reference frame. The $\lambda/2$ plate rotates the polarization state of the laser beam by a controllable angle; this rotation is exactly canceled when the light is sent through the device in the opposite direction. By proper adjustment of the first $\lambda/2$ plate, the laser beam is horizontally polarized when it arrives at the polarizing beam splitter. The polarizing beam splitter transmits the horizontally polarized laser beam, whereas it deflects a vertically polarized beam of light at an angle of 90°. The LCD rotates the polarization state of the incoming beams by an angle that depends on the applied gray level. After the LCD a polarizer is used to transform this rotation of the polarization state into a variable attenuation. The attenuated beam is vertically polarized. The two $\lambda/2$ plates before and after the second grating are added because the efficiency of the grating is higher for horizontally
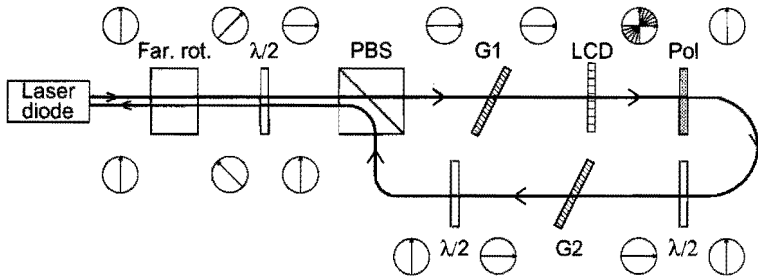
Figure 4.6 Maintaining one way optical power flow through polarization control. Polarization state is indicated with an arrow inside a circle. The initially vertical polarization of the laser beam is converted to a horizontal polarization by the Faraday rotator and the first $\lambda/2$ plate. After passing the PBS the polarization is rotated by the LCD and the $\lambda/2$ plates to a vertical polarization. The resulting beam is directed back into the laser with the initial polarization state by the PBS and the Faraday rotator.

polarized light than it is for vertically polarized light. Finally, the polarizing beam splitter directs the vertically polarized beam back into the laser diode via the first $\lambda/2$ plate and the Faraday rotator. When passed in this direction, the combination of these devices does not alter the polarization state of a passing light beam. The beam thus returns into the laser with the original, vertical polarization.

With the loop-mirror configuration the overall efficiency reaches a level of approximately 9%. With the contrast ratio of the LCD of approximately 1:30 the total percentage of optical feedback can be controlled between 0.3% and 9%.

Training Setup

For the purpose of training and monitoring the LNN a computer can control the inputs and weights of the LNN and read its outputs.

This supervising computer can send images that consist of input vectors and weight matrices to the LCD. Although the switching speed of the DHFLC material is of the order of microseconds, the rate at which images can be put on the display is limited in the setup to ~125 images per second. This limit is caused in part by the LCD driver electronics and in part by the interface between this driver and the computer.

A fast optical spectrum analyzer was built that is capable of measuring spectra at the same rate at which images can be shown on the display. By use of the spectrum analyzer, the computer reads the output state of the LNN. The spectrum analyzer consists of a grating, some lenses, a 256-element CCD array and an 8-bit analog–to–digital interface board. To analyze the power spectrum of the laser diode, light is coupled out of the LNN setup just after the polarizing beam splitter by use of a 30/70 beam splitter. The light is coupled into a single-mode fiber that is connected to the spectrum analyzer.

In the learning experiments, presented in the following section, we used a δ-rule learning algorithm, also known as Widrow Hoff learning [10]. We adapted the algorithm for our LNN in two ways. Because we are mainly interested in training digital functions to our network, that has analog outputs, digital decision levels have to be defined. These levels

correspond to the ON and OFF values of a neuron. Instead of using fixed values for these decision levels, a target extinction ratio Er between these levels is used in the learning algorithm. In this way we do not need to determine the ON and OFF levels for each neuron. As an additional advantage, a noise margin can be trained in a rather straightforward manner by simply training the network with a larger extinction ratio than needed.

```
Initialize:
    Get desired ON-OFF extinction ratio Er,
    Get learning rate η
    Calculate starting matrix W̿₀
Repeat
1:  Show all input patterns I̅ₚ to the network with W̿
    Measure all corresponding output patterns O̅ₚ,meas
2:  Calculate new target output values for each neuron j:
          ON value:  Oⱼ,des-on = Er · maximum of
              Oₚ,ⱼ,meas, all p for which j is losing neuron,
              Oₚ,ₖ,meas, all p for which j is winning neuron, all k≠j
          OFF value: Oⱼ,des-off = (1/Er) · minimum of
              Oₚ,ⱼ,meas, all p for which j is winning neuron,
              Oₚ,ₖ,meas, all p for which j is losing neuron, all k≠j
3:  Calculate error measure, Error=∑ₚ ∑ⱼ |Oₚ,ⱼ,des − Oₚ,ⱼ,meas|
4a:If (Error > 0) then for all inputs, i, and all neurons, j:
          calculate Wᵢ,ⱼ := Wᵢ,ⱼ + η ∑ₚ Iₚ,ᵢ(Oₚ,ⱼ,des − Oₚ,ⱼ,meas)
4b:If (Error = 0) then check solution W̿, N times:
          repeat step 1 and 3, accumulate error measure
Until (Error = 0)
```

Figure 4.7 Basics of our modified δ-rule algorithm. The pattern number is denoted p, j is the neuron number, the input element is denoted with i.

The learning algorithm is presented in Fig. 4.7. It starts by calculating an initial guess for the weight matrix based on the *winner-take-all* inequalities (See Section 3.6.3) of the function to be trained. Then, iteratively, the weight matrix is updated using a delta rule with learning parameter η (in step 4a) until the error measure equals zero. In step 2, the digital decision levels are recalculated for each neuron using the target extinction ratio Er and the measured output values of the neuron in the ON and OFF states. To account for the *winner-take-all* nature of our network, also the measured output values for all other neurons are included in this calculation. When an appropriate weight matrix is found the algorithm stops after this solution has been tested a number of times N to verify the stability of the solution.

4.4 Results

4.4.1 Defining Neurons

Because of imperfections in the experimental setup, not all longitudinal cavity modes of the laser diode can be activated by the applied optical feedback. Before training the LNN, we have to select the longitudinal cavity modes of the laser diode that can be used as neurons. Some criteria are formulated for a usable neuron. With a given number of input elements, a usable neuron should have a high output value when a corresponding weight is set to its maximum value, even if only one of the input elements is active. The neuron should have a low output value when all input elements are set to an inactive state. These criteria ensure that the influence of a single input element is enough to switch the neuron from an inactive to an active state.

In our setup we can test the criteria for each neuron by controlling the gray values of the pixels in the corresponding LCD column. The laser should lase at the longitudinal mode wavelength that corresponds to the neuron when a pixel of the LCD column is set to a transparent state. Such a pixel can be used as an element $W_{ij} I_i$ in the vector-matrix multiplication for neuron j.

The number of pixels that can be used depends not only on the number of illuminated rows as indicated in Section 4.3 but also on the distribution of optical power over the rows. This optical power distribution will equal the Gaussian distribution of the nondispersed laser beam. The distribution remains unchanged because the cylindrical lens CL1 focuses the beam into vertical lines perpendicular to the rows.

In Fig. 4.8 results of measuring this distribution over 19 lines of the display are shown. As can be seen from the figure, some rows have only little optical throughput; hence pixels belonging to these rows are not suitable as $W_{ij} I_i$-elements. These pixels can, however, be used to bring the corresponding mode of the laser closer to threshold when they are set to
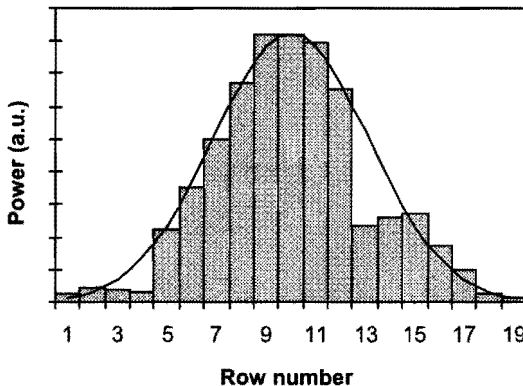
Figure 4.8 Power distribution of the light beam at the LCD in the vertical direction. Bars represent the total optical power after the LCD as measured by switching the respective rows of the display. The curve shows an approximate Gaussian fit to this data. The optical throughput of some rows will not be sufficient for the pixels of these rows to be used as elements $W_{ij} I_i$.

a fixed, transmitting state. As a result, more of the remaining pixels for the neuron will be available as a $W_{ij}I_i$-element, and the number of inputs can be increased.

We used an automated algorithm to select the modes suitable as neurons, the pixels suitable for $W_{ij}I_i$-elements, and the pixels that should be set to a permanent transmitting state. The resulting number of neurons depends on the alignment of the setup and on the target number of inputs. The maximum number of neurons we obtained was 32, each with 5 or more inputs. Whereas with 12 or more inputs, we could still define a few neurons. However, typical values were 25 neurons with 5 or more inputs or 14 neurons with 9 or more inputs.

As an example, a spectrum with 27 neurons, each with 5 or more inputs, is shown in Fig. 4.9. All inputs were set to zero when this spectrum was measured. In the figure the 27 selected modes have a higher output power than the remaining modes. The higher output power is a result of setting the unusable pixels of the columns corresponding to these modes to a transmitting state. Of those modes, the ones with the highest output power in the active state were selected for the training experiments.
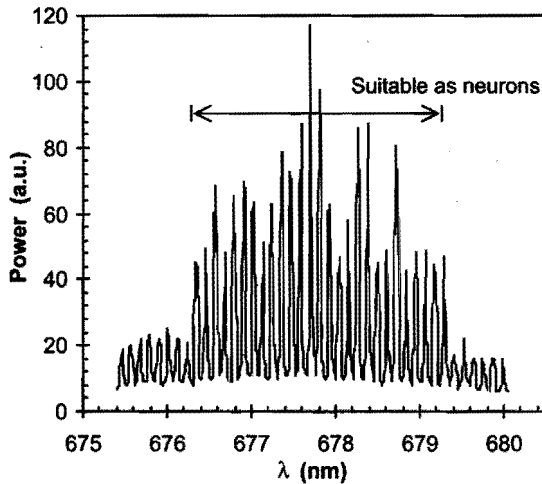
Figure 4.9 Spectrum of the LNN before training. The 27 modes of the laser that can be used as neurons in this example have a higher output power. The corresponding neurons are still in the OFF state.

4.4.2   Training Experiments

With the learning algorithm described in Section 4.3, we trained the network to perform some digital functions. The particular digital functions were chosen with the application of (telecommunication) data switching in mind.

With the 1:8 data switch function the goal is to direct one data bit to one out of eight output channels. An additional (dump) output channel is added to realize this with our *winner-take-all* neural network. A block diagram of the function is shown in Fig. 4.10. If the data input port is high, the dump output should be high, regardless of the state of

the 3-bit input address. All other output channels should be low. If the data input is low, the output channel that corresponds to the address information should be the only active one. In this way the data bit, or rather its inverse value, is routed to the output channel selected by the address data. The resulting truth table is listed in Table 4.1. The first bit of the input vector is a bias input; it is always set to a logical 1. The second bit is the data bit, the last three bits represent the address. Table 4.1 can be used as a training set for the learning algorithm.
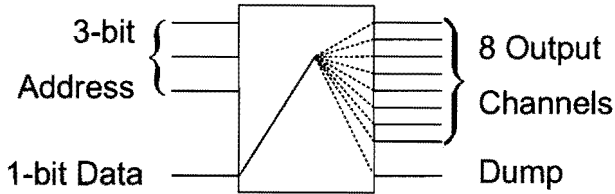
Figure 4.10 Block diagram of a 1:8 data switch. The 3-bit address selects the destination of the 1-bit data. Either the dump channel or the channel represented by the 3-bit address is active, depending on the state of the input data bit.

Aiming at a guaranteed minimum ON–OFF ratio (See Section 4.3) of 4, we set the ON–OFF ratio to be trained to 5. The evaluation of the error measure as a function of iteration count is presented in Fig 4.11. The figure shows the error measure of the learning algorithm as a function of iteration count for five typical training-sessions of the 1:8 data switch example. Each training-session is a completion of the algorithm of Fig. 4.7.

In Fig. 4.12 a resulting typical weight matrix for the 1:8 data switch function is presented. The weights in the top row of this figure correspond to the bias weights, needed to adjust the neural threshold. The weights in the second row correspond to the data bit input. The remaining rows are the weights that correspond to the three input bits containing the address information.

Table 4.1 Truth table of 1:8 data switch function. The first bit of the input vector is the bias input, the second is the data bit, the last three represent the address.

Input Vector	Output Vector	Input Vector	Output Vector
10000	100000000	11000	000000001
10001	010000000	11001	000000001
10010	001000000	11010	000000001
10011	000100000	11011	000000001
10100	000010000	11100	000000001
10101	000001000	11101	000000001
10110	000000100	11110	000000001
10111	000000010	11111	000000001
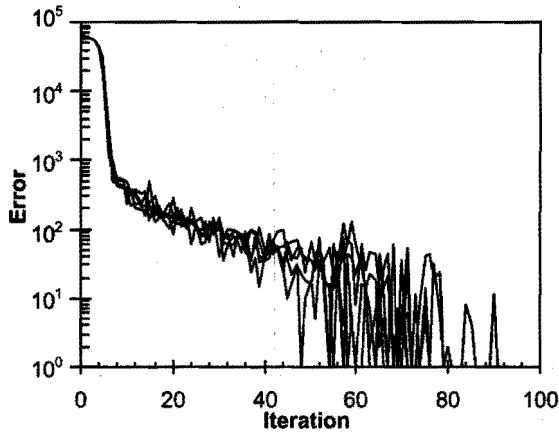
Figure 4.11 Error measure as a function of iteration count for five training sessions of the 1:8 data switch example.
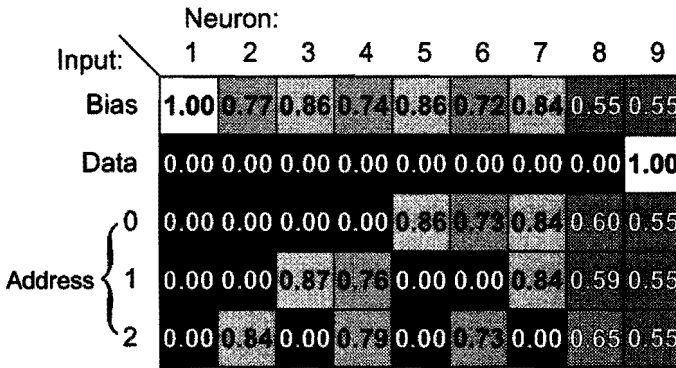
Figure 4.12 Typical weight matrix after training the 1:8 data switch, as it would appear on the LCD. Black areas denote nontransmitting pixels, white areas correspond to fully transmitting pixels. The weight values are indicated in the figure.

With this weight matrix the LNN correctly responds to the input patterns presented to it. For each input pattern the LNN responds by emitting light at a single wavelength. In Fig. 4.13 the spectral response of the LNN is shown for the input vectors 10000 (top graph) to 11111 (bottom graph).

By use of training sets similar to that of the 1:8 data switch, the LNN was also trained to perform a 1:8 decoder (without data), a 1:16 data switch and a 1:16 decoder without data. All functions were trained 100 times. In Table 4.2 some statistics of the learning behavior of the LNN are presented. In Table 4.2 the average number of iterations and the standard deviation on this average are listed.

In the learning trials presented above, the modes that had the highest output power were
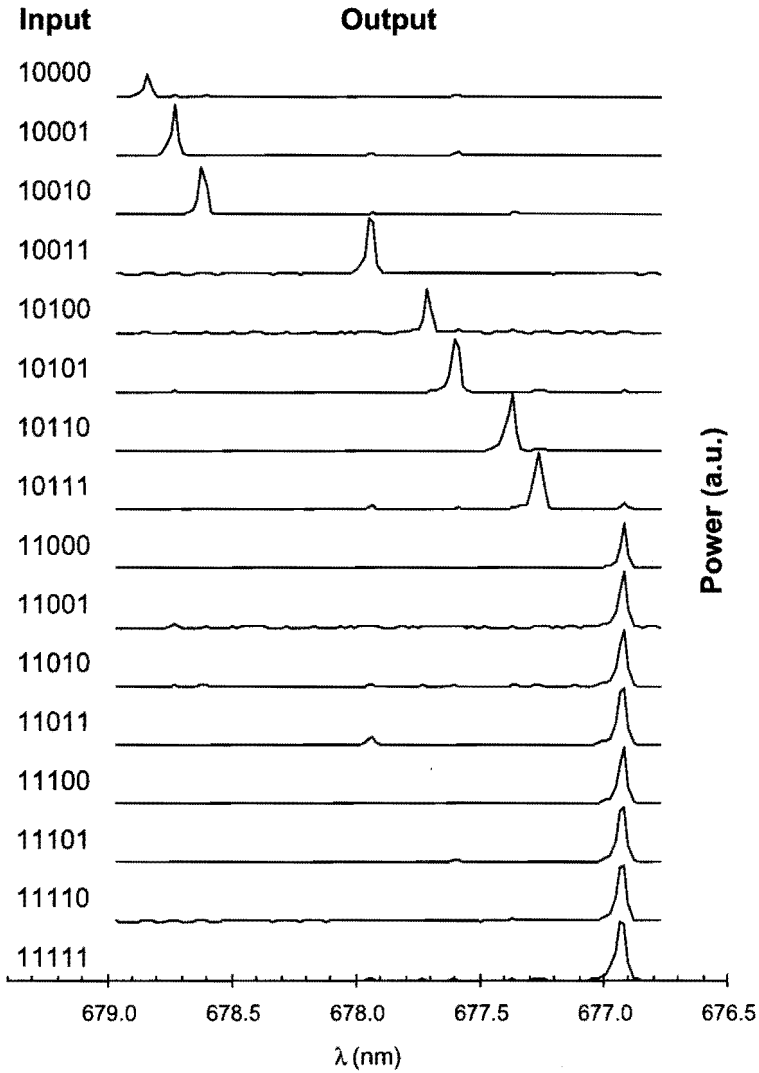
Figure 4.13 Typical output spectra of a trained LNN. The figure shows the measured spectra for all possible input patterns 10000–11111 of the 1:8 data decoder problem (Compare Table 4.1).

Table 4.2 Statistics of training. The average number of iteration and the standard deviation on this average are tabulated for a number of trained problems using data from 100 training trials.

Problem	Average Iterations	Standard Deviation
1:8 Decoder	69	16
1:8 Data Switch	77	12
1:16 Decoder	105	27
1:16 Data Switch	85	50

selected as neurons. As a result, holes appear in the output spectra of Fig. 4.13. In Fig. 4.14 the output spectra of the 1:16 data switch function are presented where adjacent modes were selected instead of those with the highest output power. In the figure the 32 spectra corresponding to input patterns 100000–111111 are plotted superimposed.
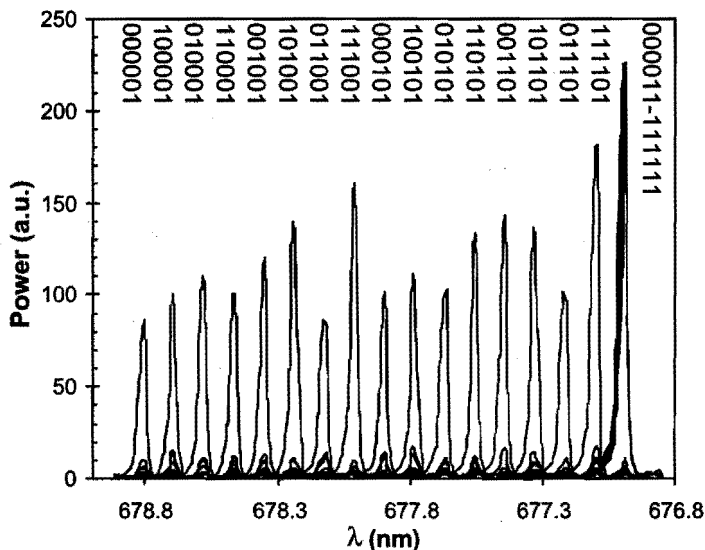
Figure 4.14 Spectra of the LNN after training the 1:16 data switch problem. The measured 32 spectra are plotted superimposed. For each input pattern, the laser emits at a single wavelength. Input vectors are indicated above the corresponding output wavelength.

After training, we subjected all solutions to a test by providing 10000 example input vectors to the trained network. The results of these tests are listed in Table 4.3. The fraction of these tests for which the neural network reproduced the trained function with the desired ON-OFF ratio of 4 is listed in the second column of Table 4.3 (OK). For all trained functions this fraction was greater than 99%. With a digital decision level set halfway between the ON and OFF decision level, the bit error rate (BER) of the trained

Table 4.3 Test results of trained problems. The percentage of test input vectors for which the neural network reproduced the trained output vector within the specified ON-OFF ratio of 4, OK, and the bit error rate during these test BER are listed for 10,000 tests.

Problem	OK (%)	BER
1:8 Decoder	99.96	$< 10^{-5}$
1:8 Data Switch	99.96	$< 10^{-5}$
1:16 Decoder	99.52	9×10^{-5}
1:16 Data Switch	99.57	$< 10^{-5}$

network was measured. Some bit errors occurred during testing of the 1:16 decoder. For the other functions no bit error was observed, resulting in a bit error rate of less than 10^{-5}.

We can obtain additional information on the reliability of the network by making a spectral eye pattern. In this spectral equivalent of a normal eye pattern all measured spectra are plotted superimposed to estimate the area between the ON and OFF value of all neurons. In Fig. 4.15 the spectral eye pattern is presented for the weight matrix solution of Fig. 4.12. A white area, or eye, between the high peaks and the low peaks is clearly visible for all neural wavelengths.
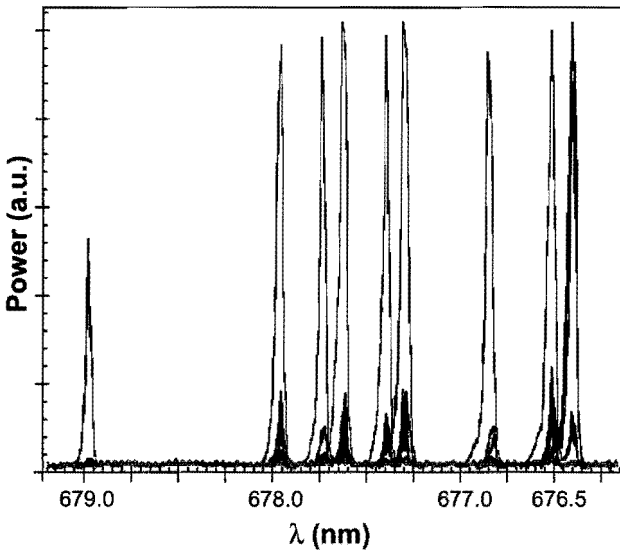
Figure 4.15 Spectral eye pattern of the 1:8 data switch. The figure is obtained by plotting 1600 measured output spectra of the LNN superimposed. A white area is clearly visible between the curves and indicates an open eye.

4.4.3 Varying the Extinction Ratio Er

We trained the 1:8 data switch function with a number of values for the target extinction ratio Er (See the algorithm presented in Fig. 4.7). Aiming at a minimum extinction ratio

of 4, we trained the network with Er = 4, 5, 6 and 7. After training we tested the behaviour of the LNN by showing 1000 input vectors to it. We repeated this for 10 learning trials for each value of Er. Since noise is obviously present in our setup, the fraction of these tests for which the measured extinction ratio was below 4 can be used as an indication of the noise margin. The higher this fraction, the smaller the noise margin. With Er set to 4, this fraction was 4.5%, for Er = 5 it was 1.0%, for Er = 6 about 0.3%, and with Er set to 7 it was below 0.1%.

4.4.4 Unexpected Neural Response

The response of the laser to a changing amount of optical feedback is usually a sigmoid function, as presented in Section 4.2 [See Fig. 4.2(d)]. In a significant number of measurements, however, we observed neural response curves such as presented in Fig. 4.16. A dip is visible in the power of the lasing mode P_1 in the part of the figure corresponding to region (a) of Fig. 4.2(d). The dip is accompanied by an increase in the power of the other mode.
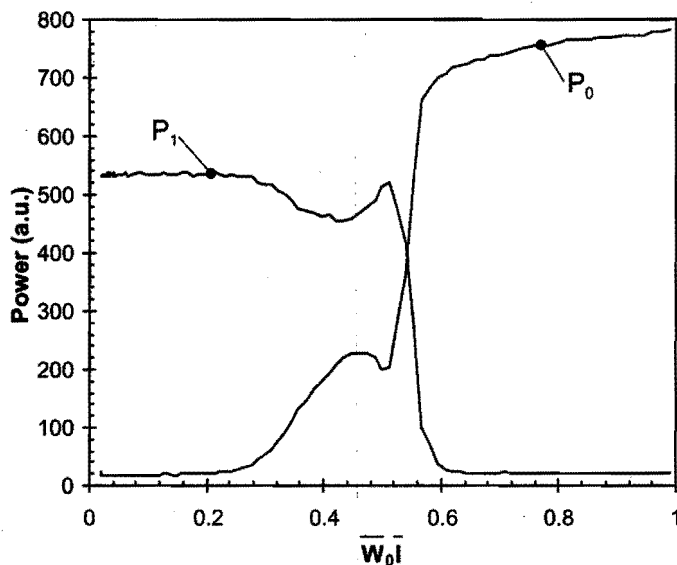
Figure 4.16 Power of two neurons as a function of weighted sum of inputs for one of the neurons. The weighted sum of inputs for neuron 1 is kept constant during the measurements; that of neuron 0 is varied. A bump occurs in the curve corresponding to the neuron with the shorter wavelength P_0. At the same point a dip in the power curve P_1 of the other mode can be observed.

In other measurements of the neural response function, we also observed this phenomenon in region (c) of Fig. 4.2(d). When this phenomenon occurred, the dip was always in the power curve of the mode with the longest wavelength while the increase was always in the power curve of the mode with the shortest wavelength.

The origin of the anomalous shape of the neural response function is not yet fully understood. The fact that both modes are active when the phenomenon occurs suggests a nonhomogenous line broadening and thus at the occurence of some kind of gain saturation. The wavelength asymmetry in the effect suggests an asymmetric nonlinear gain as described by Manning et al. [11],[12]. In Chapter 7, another possible explanation of this cross-modulation effect is indicated.

4.5 Discussion

4.5.1 Network Functionality

Although the functions that the network was trained to perform did not use all available inputs and neurons, they clearly demonstrate the capabilities of the LNN concept.

The demonstrated functions can be used in a router in a packet switched optical telecommunication network. In this type of telecommunication network, data is sent in packets. Each packet has a header that begins with a bit sequence, called the header detect sequence, that marks the start of the packet. The header also contains a bit sequence with information on the destination of the data in the packet. A router in such a network should be able to recognize the header detect sequence, decode the destination information, and route the data to the desired destination.

In Fig. 4.17 a block diagram of an all-optical router concept is presented. In this concept an optical delay line converts the serial incoming data to a parallel format. This parallel data represents a time window of the optical data stream. The header detector triggers the memory to store the destination address when a header is detected in this data stream. After passing the delay line, the serial data is sent to the 1:N data switch. This switch, finally, routes the data to the destination that was stored in the memory.
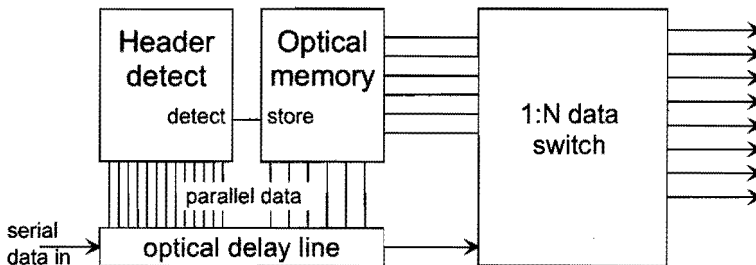
Figure 4.17 Block diagram of an all-optical router concept using the LNN. Serial data is converted to parallel data by means of an optical delay line. A header detector, possibly an LNN, detects the header detect sequence. When a header is detected, the optical memory stores the destination address. The data can then be routed by a 1:N data switch, as presented in this chapter.

A part of the routing task was performed by the LNN after it was trained with the 1:8 and the 1:16 data switch functions. The LNN decoded a destination address and, depending on this address, redirected one data bit to a destination wavelength. Another part of the routing task, the detection of the header detect sequence, is actually a pattern recognition

task. Because of their inherently parallel nature, neural networks are good at performing such tasks. Therefore we believe that our LNN can also be trained to detect the header detect sequence.

4.5.2   Network Error Performance

The tests performed after each learning trial (See Table 4.3) show a good performance of the trained network. For all trained functions the fraction of tests with an ON-OFF ratio lower than the desired value was below 1%. In most of these cases the value of the ON-OFF ratio was only slightly smaller and can be ascribed to noise. In the spectral eye pattern of Fig. 4.15 no closing of the eye at any wavelength is visible.

The observed bit errors all occurred in four training trial examples of the 1:16 decoder function. The fact that these training trial examples were run closely after one another might indicate a temporal instability in the experimental setup that is due to, for example, mechanical vibrations.

4.6   Conclusions and Further Study

4.6.1   Network Function

We demonstrated that the LNN can be trained to perform some data switching functions by use of a simple δ-rule algorithm, adapted for our digital *winner-take-all* network. The demonstrated functions had as many as 17 outputs and 5 digital inputs. A data bit could be routed to a selected output wavelength that corresponds to a destination address. Both the data bit and the address were presented to the neural network in the optical transmission domain. The results indicate the functional usefulness of our neural network concept in the area of all-optical data switching for optical telecommunication networks.

4.6.2   Learning Algorithm

The modified δ-rule learning algorithm performs well compared to the stochastic learning algorithm used in previous experiments (See Chapter 3). Less iterations are required although the complexity of the trained problems in terms of number of inputs and outputs is increased. The introduction of the extinction ratio Er in the learning algorithm enables us to control the noise margin of the LNN.

4.6.3   Network Size

The neural network presented in this study has 32 neurons and up to 12 inputs. Based on our experiments, we can estimate the ultimate network size of an optimized LNN setup.

The number of neurons in the experiments described in this chapter is limited by the number of columns of our LCD weight matrix. A dedicated LCD can have as many columns as desired. For a setup that uses such an LCD the total number of longitudinal laser modes will determine the number of neurons.

The laser diode used in the experiments described in this thesis, has approximately 100–150 modes. This number is obtained by comparison of the gain bandwidth of the laser, typically 10–15 nm wide, with the spectral mode spacing, which is ~0.1 nm. An even higher number of neurons is possible when the longitudinal mode spacing of the laser diode is reduced by use of a longer laser diode cavity.

A pixel of the LCD can be used as an input according to the definition in Section 4.4.1, if the amount of optical feedback through the pixel is sufficient to activate the corresponding longitudinal cavity mode of the laser diode. Hence the number of inputs per neuron depends on the minimum optical feedback level to activate the cavity mode, the total optical feedback, and the distribution of optical power over the rows of the LCD.

The total amount of optical feedback in our setup is ~9% (See Section 4.4.1). Considering that approximately ten inputs could be defined, we can assume that the ten rows of the LCD with the highest optical throughput are the ones that can be used as inputs. Using Fig. 4.8 to estimate the minimum throughput value of these rows, we obtain a minimum feedback level of ~0.3%.

To increase the number of inputs, the optical power can be distributed more evenly over the rows of the transmission matrix. A more even distribution can be realized by use of a variable pixel pitch in the input direction of the LCD. For a variable pixel pitch the number of inputs can be made equal to the total amount of feedback divided by the minimum feedback level. With the feedback efficiency of the setup described in this chapter this would result in ~27 inputs. If the feedback efficiency can be further enhanced, the number of inputs will increase accordingly.

4.6.4   Future Study

For application of the LNN in optical telecommunication networks the speed of operation, estimated to reach the gigahertz region [4], needs to be verified in future experiments.

For this application the input vector needs to be optically addressed. Hence it is necessary to convert incoming optical (power) data to optical transmission information by means of some opto-optical modulator. Examples of experimental opto-optical modulators can be found in Refs. [13] and [14].

Although bit error rates as low as 10^{-5} have been measured, further improvements are required, since telecommunication applications typically require a much lower bit error rate.

Acknowledgments

References

[1]   N. H. Farhat, D. Psaltis, A. Prata, and E. Peak, "Optical implementation of the Hopfield model," *Appl. Opt.* **24**, 1469–1475, 1985.

[2] H. J. Caulfield, J. Kinser, and S. K. Rogers, "Optical neural networks," *Proc. IEEE* **77**, 1573–1583, 1989.

[3] S. Jutamulia and F. T. S. Yu, "Overview of hybrid optical neural networks," *Opt. Laser Technol.* **28**, 59–72, 1996.

[4] S. B. Colak, J. J. H. B. Schleipen, and C. T. H. Liedenbaum, "Neural network using longitudinal modes of an injection laser with external feedback," *IEEE Trans. Neural Networks* **7**, 1389–1400, 1996.

[5] E. C. Mos, J. J. H. B. Schleipen, and H. de Waardt, "Optical mode neural network by use of the nonlinear response of a laser diode to external optical feedback," *Appl. Opt.* **36**, 6654–6663, 1997.

[6] J. J. H. B. Schleipen, S. B. Colak, E. C. Mos, and C. T. H. Liedenbaum, "An injection laser neural network," in *Fourth int. conf. on microelectronics for neural networks and fuzzy systems*, (IEEE Computer Society Press, Los Alamitos, CA, 1994), pp. 8–12.

[7] K. Petermann, "Laser diode modulation and noise," in *Advances in Optoelectronics* T. Okoshi Ed., (Kluwer Academic, Dordrecht, The Netherlands, 1991).

[8] J. W. Goodman, A. R. Dias, and L. M. Woody, "Fully parallel, high-speed incoherent optical method for performing discrete Fourier transforms," *Opt. Lett.* **2**, 1–3, 1978.

[9] A. G. H. Verhulst, G. Cnossen, J. Fünfschilling, and M. Schadt, "A wide-viewing-angle video display based on the deformed-helix ferroelectric liquid-crystal effect and a diode active matrix," *Journal of the SID* **3/3**, 133–138, 1995.

[10] B. Widrow, and M. E. Hoff, "Adaptive switching circuit," in *Western Electronic Show and Convention, Convention Record, Part 4*, (Institute of Radio Engineers, 1960), pp. 96–104, Reprinted in *Neurocomputing*, J. Anderson, and E. Rosenfeld Eds., (MIT Press, Cambridge, MA., 1989), pp. 126–134.

[11] J. Manning, R. Olshansky, D. M. Fye, and W. Powazinik, "Strong influence of non-linear gain on spectral and dynamic characteristics of InGaAsP lasers," *Electron. Lett.* **21**, 496–497, 1985.

[12] J. Manning, R. Olshansky, and W. Powazinik, "Measurement of nonlinear gain spectra in 1.3 μm InGaAsP," in *Proceedings of the 9 th IEEE International Laser Conference*, (IEEE, 1984), pp. 150.

[13] G. W. Yoffe, J. Brübach, F. Karouta, and J. H. Wolter, "Single-wavelength all-optical phase modulation in GaAs/AlAs hetero-*nipi* waveguide: Towards an optical transistor," *Appl. Phys Lett.* **63**, 2318–2320, 1993.

[14] H. S. Loka, S. D. Benjamin, and P. W. E. Smith, "Optical characterization of low-temperature-grown GaAs for ultrafast all-optical switching devices," *IEEE J. Quantum Electron.* **34**, 1426–1437, 1998.

5

Longitudinal Mode Switching Dynamics in a Dual External-Cavity Laser Diode

We study the potential speed of an optical neural network that uses the longitudinal cavity modes of an external-cavity laser diode as neurons. For this purpose we use a laser diode that is coupled to two external cavities, each corresponding to one longitudinal cavity mode. The process of longitudinal mode-switching is investigated for the case of intra-cavity optical modulation. In this experiment, the feedback for the mode in one cavity is modulated, the length of the other cavity can be controlled. Three limitations are imposed on the switching speed. A number of external-cavity round-trips are needed to switch from one mode to the other. It is observed that, depending on the amount of optical feed-back in both cavities, between 7 and 21 round-trips are needed. When the experimental results for varying cavity length are extrapolated to zero cavity length, a residual delay of a few nanoseconds remains. It is believed that this delay is due to a change in carrier density, needed to switch from one mode to another. Modified rate-equations are used to model our experiments. The results of numerical simulations are in good agreement with the experimental results and predict the residual delay. The model also predicts a turn-on delay that is related to relaxation oscillations and imposes a third limitation on the operation speed of our optical neural network. Implications of our findings on the potential operation speed of the optical neural network are discussed and suggestions are made for optimization.

5.1   Introduction

external-cavity laser diodes have been the subject of many studies. A few examples of applications are narrow-linewidth tunable sources [1], remote sensing [2], blue light generation by intra cavity frequency doubling [3] and intra-cavity spectroscopy [4]. In the laser neural network (LNN) described in this thesis we employ an external-cavity laser diode to build an all-optical neural network [5]–[8].

To build a neural network we need a set of simple computing elements, neurons, that receive a weighted sum of inputs [9]. The computing elements should have an active output if the weighted sum is higher than a certain threshold level. If the neurons are combined to form a network, the resulting device can be used to compute an output vector from a vector of input elements. The computation in such a network is done in parallel and is distributed over the neurons. The function implemented by the neural network is stored in the weights that connect the neurons with other neurons and the inputs.

In the LNN each longitudinal cavity mode of the laser diode represents a neuron, and the output vector corresponds to the power spectrum of the laser diode. A liquid-crystal display (LCD), consisting of a matrix of transmission elements, is placed in an external-cavity setup and enables us to control the amount of optical feedback for each longitudinal cavity mode individually. We use the LCD to implement the inputs and weights of the network by setting the transmission values of the pixels according to a sum of weighted neural inputs. In this way the optical feedback is made proportional to the weighted sum of inputs for each longitudinal cavity mode of the laser individually. A longitudinal cavity mode starts lasing when the optical feedback exceeds a certain level. This means that the corresponding neuron becomes active when the weighted sum of inputs is above a certain threshold level. Thus a neural network is formed with inputs in the optical transmission domain and outputs in the wavelength domain.

Applications of the LNN are envisioned in the area of pattern recognition and routing of data in high speed (> 1 Gbit/s) optical telecommunication systems. For this type of applications it is desirable that the output state of the LNN changes within a nanosecond after the input vector is applied. Changing between output states in the LNN implies switching between longitudinal cavity modes of the laser diode. In this chapter we investigate the mode switching transient behavior of an external-cavity laser diode subjected to a change in optical feedback.

To our knowledge the transient response of a laser diode subjected to a change in external optical feedback has not yet been investigated. Reports have been made on directly modulated external-cavity laser diodes [10]–[13]. Olsson and Tsang [10] reported a transient time of a few external-cavity round-trips when an external-cavity laser diode was driven with a step current excitation. A similar experiment was carried out by Kanjamala and Levi [11] for a laser diode that is coupled to a fiber grating external cavity.

The LNN setup described in previous Chapters 3 and 4 (See also Refs. [5]–[8]) is unsuited to measure the transient response of the laser diode. The switching time of the LCD is in the order of milliseconds, while the round-trip time of our current LNN is in the order of microseconds. A dual external-cavity setup with a fast intra-cavity electro-optical modulator is built to emulate our LNN. The modulator is used to emulate the change in optical feedback for one longitudinal mode when the input vector is changed from one

state to another. With this setup we measure the mode switching transient behavior.

In Section 5.2 we present our experimental setup. In Section 5.3 we describe the rate-equation model that is used to compare the measured results with laser theory and to estimate the speed of an LNN that is aimed at telecommunication applications. In Section 5.4 we present experimental results as well as results from numerical simulations that use the rate-equation model. We discuss the results and estimate the speed of a feasible, integrated optics device based on extrapolated experimental data and simulated results in Section 5.5. We conclude the paper in Section 5.6 where we make recommendations for future work on the LNN.

5.2   Experiment

The longitudinal mode switching behavior of an external-cavity laser diode is examined for variable feedback conditions and a range of external-cavity lengths. The experimental setup is shown in Fig. 5.1. It consists of a 670 nm multiple-quantum-well laser diode (Uniphase CQL806) coupled to two external cavities A and B by means of a polarizing beam splitter PBS. An antireflection coating with a residual reflectivity of approximately 5×10^{-4} is deposited on the front facet of the laser diode. The threshold current before the laser was antireflection coated measured $\sim$25 mA. With the applied coating the threshold current of the laser diode without optical feedback was higher than 70 mA, the driving current in our experiments. The laser diode is temperature stabilized to prevent thermal drift of the internal longitudinal mode wavelengths.
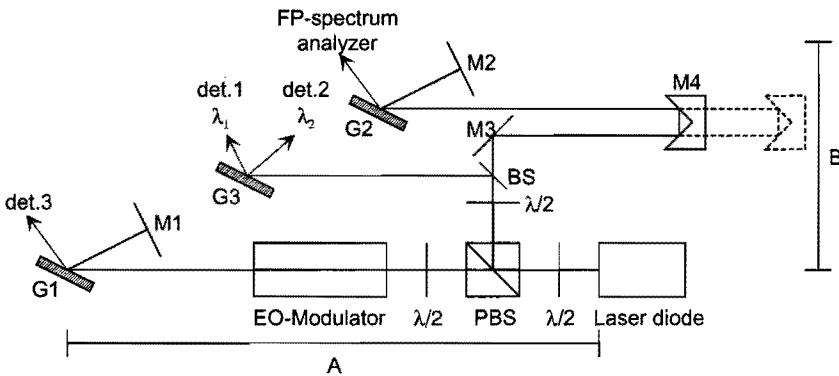
Figure 5.1 Schematic drawing of the experimental setup. A laser diode is coupled to two wavelength selective cavities A and B via a polarizing beam splitter PBS. With mirrors M1 and M2 the cavities are tuned to $\lambda 1$ and $\lambda 2$. The time varying optical output power at these two wavelengths is monitored via grating G3 with detectors (det. 1 and 2). The feedback for cavity A is modulated with an electro-optical modulator. The length of cavity B can be controlled by moving mirror M4. $\lambda/2$-plates are inserted to control the power flow. The zeroth order of gratings G1 and G2 are used to monitor the temporal behavior of the electro-optical modulator (det. 3) and the spectral behavior of the laser diode.

To obtain wavelength selective feedback, both external cavities are built according to the Littman configuration [14] that is formed by diffraction gratings G1 and G2 and mirrors M1 and M2. The wavelength selectivity of the two external cavities is approximately 10^{-2} nm. By rotating a mirror the corresponding cavity A or B can be tuned to an internal longitudinal cavity mode wavelength of the laser diode. In the rest of this text we will refer to these modes as mode A and B. The internal-cavity modes are spaced at 0.1 nm. A $\lambda/2$-plate is placed between the laser diode and the PBS to enable us to direct a controllable portion of light to the two cavities, thereby controlling the amount of optical feedback for both cavities. By measuring the optical power at the end mirrors, we estimate the maximum feedback efficiency for both cavities to be approximately 10%. By use of a ray-tracing program we estimated the overall power efficiency of the external-cavity setup to be 20%. The resulting maximum feedback levels for modes A and B are approximately 2%.

An amplitude modulator, placed in cavity A, switches the feedback efficiency of this cavity between two levels. The modulator (Coherent, model 20/317) has rise and fall times of approximately 8 nanoseconds. It is driven with a 50% duty-cycle square wave of ∼3 MHz. The length of cavity A is 1.05 m corresponding to a round-trip time of approximately 7 ns.

The length of cavity B can be controlled by changing the position of the retroreflecting mirror M4. In this way we are able to set the round-trip time of this cavity to any value between approximately 2 and 16 nanoseconds. The $\lambda/2$-plate in cavity B is inserted to control the polarization state of the laser beam in this part of the setup for optimal reflection at grating G2.

We measured the temporal response of the laser diode with a number of high speed detectors, det. 1–3 (Opto Electronics Inc., PD10). To measure the optical power of the two longitudinal cavity modes, a part of the intra-cavity optical power is coupled out by a beam splitter and dispersed by a third grating G3. The resulting, spectrally resolved, beams are imaged onto detectors 1 and 2. For timing calibration purposes the zeroth order reflection of grating G1 is used to monitor the optical response of the electro-optical modulator with detector 3. The electrical signals from detectors 1 and 2 are amplified and subsequently recorded with a sampling oscilloscope (Tektronix, 11802 with SD-26 sampling heads). The amplifiers (HP-8447) limit the detection bandwidth to a frequency range of 0.1–1300 MHz.

We monitored the internal mode power spectrum of the laser diode on a nm scale with an optical multichannel analyzer (EG&G, OMA 1460). The external-cavity mode power spectrum is measured with a 1.5 GHz free spectral range Fabry-Perot spectrum analyzer (Tropel model 240), with a resolution of approximately 10 Mhz which corresponds to ∼10^{-5} nm.

5.3 Theory

In this section we derive a theoretical description of our external-cavity laser diode to predict the time dependent output power of the diode laser at the two wavelengths selected by the external cavities. The behavior of the laser diode will be dominated by the two

external cavities because the reflectivity of the external mirrors is much higher than the residual reflectivity of the antireflection coated front facet.

A theoretical description of the dynamic behavior of a laser diode subjected to weak external optical feedback has been introduced by Lang and Kobayashi [15]. Although the feedback in our setup can hardly be referred to as weak, the same method with a slight modification can be used to describe our experiments. In an analysis for weak feedback, a one-dimensional model of a laser with external optical feedback as presented in Fig. 5.2 is used. In the figure R_1 and R_2 denote the power reflectivity of the back and front facets of the laser diode. An external reflector with power reflection R_{ext} is placed at a distance L_{ext}. Since R_{ext} is assumed to be weak in the original model, multiple reflections in the external cavity can be neglected. In our case the reflectivity of the coated front facet of the laser diode R_2 is small, which means that this is also a valid assumption for our experiment.
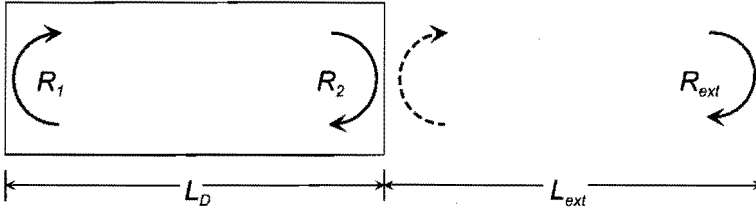
Figure 5.2 One-dimensional model for an external-cavity laser diode. R_1 is the un-coated back facet reflectivity. R_2 is the reflectivity of the antireflection coated front facet and is approximately 5×10^{-4}. R_{ext} represents the reflectivity of an external mirror at a distance L_{ext} away from the laser diode. Multiple reflections can be ignored because of the antireflection coating.

With this assumption a set of rate-equations [16],[17] can be formulated for the electro-magnetic field of the compound -cavity modes inside the external-cavity laser diode. For this purpose, an effective facet (amplitude) reflectivity $r_{eff,m}$ can be introduced for each compound-cavity mode, to replace the reflectivity of the front facet in the expression for the distributed mirror losses. For a compound-cavity mode m we find:

$$r_{eff,m} = \sqrt{R_2} + \sqrt{R_{ext,m}} \, (1 - R_2) \exp\left(-i\omega_m \tau_m\right) \tag{5.1}$$

In this equation $\exp\left(-i\omega_m \tau_m\right)$ represents the phase delay caused by the external-cavity round-trip time τ_m of the reflected electromagnetic field of a compound-cavity mode m with frequency ω_m, and $R_{ext,m}$ is the external reflectivity for mode m. The real part of Eq. 5.1 is:

$$\left|r_{eff,m}\right| = \sqrt{R_2}\left(1 + \kappa_m \cos(\omega_m \tau_m)\right) \tag{5.2}$$

with κ_m the coupling coefficient for mode m according to:

$$\kappa_m = \sqrt{\frac{R_{ext,m}}{R_2}} \, (1 - R_2) \tag{5.3}$$

Using Eq. 5.2 in the rate-equation for the modal electromagnetic field [16],[17] we find
for the photon density $S_m(t)$ of compound-cavity mode m:

$$\dot{S}_m(t) = (G - \gamma_o) S_m(t) + R_{sp} +$$
$$\Delta\gamma_m \sqrt{S_m(t)S_m(t - \tau_m)} \cos(\phi_m(t) - \phi_m(t - \tau_m)) \qquad (5.4)$$

where G is the modal gain and R_{sp} the spontaneous emission as defined in Table 5.1 and
a dot denotes time derivative. In Eq. 5.4 $\phi_m(t)$ is the phase of the modal optical field. The
optical losses γ_0 of the diode laser without feedback are given by:

$$\gamma_0 = v_g \left(\alpha_{int} + \frac{1}{2L_D} \ln\left(\frac{1}{R_1 R_2}\right) \right) \qquad (5.5)$$

with α_{int} the internal material losses, v_g the speed of light inside the laser diode and L_D
the length of the laser diode chip.

Lang and Kobayashi used an approximate solution for the external mirror induced
change in optical losses $\Delta\gamma_m$, based on the assumption that the external reflection adds a
small disturbance to the front facet reflectivity R_2. In our case the external mirror dom-
inates the behavior of the laser diode and thus the influence of this mirror on the optical
losses needs to be included without approximation. The change in optical losses caused
by the external reflection for mode m is:

$$\Delta\gamma_m = \frac{v_g}{L_D} \ln(1 + \kappa_m \cos(\omega_m \tau_m)) \qquad (5.6)$$

In this equation $\cos(\omega_m \tau_m)$ is a constant describing the phase matching between the
internal and external optical fields. For a number of compound-cavity modes with a fre-
quency around an internal mode frequency of the laser diode, the phase matching constant
in Eq. 5.6 approximately equals unity.

To find the time dependent optical output power at the two wavelengths selected in
cavity A and B, the rate-equations for the photon densities of all compound-cavity modes
selected in cavity A and B can be solved together with the corresponding phase equations.
The resulting photon densities can be summed to find the output power at the two selected
wavelengths. The selectivity of the gratings is such that, depending on the length of the
cavity, a group of approximately 10 to 100 compound-cavity modes will be selected in
each cavity.

In this chapter we are not concerned with finding the power distribution of the compound
cavity modes within the group of selected modes in each cavity; we are merely interested
in the averaged photon density of the compound-cavity modes in each group. Assuming
the number of compound-cavity modes to be large enough, at each point in time a mode
will exist for which $\phi_m(t) - \phi_m(t - \tau_m)$ is an integer multiple of 2π. This will be the
lasing mode because the cosine in Eq. 5.4 is maximal for this mode.

Noise induced changes in the phase of the compound-cavity modes will result in mode-
hopping between the compound-cavity modes. The total photon density contained in a
group of compound-cavity modes will only change if a mode hop occurs from a mode
inside a group to a mode outside a group or vise versa. This means that the effect of

the phase changes on the total photon number in a group disappears when the number of compound-cavity modes in the group is large enough. Therefore we neglect the influence of the phase term in Eq. 5.4.

Including a rate-equation for the carrier density inside the active region $N(t)$, this results in the following set of equations:

$$\dot{N}(t) = I/qV - \gamma_e N(t) - G\big(S_A(t) + S_B(t)\big) \tag{5.7}$$

$$\dot{S}_A(t) = (G - \gamma_0) S_A(t) + R_{sp} + \Delta\gamma_A(t)\sqrt{S_A(t)S_A(t - \tau_A)} \tag{5.8}$$

$$\dot{S}_B(t) = (G - \gamma_0) S_B(t) + R_{sp} + \Delta\gamma_B(t)\sqrt{S_B(t)S_B(t - \tau_B)} \tag{5.9}$$

where $S_A(t)$ and $S_B(t)$ are the group averaged photon densities in mode A and B, I is the electrical current, q the elementary charge, V the active volume of the laser diode and γ_e the carrier recombination rate.

The parameter values in Table 5.1 are estimated for our multiple-quantum-well laser diode emitting in the red. In our estimate of the spontaneous emission factor β_{sp} we took into account the enhancement factor for antireflection coated laser diodes [18],[19].

Table 5.1 Parameters used in simulations, their symbols and their values.

Parameter	Symbol	Value
Modal Gain	G	$a_0 v_g \Gamma (N - N_0)$
Gain Constant	a_0	4×10^{-16} cm^2
Group Speed	v_g	0.75×10^{-10} cm s^{-1}
Confinement Factor	Γ	0.02
Transparency Carrier Density	N_0	2×10^{18} cm^{-3}
Modal Spontaneous Emission Rate	R_{sp}	$\Gamma \beta_{sp} \gamma_e N$
Spontaneous Emission Factor	β_{sp}	1×10^{-3}
Carrier Life Time ($1/\gamma_e$)	τ_e	1×10^{-9} s
Internal Material Losses	α_{int}	10 cm^{-1}
Back Facet Reflectivity	R_1	0.32
Coated Front Facet Reflectivity	R_2	5×10^{-4}
Active Region Volume	V	$L_D W D$
Length,	L_D	500×10^{-4} cm
Width and	W	1×10^{-4} cm
Thickness of Active Region	D	0.04×10^{-4} cm

5.4   Measured and Simulated Transient Responses

With the experimental setup described in Section 5.2 the transient behavior of the external-cavity laser diode was studied under various conditions. We varied the amount of feedback for the mode selected in cavity A. For the mode selected in cavity B we varied the cavity round-trip time. In this section the measurement results are presented for the time varying optical power of the two corresponding modes, mode A and mode B.

The wavelength corresponding to these modes was 683 nm and 679 nm respectively. These wavelengths were chosen around the gain maximum of the laser diode to make the modal gain for mode A and B approximately equal. When the feedback path for mode B is blocked and the modulator is continuously open, the laser operates in a single external cavity (A) mode, as measured with the etalon spectrum analyzer. The same holds if the feedback path for mode A is blocked. Thus the external feedback is sufficiently high to dominate the behavior of the laser diode and the laser is operated in the strong feedback regime [20].

Also presented in this section are the results of computer simulations using the rate-equations 5.7–5.9. The rate-equations were numerically solved with a fourth order Runge Kutta routine with a two picosecond step size. In Table 5.1 the used parameter values are listed. To match the simulation results to the experimental result we used the reflectivity values for cavity A and B as fitting parameters.

5.4.1   Varying the Feedback Level for Cavity A

In a first measurement we adjusted the $\lambda/2$-plate in such a way that the estimated feedback for mode A is about 2% when the modulator is open. Considering the extinction ratio of the modulator, the feedback for this mode is about 2×10^{-6} when the modulator is closed. The maximum feedback level for mode A was varied by inserting neutral density filters in cavity A.

The estimated feedback for mode B was about 0.5% for all measurements. The length of cavity A and B was fixed and corresponded to a round-trip time of 6 ns and 7 ns respectively. In Fig. 5.3 the measured transient response of both modes is shown. At t=0, the modulator opens; the transmission is then at 50% of its maximum value. In Fig. 5.3(a) the measured results are plotted for mode A without neutral density filter (ND=0) and with neutral density filters (ND=0.1 and ND=0.2). The corresponding estimated feedback levels for mode A are 2%, 1.3% and 0.8% respectively. The transient response for mode B, that switches off due to mode competition, is presented in Fig. 5.3(b). Depending on the amount of feedback for mode A, it takes between 7 and 21 round-trip times of cavity A for the power to switch from mode B to mode A.

In Fig. 5.4 the simulation results for these experiments are presented. Again, the modal response of mode A and B are presented. The value for the external reflectivity of cavity A in the open state of the modulator was 2.0% (ND=0). In order to match the simulation results to the experimental data we had to assume an extra loss due to the insertion of the neutral density filters. This extra loss was estimated at 10% and can be due to mis-alignment and phase front distortion caused by the neutral density sheets. The resulting external reflection values are 1.0% for ND=0.1 and 0.65% for ND=0.2. In the closed state of the modulator the external reflection for mode A was a factor 10^4 lower than in the open state. As with the modulator used in the experiment, the simulated modulator has a transient time of 8 ns; at t = 0 it reaches 50% of the maximum transmission value. For mode B the external reflectivity was constantly 0.3% in all cases.

(a)

(b)
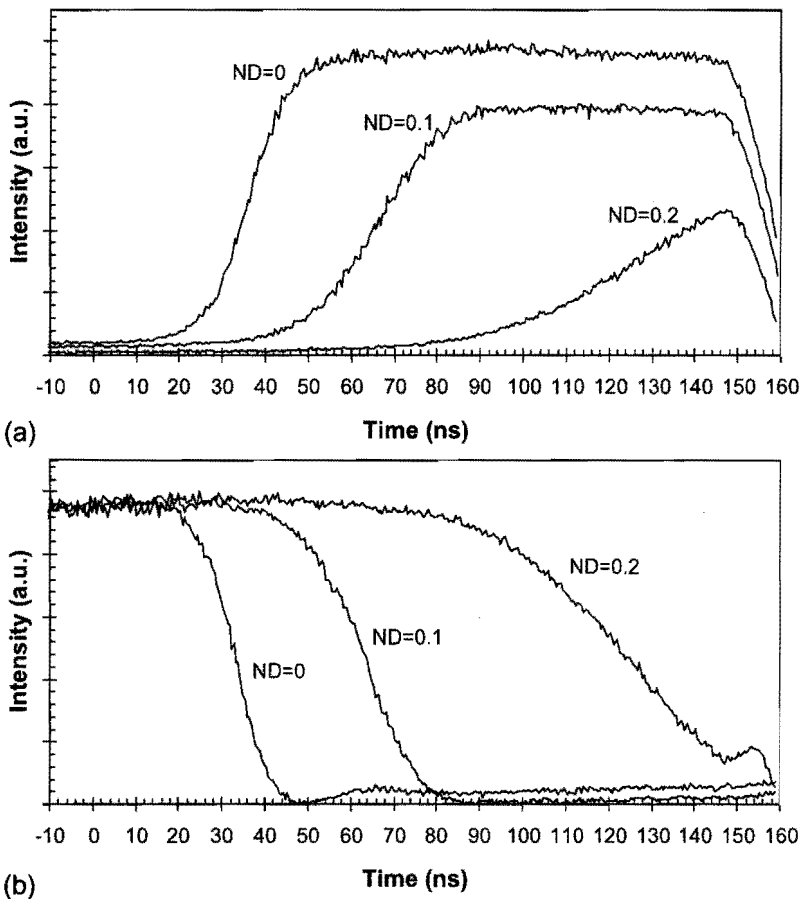
Figure 5.3 Measured transient response of the two selected modes.(a) Mode A, (b) mode B. The modulator opens at t=0, resulting in a switching-on of mode A. Mode B switches of due to mode-competition. Neutral density filters are inserted in the mode A cavity to vary the external reflection for this mode. The value of the neutral density filter (ND) is inserted in the figure for each curve. The estimated external optical feedback is 2% (ND=0), 1.3% (ND=0.1) and 0.8% (ND=0.2) in the open state of the modulator for mode A. The extinction ratio of the modulator measures approximately 10^4. The feedback for mode B is estimated at 0.5%.

5.4.2   Varying the Round-Trip Time of Cavity B

In a next experiment, the round-trip time of cavity B was set to ten different values between 2.1 ns and 15.4 ns. The round-trip time for cavity A was 7.0 ns in this experiment. The estimated reflectivity for cavity A in the open state of the modulator was 2%, the reflectivity for mode B measured approximately 0.5%. The transient response of mode B to a closing of the modulator in cavity A was recorded for all ten cavity lengths.

(a)

(b)
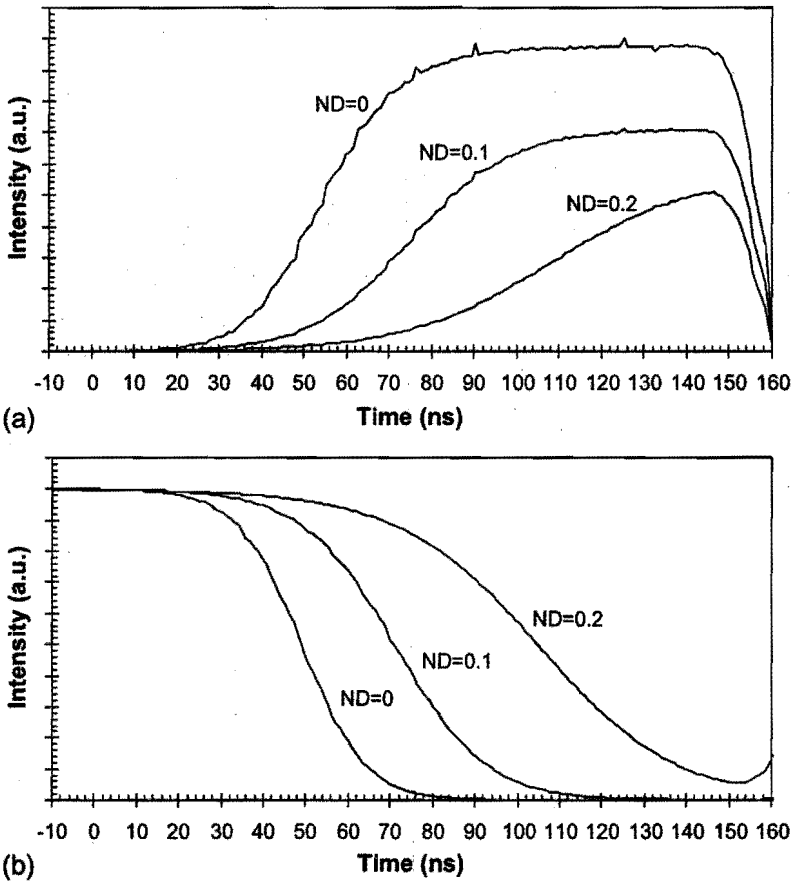
Figure 5.4 Simulation results corresponding to the experimental results presented in Fig. 5.3. (a) Mode A, (b) mode B. In the simulations the following external optical feedback levels were used: 2.0% (ND=0), 1% (ND=0.1) and 0.65% (ND=0.2) in the open state of the modulator for mode A, 0.3% for mode B. In the closed state of the modulator, the feedback for mode A is a factor 10^4 lower than in the open state.

In Fig. 5.5, the transient behavior of mode B is shown for five of these external-cavity lengths corresponding to τ=2.1 ns, τ=4.3 ns, τ=7.0 ns, τ=12.3 ns and τ=15.4 ns. For clarity, the measured results for other cavity lengths are not included. Steps in the time evolution of the intensity for mode B can be clearly distinguished in the figure. The duration of these steps is approximately equal to the round-trip time. Also visible are relaxation oscillations that gradually build up during the transient and mark the beginning of each step. A steady state is reached after about ten round-trip times of cavity B.

The response of mode A was the same for all the measurements; the mode switches off within one round-trip time of cavity A after the modulator is fully closed. For time reference, the transient response of this mode is included in the figure.
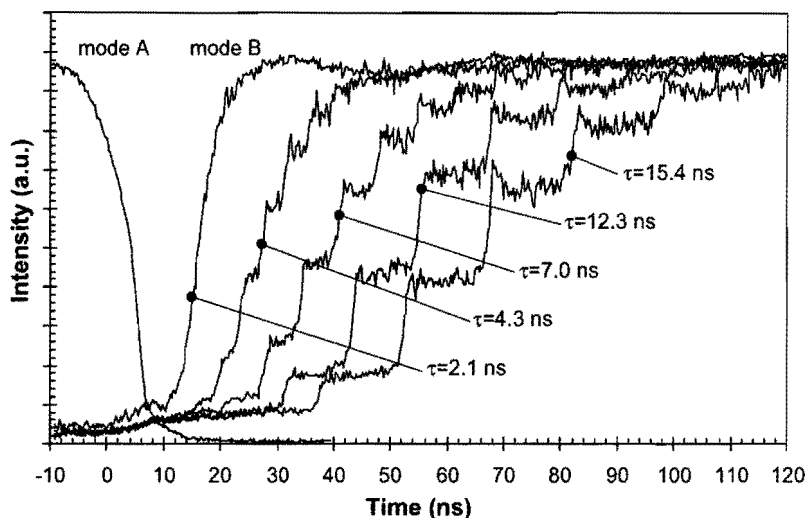
Figure 5.5 Measured transient response of mode A and B for various values of the round-trip time τ of cavity B. The round-trip time in cavity A is about 7 ns, the modulator closes at t = 0. The transient response of mode A does not depend on the cavity round-trip time of mode B. Steps are visible in the transient response of mode B. The duration of the steps is approximately equal to the round-trip time of cavity B. Also visible are relaxation oscillations that gradually build up and mark the beginning of each step.

The simulation results corresponding to this experiment are shown in Fig. 5.6. In the model the external reflectivity for mode A is switched from 2% to 2×10^{-6} at t = 0 in the same way as in the previous simulations. The external reflectivity for mode B is set to a constant value of 0.4% to obtain an optimal fit with the experimental data. Just like in the experimental results, steps and a gradual buildup of relaxation oscillations are visible. Again a steady state is reached after approximately 10 round-trip times.

The operating current of the laser diode was 70 mA during the measurements presented in this section. The measurements were repeated with a driving current of 50 mA and 60 mA with similar results. Also the selected wavelengths of mode A and B were varied. Again similar results were obtained.

When the reflectivity for mode A is modulated, a multi external-cavity mode spectrum is observed with the Fabry-Perot spectrum analyzer. This means that the laser is hopping between external-cavity modes during the transient. The simulations are in good agreement with the experimental results and thus we can deduce that the mode-hopping only influences the distribution of optical power within the selected group of external-cavity modes, as assumed in Section 5.3.
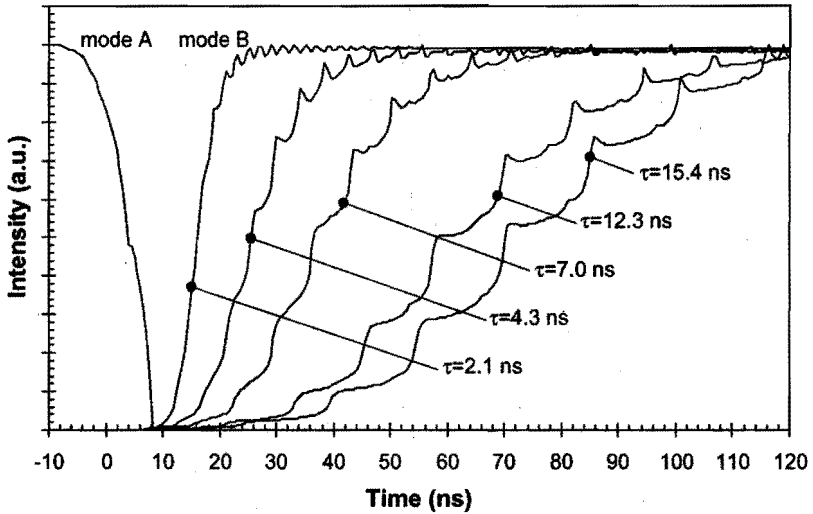
Figure 5.6 Simulated transient response of mode A and B for various values of the round-trip time τ of cavity B, the modulator closes at t = 0. The simulated transient curves show the same features as the experimentally obtained curves presented in Fig. 5.5.

5.5   Discussion

In this section we examine the implications of our measurements and simulation results on the operation speed of the experimental LNN of Chapters 2–4 and a proposed LNN using integrated optics devices [21]. The proposed LNN has an optical length of a few cm that corresponds to a cavity round-trip time of 0.1 ns. With the proposed integrated optics LNN we aim, among other things, at increasing the operation speed of the LNN.

5.5.1   Round-Trip Delay

The experiments with varying external reflection show that, depending on the difference in external reflection between the two modes, up to 21 round-trips are needed to switch the optical power from one mode to the other. The highest number of round-trips were needed with the lowest difference in optical losses for mode A and B. This occurred when the feedback for mode A and B was about 0.8% and 0.5% respectively.

Olsson and Tsang measured the transient behavior of a single mode external-cavity laser diode [10]. They reported that a steady state was reached in three round-trips of the external cavity near the gain peak of the laser. When the gain was reduced by shifting the feedback from the gain peak, they reported 20 or more round-trips before a steady state was reached. Although they modulated the driving current instead of the external optical losses, these findings are in agreement with our experimental results.

In the LNN setup of Chapter 4 the maximum feedback per mode measures approximately $R_{ext} = 9\%$. Each of the neurons receives six or more inputs. This means that for

each input the external reflectivity for a mode can be changed by about $\Delta R_{ext} = 0.015$. To estimate the number of round-trips needed to switch from one output state of the LNN to another output state we assume that the change in output state is caused by switching only one input element. In this worst case the amount of feedback for a mode will change by less than $\Delta R_{ext} = 0.015$ considering the weighting of inputs by a factor smaller than unity. This results in a difference in feedback approximately equal to that for the transient with ND=0.1 reported above, where ∼12 round-trips were needed to reach a steady state. The number of round-trips needed to reach a steady output state after a change of input state in our current experimental LNN will therefore be 12 or higher.

If the feedback level of the proposed integrated optics LNN is the same as in our current experimental LNN, the fastest transient response will be about $12 \times 0.1 = 1.2$ ns. In order to reach a computational speed higher than 1 GBit/s the difference in the amount of external feedback between two input states needs to be increased. This can simply be achieved by reducing the number of inputs, which is undesirable from a functional point of view. A better solution would be to optimize the design of the integrated optics devices for maximum feedback efficiency. For this it might be necessary to introduce extra gain regions in the design.

5.5.2 Residual Delay

The measurements with varying round-trip time were used to extrapolate the experimentally recorded transient curves for zero cavity length. For this purposes the time t_x at which the optical power of mode B reaches a given amount x is extracted from the measurement data presented in Section 5.4.2 as a function of cavity round-trip time. By use of a linear fit [22] on t_x we extrapolated the time at which this amount of power would have been reached if the cavity length for mode B was zero. In this fit we used the round-trip time of the cavity as an estimate on the uncertainty of the t_x-values. The results are plotted in Fig. 5.7 using the ten recorded transient curves discussed in Section 5.4.2. The horizontal error bars in these plots indicate the 95% confidence intervals of the extrapolated data. For reference, the intensity development of mode A and B with a cavity B round-trip time of 2.1 ns are included in the figure.

The extrapolated transient curves for a zero round-trip time of cavity B clearly show a residual delay between the switching off of mode A and the switching on of mode B. The delay is in the order of nanoseconds and will put an additional limit on the operation speed of the LNN on top of that imposed by the number of needed round-trips. We believe that the residual delay is due to the fact that the total external reflectivity before and after the transient is different. As a result the total emitted optical power will be different. Consequently the number of charge carriers needs to change. Since the optical feedback for mode B is lower than that for mode A, the change in the number of charge carriers is also needed to reach the threshold condition for mode B.

To test our hypothesis on the origin of the residual delay, and to estimate the operation speed of the proposed integrated optics LNN device [21], we carried out simulations with a cavity round-trip time of 0.1 ns for both cavities. As a transient time of the modulator we choose 0.1 ns, a modest value for integrated optics modulators [23]. Although the rate-equation model (See Eqs. 5.7–5.9) was derived for a large group of compound-cavity
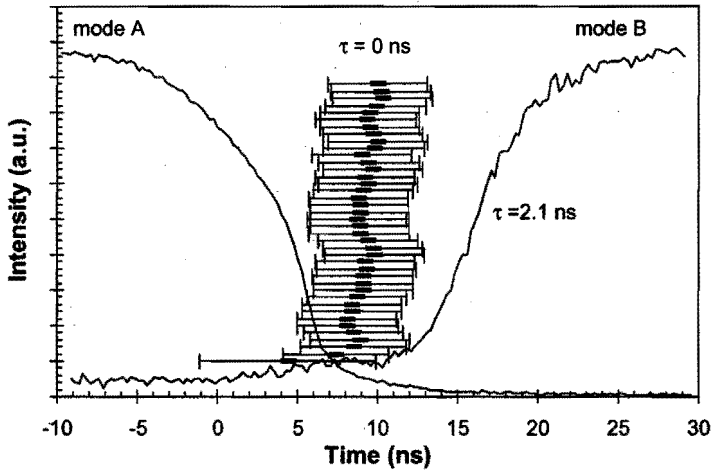
Figure 5.7 Extrapolated transient response curve for cavity B with a zero round-trip time using data of Fig. 5.5. The points are obtained by linear extrapolation of the time at which the intensity of mode B reaches a certain level for various round-trip times, to a round-trip time of 0. Error bars indicate 95% confidence intervals of the linear fit. Measured response curves of mode A and B for a cavity B round-trip time of 2.1 ns are included for comparison.

modes, we will also use the model for this cavity length with just one compound-cavity mode per group. If the mode spacing is sufficiently large, changes in the modal phase are not expected to cause a mode hop to another compound-cavity mode and therefore also in this case the phase term in Eq. 5.4 can be neglected.

In a first simulation we switched off the external reflectivity for mode A at t = 0 while keeping the external feedback for mode B constant. In a second simulation the external reflectivity values for mode A and B were interchanged at t = 0. We used the same values for the external reflectivities as in the simulations of Section 5.4.2, so we expect a delay of approximately 10 round-trip times.

The results of these simulations are presented in Fig. 5.8. Figure 5.8(a) corresponds to the situation with a constant feedback level for mode B, in Fig. 5.8(b) results are shown for the simulated interchanging of the external reflectivity of mode A and B. The figures show the optical intensity of the modes, mode A and B, and the carrier density normalized to the transparency value N0. The steady state of the optical intensity of mode B is indicated with a dotted line.

In Fig. 5.8(a) a difference in the carrier density before and after the transient is visible. The time delay between the complete extinction of mode A and the point at which the intensity of mode B first reaches the steady state value is about 1.7 ns. This is more than 10 round-trip times. In Fig. 5.8(b) this time delay is about 1.1 ns, approximately equal to the expected 10 round-trips. The carrier densities before and after the transient are equal in Fig. 5.8(b). Thus we can conclude that the change in charge carrier density introduces a delay of about 0.6 ns. This value is in reasonable agreement with the measured residual delay.
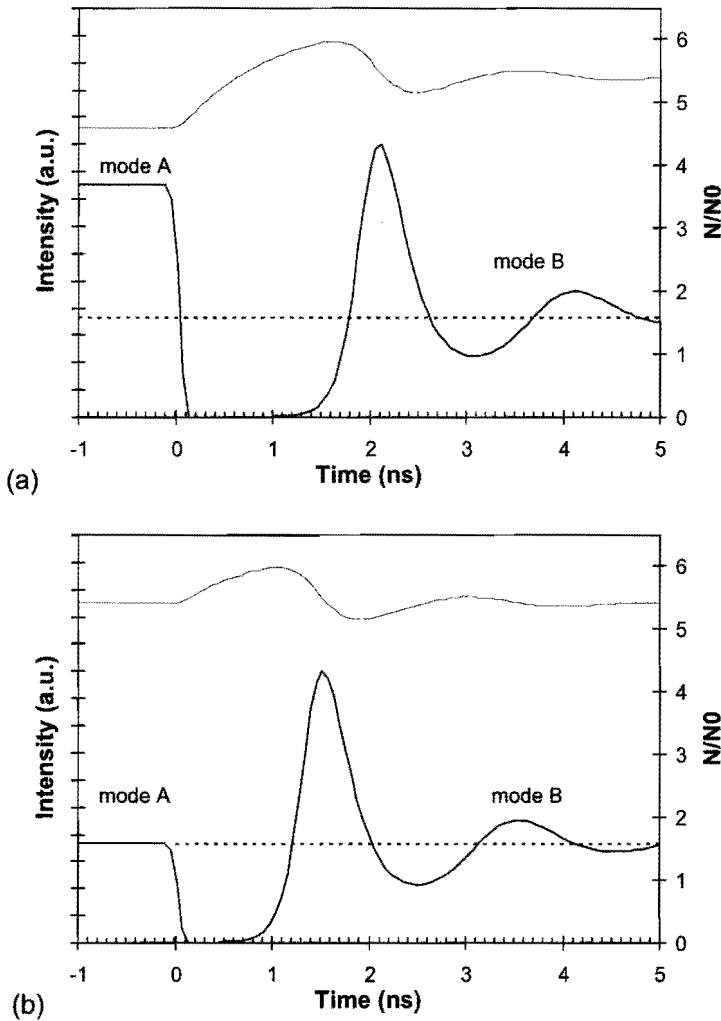
Figure 5.8 Results of simulation of the time development of optical power for both modes with a cavity round-trip time of 0.1 ns. The light intensity of mode A and B are plotted, together with the normalized carrier density N/N0. The steady state of mode B is indicated with a dotted line. (a) At t = 0, the modulator closes with a transient time of 0.1 ns. Relaxation oscillations and a delay of about 1.7 ns can be observed in the transient response of mode B. The carrier density is different before and after the transient. (b) At t = 0 the optical feedback levels of mode A and B are interchanged. The carrier density is the same before and after the transient. The delay is reduced to 1.1 ns or approximately 10 round-trip times of the external cavities.

The simulations of Fig. 5.8(b) show that the delay can be avoided by controlling the total external reflectivity in such a way that it is equal before and after the transient. To avoid the residual delay, the total amount of external reflectivity should be the same for each state of the LNN. Although this should be possible, it will considerably complicate implementations of the LNN. The resulting constraint on the input vectors and the weight matrix will reduce the functional capabilities of the LNN.

5.5.3   Relaxation Oscillations

In Fig. 5.8 relaxation oscillations can be observed. These relaxation oscillations originate from the change in charge carrier density during the transient which in turn is caused by the temporary change in total emitted light intensity. Compared to the oscillations that are visible in the measurements and simulations with longer cavity round-trip times, the oscillations are more pronounced in these simulations with a round-trip time of 0.1 ns. With still lower round-trip times, the relaxation oscillations will dominate the behavior during the transient. This is illustrated in Fig. 5.9 where we show simulation results for a zero cavity length.
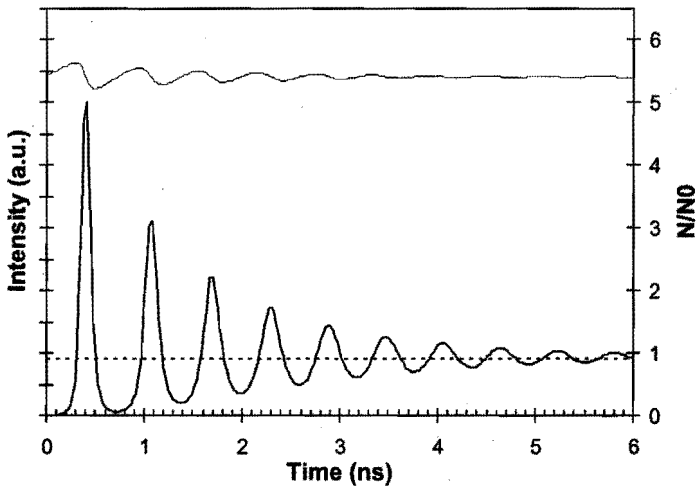
Figure 5.9 Simulated time evolution of the intensity of mode B for zero cavity length of both cavities. Steady state is indicated with a dotted line. Relaxation oscillations in the intensity of mode B can be observed. The oscillation frequency is about 1.7 Ghz. A switch-on time of ~0.3 ns can be observed.

The relaxation oscillation frequency is proportional to the square-root of the optical output power of the laser and has a typical value of ~5 GHz [16],[17] for laser diodes operated well above threshold. The frequency of the relaxation oscillations in Fig. 5.9 is about $f_r = 1.7$ GHz. This relatively low value is caused by the fact that the laser diode in the experiments and simulations is operated close to threshold.

A switch-on time t_{on} can be associated with the relaxation oscillation frequency according to [16]:

$$t_{on} = \frac{\sqrt{2}}{\omega_r} \left[\ln \left(\frac{S_{on}}{S_{off}} \right) \right]^{1/2} \tag{5.10}$$

with S_{on}/S_{off} the intensity ratio of the considered mode and ω_r the angular relaxation oscillation frequency. The value of t_{on} resulting from Eq. 5.10 is about 0.35 ns and is in agreement with the simulation results of Fig. 5.9. The bandwidth of the system will essentially be limited by the relaxation oscillation frequency [16],[17], hence the current LNN will be bandwidth limited to about 1.7 GHz even if the round-trip delay is zero.

5.6 Conclusions

In conclusion we have studied the mode switching behavior of an external-cavity laser diode under optical modulation conditions to estimate the feasible operation speed of a LNN implemented with integrated optics. In our experiments the feedback level for one mode of the external-cavity laser diode was kept at a constant value, while the feedback level for another mode is switched by means of an optical modulator. The round-trip delay for one of the modes is varied.

It was found, both experimentally and theoretically, that depending on the amount of external optical feedback between 7 and 21 round trips of an external cavity are needed to reach a steady state. Switching between two states in our LNN is expected to take more than 12 round-trips considering the feedback level of our experimental LNN setup. To obtain switching times <1 ns in an integrated optics LNN with a cavity length of a few cm, the amount of optical losses needs to be reduced or extra optical gain should be introduced.

For a zero cavity length a residual delay of a few nanosecond is identified by extrapolation of experimentally obtained transient curves for various cavity lengths. Simulations indicate that this delay is due to a change in charge carrier density, needed to reach the threshold condition for the initially nonlasing mode. Simulations indicate that this delay can be a avoided by ensuring an equal feedback level in each state of the LNN.

A third limitation on the operation speed of the LNN is imposed by the occurrence of relaxation oscillations. This limits the bandwidth of the current LNN to about 1.7 GHz. To increase the relaxation oscillation frequency of the laser diode, the feedback efficiency can be increased to operate the laser diode further above threshold in the on state.

Acknowledgements

References

[1] V. Vassiliev, V. Velichansky, P. Kersten, T. Trebst, and E. Riehle, "Subkilohertz enhanced-power spectrometer in the visible," *Opt. Lett.* **23**, 1229–1231, 1998.

[2]   P. de Groot, "Use of multimode short-external-cavity laser diode for absolute-distance interferometry," *Appl. Opt.* **32**, 4193–4198, 1993.

[3]   W. J. Kozlovsky, W. P. Risk, W. Lenth, B. G. Kim, G. L. Bona, H. Jaeckel, and D. J. Webb, "Blue light generation by resonant-enhanced frequency doubling of an extended-cavity diode laser," *Appl. Phys. Lett.* **65**, 525–527, 1994.

[4]   V. M. Baev, J. Eschner, E. Paeth, R. Schuler, and P. E. Toschek, "Intra-cavity spectroscopy with diode lasers," *Appl. Phys. B* **55**, 463–477, 1992.

[5]   S. B. Colak, J. J. H. B. Schleipen, and C. T. H Liedenbaum, "Neural network using longitudinal modes of an injection laser with external feedback," *IEEE Trans. Neural Networks* **7**, 1389–1400, 1996.

[6]   E. C. Mos, J. J. H. B.Schleipen, and H. de Waardt, "Optical mode neural network by use of the nonlinear response of a laser diode to external optical feedback," *Appl. Opt.* **36**, 6654–6663, 1997.

[7]   E. C. Mos, J. J. H. B. Schleipen, and H. de Waardt, "Laser neural network demonstrates data switching functions," in *Proc. of the 8th int. conf. on artificial neural networks*, Niklasson, Bodén and Ziemke Eds., (Springer-Verlag, Berlin, Germany, 1998), Vol. 2, pp. 1165–1170.

[8]   E. C. Mos, J. J. H. B. Schleipen, H. de Waardt, and G. D. Khoe, "Loop-mirror laser neural network using a fast liquid-crystal display," *Appl. Opt.* **38**, 4359–4368, 1999.

[9]   R. P. Lippman, "An introduction to computing with neural nets," *IEEE Acoustics, Speech and Signal Processing Mag.* **4**, 4–22, 1987.

[10] N. A. Olsson and W. T. Tsang, "Transient effects in external cavity semiconductor lasers," *IEEE J. Quantum Electron.* **19**, 1479–1481, 1983.

[11] A. P. Kanjamala and A. F. J. Levi, "Transient response of wavelength switching in multicavity mode-locked laser diodes," *Appl. Phys. Lett.* **69**, 3647–3649, 1996.

[12] C. L. Wang, J. C. Kuo, C. S. Chang, and C. L. Pan, "Pulse buildup dynamics of an actively mode-locked laser diode array in the external cavity," *IEEE J. Quantum Electron.* **20**, 439–446, 1995.

[13] J. Dellunde, C. R. Mirasso, M. C. Torrent, J. M. Sancho, E. Hernández-García, "Transient dynamics of a single-mode semiconductor laser subjected to both optical feedback and external light injection," *Optical and Quantum Electron.* **27**, 755–760, 1995.

[14] M. G. Littman and H. J. Metcalf, "Spectrally narrow pulsed dye laser without beam expander," *Appl. Opt.* **17**, 2224–2227, 1978.

[15] R. Lang and K. Kobayashi, "External optical feedback effects on semiconductor laser properties," *IEEE J. Quantum Electron.* **16**, 347–355, 1980.

[16] K. Petermann, "Laser diode modulation and noise," in *Advances in Optoelectronics*, T. Okoshi ed., (Kluwer Academic, Dordrecht, The Netherlands, 1991).

[17] G. P. Agrawal and N. K. Dutta, *Long wavelength semiconductor lasers*, (van Nostrand Reinhold, New York, 1986).

[18] K. Ujihara, "Phase noise in a laser with output coupling," *IEEE J. Quantum Electron.* **20**, 814–818, 1984.

[19] C. H. Henry, "Theory of spontaneous emission noise in open resonators and its application to lasers and optical amplifiers," *J. Lightwave Techn.* **4**, 288–297, 1986.

[20] R. W. Tkach and A. R. Chraplyvy, "Regimes of feedback effects in 1.5 μm distributed feedback lasers," *J. Lightwave Techn.* **4**, 1655–1661, 1986.

[21] J. H. Wolter, G. D. Khoe, and M. K. Smit, "Photonics in communication technologies," COBRA-NWO-NRC-Programme proposal (Granted), 1998.

[22] W. H. Press, B. P. Flannery, S. A. Teukolsky, and T. Vetterling, *Numerical recipes*, (Cambridge University Press, Cambridge, 1986).

[23] H. S. Loka and P. W. E. Smith, "Ultrafast all-optical switching in an asymmetric Fabry-Perot device using low-temperature-grown GaAs," *IEEE Phot. Techn. Lett.* **10**, 1733–1735, 1998.

6

Optical Neuron by use of a Laser Diode with Injection Seeding and External Optical Feedback

We present an all-optical neuron by use of a multimode laser diode that is subjected to external optical feedback and light injection. The shape of the threshold function, that is needed for neural operation, is controlled by adjusting the external feedback level for two longitudinal cavity modes of the laser diode individually. One of the two modes corresponds to the output of the neuron; light injection at the wavelength of this mode provides excitatory input. Light injection in the other mode provides inhibitory input. When light corresponding to two input signals is injected in the same mode, summation of input signals can be achieved. A rate-equation model is used to explain the operating principle theoretically. The proposed injection seeding neuron is built using free-space optics to demonstrate the concept experimentally. The results are in good agreement with predictions from the rate-equation model. Some experimental results show threshold functions that are preferable from a neural network point-of-view. These results agree well with injection locking theory and experiments reported in literature.

6.1   Introduction

The optical domain is attractive for hardware implementation of neural networks because of the high degree of parallelism that can be achieved in optical systems. An optical neural network was first presented by Psaltis and Farat [1]. Since then, optical implementation of neural networks has been the subject of many studies (for an overview see e.g. [2],[3]).

As pointed out by Jutamulia and Yu [3], the threshold function needed for neural operation is realized in the electrical domain for most of the proposed optical neural networks. In this chapter we describe a method to apply inputs and provide threshold operation in the optical domain. The threshold operation is implemented by use of the sensitivity of a multimode laser diode to external light injection. The threshold can be controlled by applying external optical feedback to the laser diode. The work presented here is closely related to the laser neural network (LNN) discussed in Chapters 2–5 of this thesis (See also Refs. [4]–[6]) in which we use external optical feedback to implement the threshold operation. The inputs in the LNN are implemented in the optical transmission domain.

With the work presented in this chapter as well as with the LNN we aim at applications in optical telecommunications. For this application area it is especially important to have all-optical neural operation. The inputs and outputs of such a neural network should preferably be in the optical power domain. The all-optical neuron presented in this chapter has inputs as well as output in the optical power domain.

Laser source   Laser diode
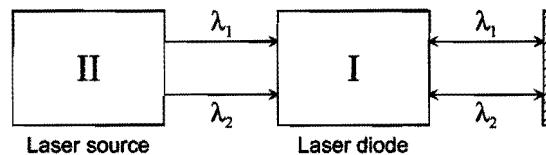
Figure 6.1 Schematic drawing of the injection seeding neuron concept. A laser diode I is provided with external optical feedback for two wavelengths (λ_1 and λ_2) to control the net optical gain at these wavelengths. By use of a tunable laser source II, light can be externally injected in laser diode I to switch the laser to one of the selected wavelengths.

The concept of the all-optical neuron is explained in Fig. 6.1 and relies on the injection of light from a source laser (II) into a laser diode (I). This technique, commonly known as injection seeding or injection locking is well documented [7]–[16] and has applications such as frequency conversion for telecommunication applications [11],[12]. With our optical neuron, we combine injection seeding and optical feedback to obtain neural-like operation. The laser that receives the injected light will represent a single neuron. This is in contrast with the LNN where a single laser diode provides a multitude of neurons.

The principle of operation of the proposed injection seeding neuron is illustrated in Fig. 6.2. By use of controlled external optical feedback laser diode I can only operate in one of two longitudinal modes. The figure shows conceptual drawings of the power spectra of the laser diode in two states. The left part of the figure shows the spectrum of the laser diode that is lasing in a certain mode 1, at wavelength λ_1, and corresponds to
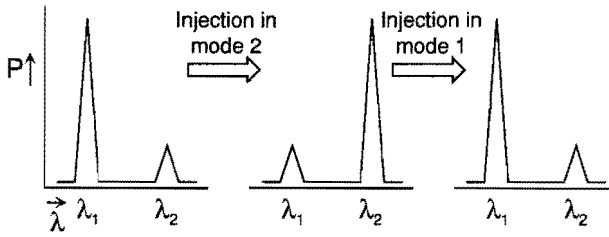
Figure 6.2 Illustration of the operating principle of our injection seeding neuron. The left part of the figure shows the spectrum of a laser emitting at wavelength λ_1 (mode 1) without injection seeding. By injecting light in mode 2 the emission spectrum of the laser can be locked to λ_2, the output wavelength of the neuron. The output power at λ_2 will vary nonlinearly with the amount of injected power yielding neural-like behavior with an excitatory input. When the neuron is active, the laser emits at λ_2, as shown in the middle part of the figure. In this state injection of light at λ_1 can force the laser back to emit at λ_1. Again a nonlinear, neural-like function is associated yielding an inhibitory input. The resulting state is shown in the right part of the figure.

the state of our laser neuron without external light injection. Mode 2, corresponding to wavelength λ_2, is just below threshold and its optical power is defined as the output of our injection seeding neuron. Laser diode I can be made to emit this spectrum by carefully controlling the amount of external optical feedback for wavelengths λ_1 and λ_2.

If the source laser II operates at λ_2, and the amount of injected optical power is high enough, laser diode I will be locked to the injected light at wavelength λ_2. The power spectrum of the resulting state is shown in the middle part of Fig. 6.2. The optical power at wavelength λ_2, and thus the output of our injection seeding neuron, will vary nonlinearly with the amount of externally injected light at wavelength λ_2. It is this nonlinear response that is used to obtain neural-like action. The injected signal at wavelength λ_2 corresponds to an input signal of the neuron. From the preceding it is clear that this input signal causes the output of the neuron to increase and hence it is excitatory.

Inhibitory inputs can be obtained by injecting light at wavelength λ_1. Injection of light at this wavelength can cause laser diode I to go back to the original state where mode 1 dominates over mode 2 as drawn in the right part of Fig. 6.2. Again a nonlinear, neural-like response is associated with the amount of injected light and the output power of the neuron. In the case of injection in mode 1 the input has a decreasing effect on the output of the neuron.

The shape of the nonlinear threshold function and the level of the threshold will depend on the amount of optical gain and losses of laser diode I at wavelengths λ_1 and λ_2. By controlling the external optical feedback conditions for laser diode I, the optical losses can be controlled for each wavelength of the laser diode independently. This can be used as a way to control and shape the threshold function of our injection seeding neuron.

Summation of inputs can be obtained by simultaneous injection of several optical input signals. Excitatory inputs should be injected at wavelength λ_2, inhibitory inputs at wavelength λ_1. Weights can be assigned to the inputs by attenuating the optical signals prior to injection into the laser diode.

The operating principle will be theoretically verified in Section 6.2 where we use a rate-equation analysis to model our laser diode with light injection and optical feedback. In Section 6.3 we present the experimental setup used to demonstrate the injection seeding neuron. The results are presented in Section 6.4 and discussed in Section 6.5. We conclude the chapter in Section 6.6 by giving recommendations for future work.

6.2   Theory

Injection locking of semiconductor lasers has been studied extensively in literature [7]–[16]. A laser diode can be locked to an externally injected signal if the wavelength of the injected signal is inside a wavelength range around a fundamental wavelength of the laser diode. The size of this locking range depends on the amount of externally injected power and the linewidth and power of the originally lasing mode.

6.2.1   Rate-Equation Analysis

In this section, we examine the combined effect of injection seeding and external optical feedback theoretically. To verify the concept of the injection seeding neuron, we model the laser as having two longitudinal modes with external light injection and external optical feedback for both of the modes.

As will be described in subsequent sections, the experimental injection seeding neuron consists of an antireflection coated laser diode that is coupled to an external cavity. However, for simplicity we model the system as a solitary laser diode with two longitudinal modes. The external reflectivity will be incorporated in the model as the effective reflectivity of the laser diode facet facing the external cavity. The simplified model is valid in our situation because the external-cavity reflectivity is much larger than the residual reflectivity of the antireflection coated laser diode facet. In other words, the laser diode operates in the strong feedback regime [17].

The two longitudinal modes of the laser are labeled mode 1 and mode 2. As mentioned previously, the output of our neuron corresponds to mode 2 of the laser. Light can be injected in mode 1 and 2. The laser diode subjected to external light injection can be described by a set of rate-equations [18] for the complex optical field and the number of carriers inside the active region.

To simplify the analysis we constrain the problem to externally injected light with a frequency that is inside the stable part of the locking range for both modes [13]. Furthermore we assume a constant phase difference between the externally injected optical field and the internal optical field. With these simplifications the photon phase can be omitted from the rate-equation model and instead of the complex field equations we can use the equations for the photon number of the two modes. The photon number $P_m(t)$ of the two modes $m = 1, 2$ can be described with [18]:

$$\frac{dP_m(t)}{dt} = (G_m - \gamma_m) P_m(t) + R_{sp} + 2k_c \sqrt{P_m(t) P_m^{inj}} \qquad (6.1)$$

The first term in the right part of Eq. 6.1 represents the net gain, where G_m is the wavelength dependent optical gain and γ_m is the photon decay rate for a mode. In this

theoretical description we assume that both modes have approximately the same wavelength and thus experience the same optical gain, G. The second term in the right part of Eq. 6.1, R_{sp}, is the rate of spontaneous emission in mode m. Both gain and spontaneous emission are linear dependent on the carrier number [18].

In the injection seeding neuron, external feedback is used to control the net modal gain via the photon decay rate γ_m. For mode m we can write:

$$\gamma_m = v_g \left(\alpha_{int} + \frac{1}{2L} \ln \left(\frac{1}{R_0 R_{ext,m}} \right) \right) \tag{6.2}$$

where v_g is the speed of light inside the laser material, α_{int} is the internal cavity loss and L the cavity length. R_0 is the facet reflectivity of the uncoated laser diode back facet and $R_{ext,m}$ is the effective facet reflectivity controlled by the external optical feedback for mode m.

External light injection is represented in the model by the injected photon number for mode m, P_m^{inj}. The coupling between the externally injected photons and the photons inside the active region is accounted for by a coupling constant k_c [18].

The rate-equation model is completed with an equation for the carrier number $N(t)$ given by:

$$\frac{dN(t)}{dt} = \frac{I}{q} - \gamma_e N(t) - \sum_{m=1}^{2} G_m P_m(t) \tag{6.3}$$

The first part of the righthand side of Eq. 6.3 accounts for the electrically injected carriers in the active region, the second part for the spontaneous carrier decay and the third part for the stimulated carrier decay.

In this section we are concerned with finding the laser output power in the two modes as a function of the power injected into one (or both) of the modes. We now define this nonlinear function of output power versus externally injected power as the threshold function for the laser. This threshold function can be found from the steady state solution of the photon rate-equation 6.1 for modes $m = 1, 2$, and the carrier rate-equation 6.3. The steady solution can be found by solving the following equations for N, P_1 and P_2:

$$(G - \gamma_1) P_1 + R_{sp} + 2k_c \sqrt{P_1 P_1^{inj}} = 0 \tag{6.4}$$

$$(G - \gamma_2) P_2 + R_{sp} + 2k_c \sqrt{P_2 P_2^{inj}} = 0 \tag{6.5}$$

$$\frac{I}{q} - \gamma_e N - G (P_1 + P_2) = 0 \tag{6.6}$$

6.2.2 Numerical Simulations

A set of threshold functions for the laser was found by numerically solving Eqs. 6.4–6.6 for N, P_1 and P_2. The amount of light injected into each mode was varied. Furthermore the amount of external feedback for mode 2, $R_{ext,2}$ was varied. For the parameter values used in these simulations, we refer to Ref. [18]
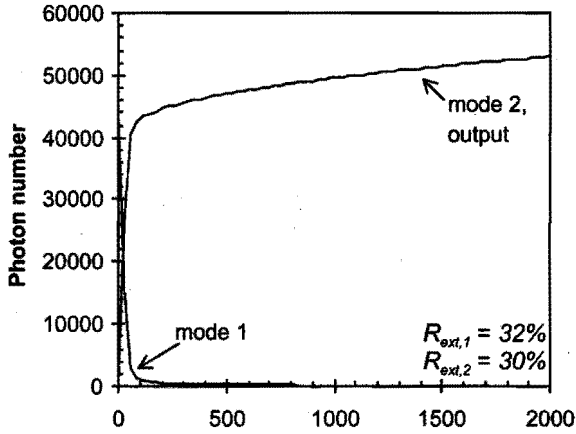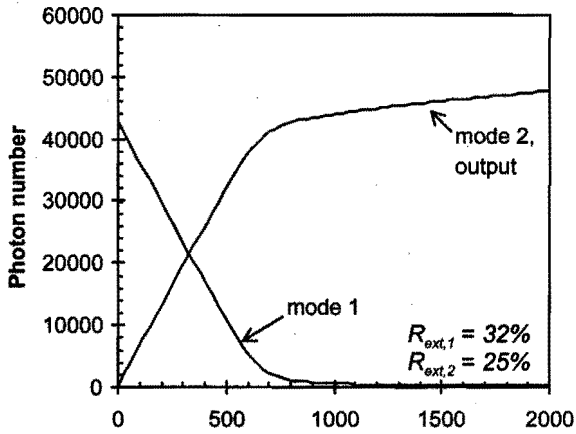
Figure 6.3 Simulation results of the photon number in the two modes 1 and 2, as a function of injected photon number in mode 2. The optical losses for mode 2 is lower in (a) then it is in (b). In Fig. (a) $R_{ext,2}= 30\%$, in Fig. (b) $R_{ext,2}= 25\%$. Both figures show a nonlinear relation between the amount of injected photons in mode 2 and the photon number of mode 2, the output of our proposed neuron.

Let us first consider injection of light in mode 2 to verify excitatory input. The output of the neuron versus injected photon number in mode 2 is shown in Fig. 6.3 for different values of $R_{ext,2}$. The figure shows two threshold functions with reflectivity $R_{ext,2}$ set to 30% (a) and 25% (b). The laser diode back facet reflectivity for both modes, R_0, was set to 32%, which is the reflectivity for the uncoated laser diode facet. The front facet reflectivity for mode 1, $R_{ext,1}$, was arbitrarily set to same value. As can be seen from

Fig. 6.3, increasing the injected light power causes mode 1 to be switched off and mode 2 to start lasing, as expected. Note that for a lower external reflectivity for mode 2, more power is required to switch the laser from mode 1 over to mode 2. This can be used to control the shape of the threshold function. The slope of the threshold function decreases with decreasing $R_{ext,2}$.
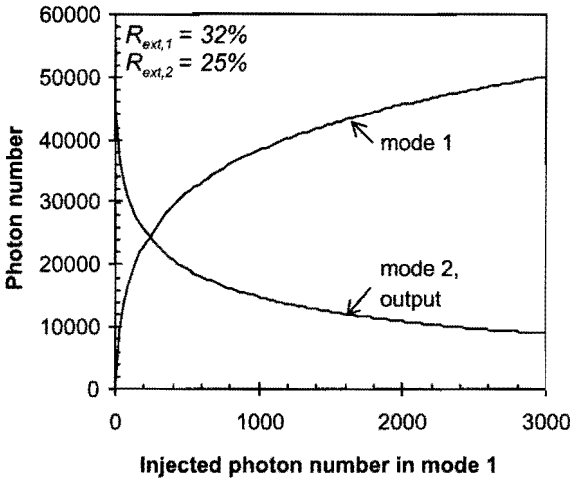
Figure 6.4 Simulation results of the photon numbers in two modes 1 and 2 as a function of injected photon number in mode 1 with a constant injection of 1200 photons in mode 2. The photon number of mode 2 is a nonlinear, decreasing function of the number of injected photons in mode 1.

The results presented in Fig. 6.4 demonstrate an inhibitory input signal. A constant amount of photons, 1200 in our simulations, is injected into mode 2, so that mode 1 is initially turned off and the laser is in the state corresponding to the middle part of Fig. 6.2. To turn mode 1 on again light is injected into mode 1, the inhibitory input. The results were obtained with $R_{ext,2}$ at 25% and $R_{ext,1}$ set to 32%. Due to the constant injection in mode 2, this mode does not switch off completely.

In order to relate the results of this section to the experimental results, it should be noted here that the photon number is directly proportional to optical power. From Figs. 6.3 and 6.4 it can be seen that injection of about 1% of the optical power is sufficient to switch the laser between modes 1 and 2.

6.3   Experimental Setup

In order to experimentally verify the concept of the all-optical neuron a laser diode is needed with controllable optical feedback and external light injection for at least two longitudinal modes.

6.3.1   Optical Feedback

A setup is shown in Fig. 6.5. It consists of a laser diode (laser diode I, Uniphase CQL806, $\lambda \approx 680$nm) coupled via beam splitter BS1 to two external cavities, one for each mode. For each cavity the 1st order reflection of a diffraction grating (G1 and G2, 2400 l/mm) is coupled back into the laser. The optical feedback is wavelength selective in this way and gratings G1 and G2 are tuned to wavelengths λ_1 and λ_2 corresponding to modes 1 and 2.

The exit facet of the laser diode facing the external cavity is provided with an antireflection coating with a residual reflectivity of approximately 5×10^{-4}. If the external optical feedback is sufficiently high, laser action will be dominated by the external cavity instead of the internal cavity of the laser diode [17]. Consequently, the laser will oscillate at the wavelength selected by the external cavity with the highest reflectivity. Neutral density filters can be inserted in the external cavity corresponding to G2 to set the amount of optical feedback for this cavity. The laser is temperature stabilized to prevent thermal drift of
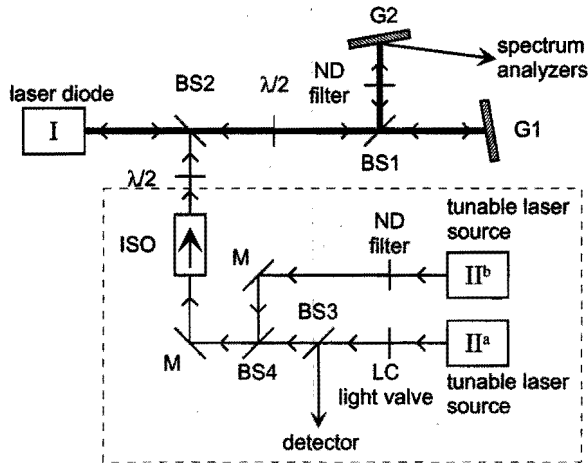
Figure 6.5 Experimental setup to demonstrate the proposed injection seeding neuron. Laser diode I is coupled to two external cavities, wavelength tunable by use of gratings G1 and G2. A neutral density filter ND controls the feedback efficiency for one cavity. Light from two continuously tunable laser sources II^a and II^b is injected via a beam splitter, BS2, and an isolator, ISO. Light from laser source II^a can be variably attenuated by use of a liquid-crystal light valve LC, and monitored via BS3 with a photodiode detector. A neutral density filter attenuates the light from laser source II^b by a fixed amount. $\lambda/2$-plates are inserted to match polarization states for optimum optical throughput.

the mode wavelengths. A $\lambda/2$ plate is inserted to tune the polarization angle for optimal reflection at the gratings.

6.3.2   Light Injection

The output of two tunable laser sources II[a] and II[b] (Sacher Lasertechnik TEC500 series) is injected in the external-cavity laser diode via beam splitter BS2. An isolator is used to prevent coupling of the light from laser diode I to the tunable laser sources. A $\lambda/2$ plate is added to match the polarization state of injected light to that of the laser diode. For one source, II[a], the amount of injected power is made continuously variable by use of a liquid crystal light valve. With a photodiode detector we measure the amount of injection from this source. We can set the amount of injected power from the second source II[b] to discrete values by use of neutral density filters. The amount of injected power from this source is measured by inserting a photodiode detector in the light path (not shown in the figure).

The wavelength of the injected light must be inside the locking range, that increases with decreasing cavity length [7],[9],[10]. For this reason, the external cavities are kept as short as possible. The resulting locking range is estimated at $\sim$10 MHz. The wavelength stability of the tunable laser sources is within this range with unchanged drive current. Controlling the amount of injected light by changing the drive current of the tunable laser diodes would cause an unacceptable wavelength change.

6.3.3   Measurements

To monitor the spectral behavior of laser diode I the 0th order reflection of one of the gratings is directed to two spectrum analyzers. An optical multichannel analyzer (OMA) is used to measure the output spectrum of the laser at a coarse wavelength scale (resolution 0.25 nm, range 26 nm). This analyzer is used to measure the output power in the modes of the laser diode. The laser spectrum is also monitored at a finer scale by a Fabry Perot etalon (resolution 10 MHz, free spectral range 1.5 GHz), to verify whether the laser is lasing at a single external-cavity mode.

With the setup of Fig. 6.5 the threshold functions can be measured by monitoring the output power in the two external-cavity modes of laser diode I (via the OMA) while the amount of power injected by laser source II is varied. Since both injection sources II[a] and II[b] can be tuned to either one of the modes at λ_1 and λ_2, excitatory and inhibitory inputs as well as the adding of input signals can be experimentally demonstrated.

6.4   Experimental Results

With the setup described in Section 6.3, the threshold functions predicted by theory are experimentally verified. In all measurements presented in this section, the wavelength separation between the two modes was about 1.5 nm to ensure equal gain for the modes. The driving current of the laser diode was in the range of 60–70 mA. The total optical output power of the laser diode at this driving current measured $\sim$5 mW.

6.4.1   Excitatory Input

In a first experiment an excitatory input is demonstrated. By controlling the feedback
for both modes, mode 1 is made to lase in the absence of injected power. Next, light is
injected at the wavelength corresponding to mode 2 with tunable laser source II^a only.
The results are shown in Fig. 6.6. The amount of power injection in mode 2 is gradually
increased from 0 μW to about 15 μW. The figure shows two nonlinear functions for
different levels of the external feedback efficiency for mode 2. In Fig. 6.6(b) the feedback
level for mode 2 is a factor of ~2 lower than that in Fig. 6.6(a). Figure 6.6 shows the basic
threshold function as well as the possibility to change the shape of the threshold function.

In the measurements corresponding to Fig. 6.6, the wavelength of the injected signal
was adjusted to obtain optimal injection locking. If the wavelength is slightly changed
(~10 MHz) from this optimal wavelength, different results are obtained. These results are
shown in Fig. 6.7 where much steeper threshold functions can be observed. Compared to
the measurements of Fig. 6.6 more injected power is needed to switch on mode 2.

6.4.2   Inhibitory Input

To demonstrate inhibitory inputs the laser is first made to lase at wavelength λ_1 by setting
the external reflectivity for the two modes 1 and 2. Now, 25 μW of optical power is
injected in mode 2 by use of tunable laser source II^b. As a result, the laser oscillates at
wavelength λ_2 as is expected. Figure 6.8 shows the optical powers in both modes when
power is injected in mode 1 by use of tunable laser source II^a with simultaneous constant
injection in mode 2. If sufficient power is injected in mode 1, the laser switches to this
mode and the power of mode 2 decreases.

Again, the experiments were repeated with a slight detuning of the injection source
wavelength (laser source II^a). The results, presented in Fig. 6.9, show a much sharper
threshold function.

6.4.3   Input Summation

To demonstrate the summation of two input signals we tuned both laser sources II^a and II^b
to wavelength λ_2 corresponding to mode 2. By controlling the external feedback, mode 1
at λ_1 was made to lase.

First we measured the threshold function with injection by laser source II^a only. The
results are represented by the drawn lines in Fig. 6.10. Next, laser source II^b is used to
inject an additional 5.6 μW in mode 2. Again the amount of power injected with laser
source II^a is varied and the optical power in the two modes is measured. The results are
plotted with dotted curves in Fig. 6.10. The dotted lines can be considered a leftward
shifted version of the drawn lines. The shift is due to the extra injection into mode 2 and
is ~4 μW. Note that only the linear part of the threshold curve is visible. This is due to
the fact that the amount of losses for mode 2 were higher then those in the measurements
presented in, for example, Fig. 6.6.
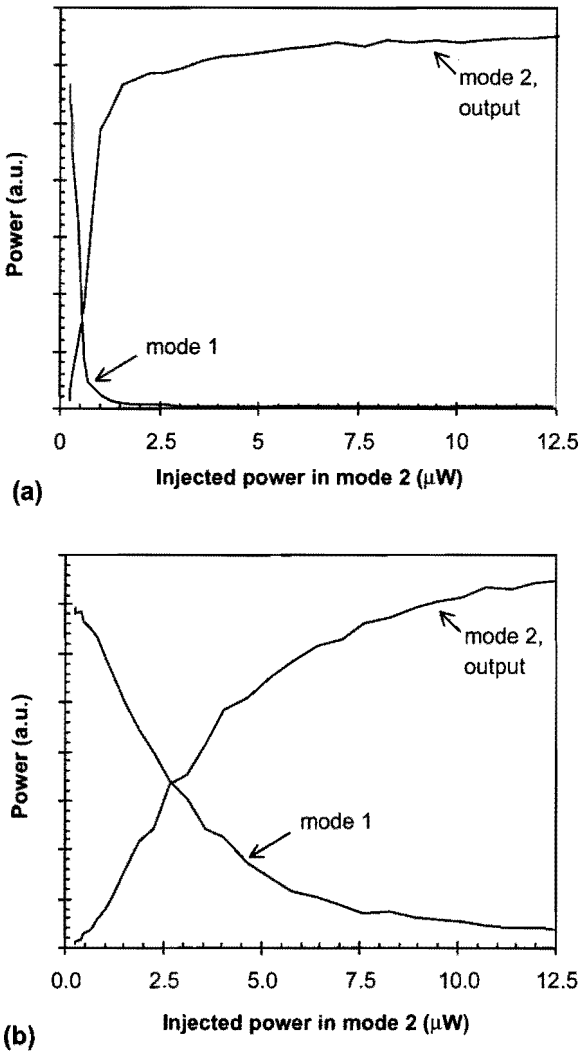
Figure 6.6 Measured optical power in the two selected modes as a function of injected optical power in mode 2. (a) Without neutral density filter, (b) with neutral density filter. The power of mode 2 increases nonlinearly with increasing injection power in this mode. The power in mode 2 increases more rapidly as a function of injected power without the neutral density filter (Compare Fig. 6.3).

6.5 Discussion

6.5.1 Basic Neural Operation

The experimental results on the excitatory and inhibitory input, presented in Figs. 6.6 and 6.8, are in close agreement with the theoretically predicted curves of Figs. 6.3 and 6.4.
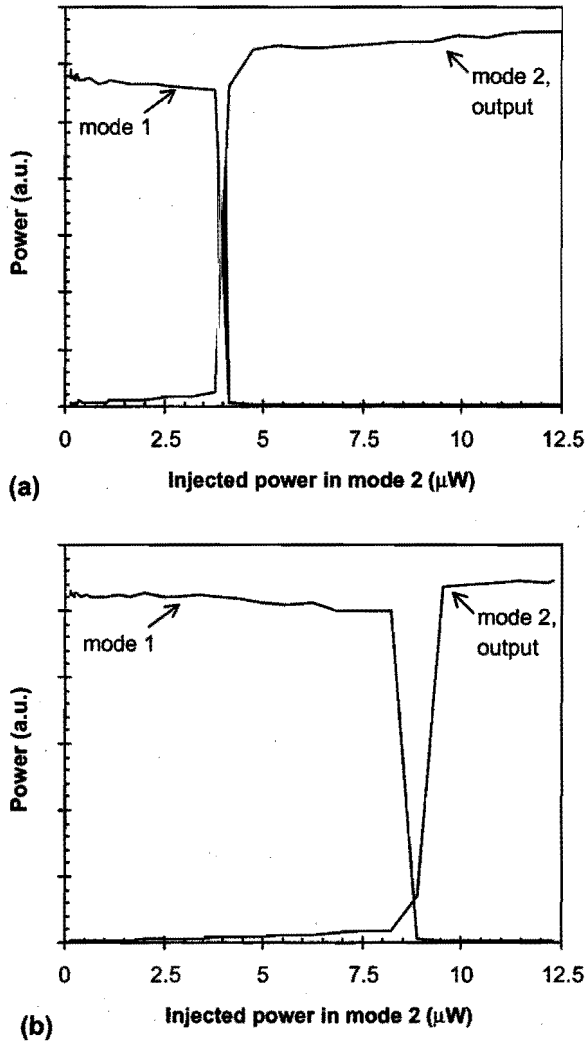
Figure 6.7 Same as Fig. 6.6. but with a slight wavelength detuning of the injected signal. Much steeper threshold functions can be observed. More power is needed to switch the active mode.

The results of simulations and experiments demonstrate that the output of our proposed injection seeding neuron exhibits neural-like behavior as a function of injected optical power. The shape and the level of the threshold can be varied by changing the amount of optical feedback for the two modes of the laser diode.

The ratio between the neuron output power and the injected optical power was about 10^3 in the measurements. In the simulations this ratio was about 10^2. This discrepancy can be due to differences between the used laser parameters, obtained from literature [18], and the actual laser parameters for our laser diode. Also the estimated optical feedback level and coupling efficiency will differ from the actual parameters.
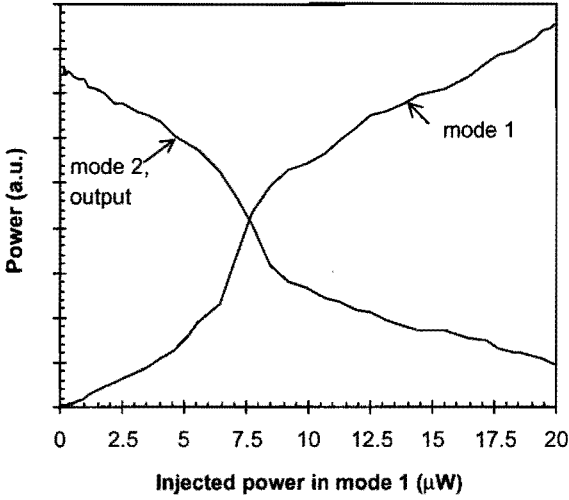
Figure 6.8 Measured optical power in the two selected modes as a function of injected optical power in mode 1 with a constant injection of 25 μW in mode 2. The power in mode 2 shows a nonlinear decrement as a function of light injection in mode 1 (Compare Fig. 6.4).
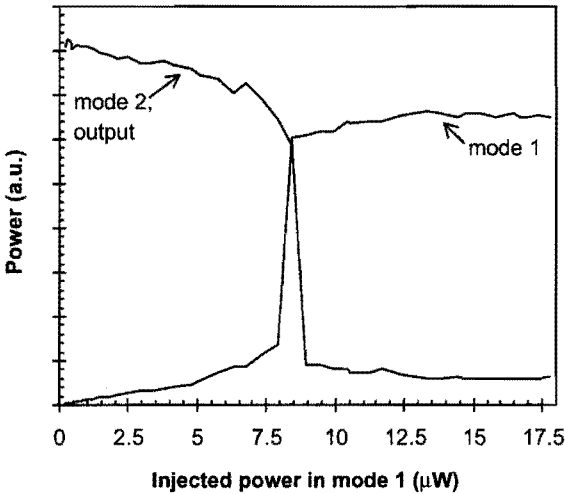
**Figure 6.9** Same as Fig. 6.8 but with a slight detuning of the injected signal in mode 1. A much steeper threshold functions can be observed.
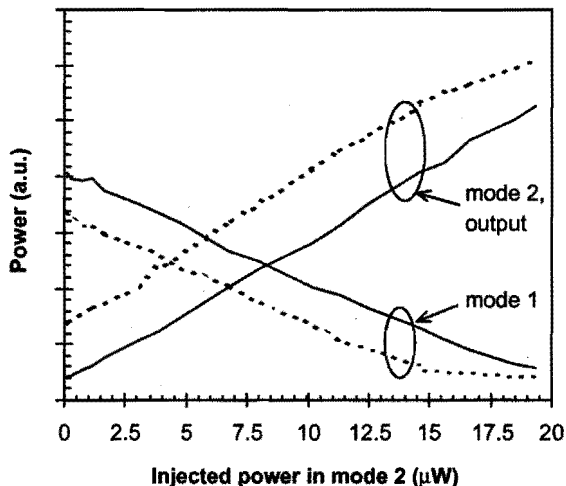
Figure 6.10 Measured optical power in the two selected modes as a function of injected optical power in mode 2 (source II^a) with and without a constant injection of 5.6 μW in mode 2 (source II^b). The drawn lines correspond to the measurements without the additional injection, the dotted lines to the measurements with the additional injection. The dotted lines can be considered a shifted version of the drawn lines.

6.5.2 Steep Threshold Functions

More discrepancy can be observed between the simulation results of Figs. 6.3 and 6.4, and the results presented in Figs. 6.7 and 6.9. The measured threshold functions have a much steeper transition region than the simulated ones. The measured results presented in these figures were obtained with a slightly detuned injection source. We believe that the differences are caused by this detuning and the shape of the locking region. The locking range, in this context, is the area in the detuning - injected power plane in which the laser locks to the injected signal. Various shapes of the locking range have been reported [9],[10],[13],[14]. Figure 6.11 shows a schematic drawing of one of the reported shapes for the locking range (after Ref. [13]). The curves in the figure represent the edges of the locking range. The area within the solid lines is the stable locking range, the area between the solid line and the dashed line is the unstable locking range.

In our theoretical model we assume that light is injected within the locking range of the laser diode. This proved to be a valid assumption for the measurements of Figs. 6.6 and 6.8. Hence, the trajectory of the light injection corresponding to these figures can be represented by arrow A in Fig. 6.11. When, however, the frequency of the injection source is detuned, as was the case for the measurements presented in Figs. 6.7 and 6.9, the injection is not always inside the locking range. This situation is indicated with trajectory arrow B in Fig. 6.11. Now, the locking range is only reached when the power exceeds a certain value. This explains why more injected power is needed to switch the active mode of the laser.
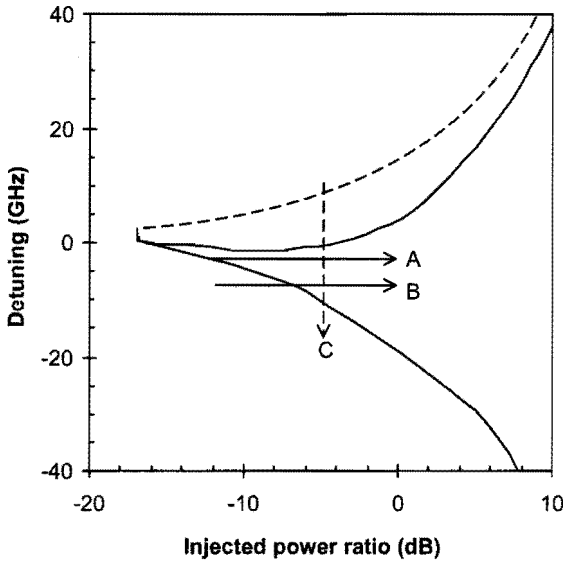
Figure 6.11 Plot of frequency difference between injected signal and free running signal of a laser diode showing various locking ranges (after Ref. [13]). Stable locking occurs in the range within the solid lines. The area between the dashed and the solid line corresponds to the unstable locking range. Solid arrows indicate measured trajectories. Arrow A corresponds to Fig. 6.6, arrow B to Fig. 6.7. The dashed arrow C is the trajectory of Refs. [7],[15] and [16]

The sharp transition in the laser output power from the unlocked to the locked condition on this side of the locking range was already reported by a number of groups [7],[15],[16]. These groups investigated the locking properties of injected light having a varying optical frequency as indicated by the dashed trajectory arrow C. They explain the sharp transition by the carrier induced refractive index change caused by the injected signal.

From a neural network point-of-view, the experimentally obtained threshold functions of Figs. 6.7 and 6.9 are preferable to the experimental results of Figs. 6.6 and 6.8 and the theoretically predicted curves of Figs. 6.3 and 6.4. A smaller change in externally injected light is needed in the results of Figs. 6.7 and 6.9 to switch the neuron from an inactive to an active state. As the amount of injected light corresponds to the weighted sum of inputs of our proposed neuron, a higher number of inputs would be possible with the threshold functions of Figs. 6.7 and 6.9. Furthermore, the shape of the threshold function of Figs. 6.7 and 6.9 is closer to a sigmoid (S-like) shape that is commonly used in neural networks [19].

6.5.3   All-Optical Bipolar Inputs

As demonstrated both in theory and experiment, excitatory as well as inhibitory inputs are possible with our conceptual all-optical neuron by simply injecting the input signals at selected wavelengths. In other optical neural networks, inhibitory inputs are usually implemented by electronic subtraction (See e.g. Refs. [1], [20]–[22]). The advantage of our approach is that no conversion from the optical to the electrical domain is necessary. Another all-optical way of implementing bipolar inputs uses interferometrical methods [23]. This method requires a high level of optical coherence and mechanical stability.

Although both phase and frequency of the two injection sources were not exactly equal in our experiment, summation of input signals by simultaneous injection is demonstrated. A 5.6 μW additional injection by a second source shifted the neural response by 4μW. Although the addition is not exact (a shift of 5.6 μW would be expected), for neural operation it is quite adequate as the neural weights can be adapted to equalize the effect of each input signal. The results indicate that the two injection signals do not need to be coherently added to obtain summation. This eases the constraints on the design of an all-optical neuron constructed from a number of injection seeding neurons. The signals, however, need to be injected inside the locking range of the laser diode.

In the laser neural network described in Chapters 2–5, the inputs are implemented in the optical transmission domain. In the all-optical neuron presented in this chapter, the inputs are transferred to the optical power domain which is advantageous for the application area of optical telecommunications.

6.5.4   Optical Neural Network

To build a neural network, a number of injection seeding neurons should be interconnected. In Fig. 6.12(a) a single injection seeding neuron with a number of connections is depicted. An input signal can either come from outside of the network or from a another injection seeding neuron in the neural network. Because in a general neural network both positively (w^+) and negatively (w^-) weighted inputs are required, the input signals $I_0 \ldots I_2$ at λ_0 are copied to wavelength λ_1 by means of a set of wavelength converters (See e.g. Refs. [11],[12]). As presented in this chapter the light at λ_0 and λ_1 can be used to provide excitatory and inhibitory input signals to an injection seeding neuron operating at λ_0. This output signal of the neuron O can serve as an input signal for other neurons to form a neural network. The weighted interconnection between the injection seeding neurons in the network can be achieved by use of a free-space optical vector-matrix multiplier [24] for each layer of the neural network. Any network topology is possible with this concept.

Alternatively, other wavelengths of the laser diode could be used to form a neural network with just one laser diode. This is shown schematically in Fig. 6.12(b). Now, all the input signals are copied to a number of wavelengths $\lambda_0 \ldots \lambda_2$ corresponding to output signals $O_0 \ldots O_2$. The resulting signals can be used to provide excitatory inputs for the corresponding output. Due to mode competition only the wavelength with the highest amount of summed excitatory input will lase, suppressing laser action at any other wavelength. Thus the resulting neural network will be limited to a *winner-take-all* neural

(a)   (b)
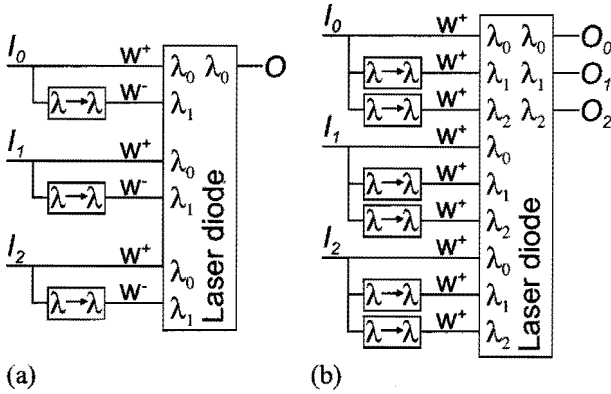
Figure 6.12 Conceptual drawing of injection seeding neuron with some connections. (a) With a number of weighted inputs and one output. Wavelength converters ($\lambda \rightarrow \lambda$) are used to copy the input signals at λ_0 to λ_1 in order to provide excitatory as well as inhibitory weighted (w^+ and w^-) input signals. (b) Injection seeding neuron with a number of weighted inputs and a number of outputs. The input signals are copied to a $\lambda_0 \ldots \lambda_2$ corresponding to outputs $O_0 \ldots O_2$. The wavelength with the highest sum of weighted (w^+) inputs will be the only one lasing, resulting in a *winner-take-all* neural network.

network that closely resembles the laser neural network.

Applications of the proposed all-optical neural network are envisioned in data processing for the field of optical telecommunications. An example is the header processing task in a network switch of a packet switched telecom network (See also Chapter 4). For such applications sufficient operation speed and functional complexity are required. The speed of the injection locking concept is already demonstrated to be compatible with the field of optical telecommunications [11],[12]. The functional complexity of the proposed *winner-take-all* injection seeding neural network is expected to be equal to that of the laser neural network. With the laser neural network we already demonstrated training of functions toward the packet switching task.

The injection seeding neuron, presented in this chapter consisted of a laser diode with controlled optical losses for two modes. The controlled losses do not necessarily have to be implemented with an external-cavity setup. From a practical point of view and considering the size of the locking range, it is preferable to come to a compact, integrated optics, injection seeding neuron.

6.6 Conclusions

We have presented all-optical neural operation by use of light injection in a laser diode. External optical feedback is used to control the shape of the threshold function. By injection of light at different wavelengths excitatory as well as inhibitory inputs are possible with this concept. Summation of input signals can be achieved by simultaneous injection of different input signals at the same wavelength.

The injection seeding neuron is theoretically demonstrated by use of a rate-equation model. An experimental setup is used to confirm the operating principle of the proposed all-optical neuron. We demonstrated basic threshold operation, excitatory and inhibitory inputs as well as summation of input signals with the experimental setup. The numerical results, predicted by the model, are in good agreement with the measurements. Under certain injection conditions a threshold function is observed that is preferable for neural operation. These results were obtained with a detuned injection frequency and can be explained by considering the shape of the injection locking range.

To examine the feasibility of the all-optical neuron, it will be necessary to build a (modest size) neural network. In such a neural network the interconnection of neurons and the weighting of these connections needs to be tested. Connecting the output of one injection seeding neuron to the input of another injection seeding neuron will require a certain level of wavelength stability of the external-cavity laser diodes as the characteristics of the injection seeding neurons depend on the injected wavelength. The needed level of wavelength stability should be investigated before starting experiments on a neural network.

For the proposed application area of optical telecommunications it is of great importance that the operation speed of the neural network is sufficiently high. Although previous work indicates the possibility of using injection seeding for telecom applications, this issue should be addressed in future work.

References

[1] D. Psaltis and N. Farat, "Optical information processing based on an associative-memory model and neural nets with thresholding and feedback," *Opt. Lett.* **10**, 98–100, 1985.

[2] H. J. Caulfield, J. Kinser, and S. K. Rogers, "Optical neural networks," *Proc. IEEE* **77**, 1573–1583, 1989.

[3] S. Jutamulia and F. T. S. Yu, "Overview of hybrid optical neural networks," *Opt. Laser Technol.* **28**, 59–72, 1996.

[4] S. B. Colak, J. J. H. B. Schleipen, and C. T. H. Liedenbaum, "Neural network using longitudinal modes of an injection laser with external feedback," *IEEE Trans. Neural Networks* **7**, 1389–1400, 1996.

[5] E. C. Mos, J. J. H. B. Schleipen, and H. de Waardt, "Optical mode neural network by use of the nonlinear response of a laser diode to external optical feedback," *Appl. Opt.* **36**, 6654–6663, 1997.

[6] E. C. Mos, J. J. H. B. Schleipen, H. de Waardt, and G. D. Khoe, "Loop-mirror neural network using a fast liquid-crystal display," *Appl. Opt.* **38**, 4359–4368, 1999.

[7] R. Lang, "Injection locking properties of a semiconductor laser," *IEEE J. Quantum Electron.* **18**, 976–993, 1982.

[8] N. Schunk and K. Petermann, "Noise analysis of injection-locked semiconductor injection lasers," *IEEE J. Quantum Electron.* **22**, 642–650, 1986.

[9] I. Petitbon, P. Gallion, G. Debarge, and C. Chabran, "Locking bandwidth and relaxation oscillations of an injection-locked semiconductor laser," *IEEE J. Quantum Electron.* **24**, 148–154, 1988.

[10] F. Mogensen, H. Olesen, and G. Jacobsen, "Locking conditions and stability properties for a semiconductor laser with external light injection," *IEEE J. Quantum Electron.* **21**, 784–793, 1985.

[11] S. Murata, A. Tomita, J. Shimizu, and A. Suzuki, "THz optical-frequency conversion of 1 Gb/s-signals using highly nondegenerate four-wave mixing in an InGaAsP semiconductor laser," *IEEE Photon. Techn. Lett.* **3**, 1021–1023, 1991.

[12] R. P. Braun, C. Caspar, H. M. Foisel, K. Heimes, B. Strebel, N. Keil, and H. H. Yao, "Transparent switching node for optical frequency division multiplexed signals," *Electron. Lett.* **29**, 912–913, 1993.

[13] P. Debernardi, "Locking characteristics of Fabry-Perot semiconductor laser oscillators with side-mode injection," *Opt. Lett.* **21**, 656–658, 1996.

[14] L. Li, "Static and dynamic properties of injection-locked semiconductor lasers—an overview," *IEEE J. Quantum Electron.* , 1701–1708, 1994.

[15] C. H. Henry, N. A. Ollson, and N. K. Dutta, "Locking range and stability of injection locked 1.54 μm InGaAsP semiconductor lasers," *IEEE J. Quantum Electron.* **21**, 1152–1156, 1985.

[16] C. E. Moeller, P. S. Durkin, and G. C. Dente, "Mapping the injection-lock band of semiconductor lasers," *IEEE J. Quantum Electron.* **25**, 1603–1608, 1994.

[17] R. W. Tkach and A. R. Chraplyvy, "Regimes of feedback effects in 1.5 mm distributed feedback lasers," *J. Lightwave Techn.* **4**, 1655–1661, 1986.

[18] G. P. Agrawal and N. K. Dutta, *Long-wavelength semiconductor lasers*, (van Nostrand Reinhold, New York, 1986).

[19] R. P. Lippman, "An introduction to computing with neural nets," *IEEE Acoustics, Speech and Signal Processing Magazine* **4**, 4–22, 1987.

[20] M. Kranzdorf, B. J. Bibner, L. Zhang, and K. M. Johnson, "Optical connectionist machine with polarization-based bipolar weight values," *Opt. Eng.* **28**, 844–848, 1989.

[21] A. P. Ittycheriah, J. F. Walkup, T. F. Krile, and S. L. Lim, "Outer product processor using polarization encoding," *Appl. Opt.* **29**, 275–283, 1990.

[22] I. Shariv, O. Gila, and A. A. Friesem, "All-optical bipolar neural network with polarization-modulation neurons," *Opt. Lett.* **16**, 1692–1694, 1991.

[23] J. H. Hong, S. Campbell, and P. Yeh, "Optical pattern classifier with Perceptron learning," *Appl. Opt.* **29**, 3019–3025, 1990.

[24] J. W. Goodman, A. R. Dias, and L. M. Woody, "Fully parallel, high-speed incoherent optical method for performing discrete Fourier transforms," *Opt. Lett.* **2**, 1–3, 1978.

7

Chaotic Self-Pulsation and Cross-Modulation in a Wavelength Selective External-Cavity Laser Diode

Chaotic self-pulsation in a single wavelength external-cavity laser diode is observed. It is shown that the self-pulsation is caused by interdependencies between the optical output power and the compound cavity losses through the refractive index of the laser diode material. On the one hand, a change in optical output power results in a change of the refractive index via the carrier density. On the other hand, it results in a change of refractive index via temperature changes. Compared to the carrier induced refractive index change, the temperature induced refractive index change is opposite in sign and factor of $\sim 10^2$ smaller. The switch-on and switch-off time of the self-pulsation is governed by the carrier life-time. The repetition rate of the self-pulsation is governed by the thermal time constant and is in the megahertz region. Cross-modulation resulting from the thermal induced refractive index change is demonstrated. In a two wavelength double external-cavity laser diode optical power at one wavelength affects the optical power at the other wavelength. This cross-modulation is shown to be related to previous experiments on a laser neural network. A novel technique is introduced to measure the thermal impedance of a laser diode that is based on the cross-modulation.

7.1   Introduction

Grating tuned external-cavity laser diodes are widely used as narrow linewidth tunable sources for many applications. These sources consist of a laser diode that is coupled to an external wavelength selective resonator. Although the facet of the laser diode facing the external resonator is usually antireflection coated, the reflectivity of the facet is finite and thus the laser should be treated as a compound cavity laser diode.
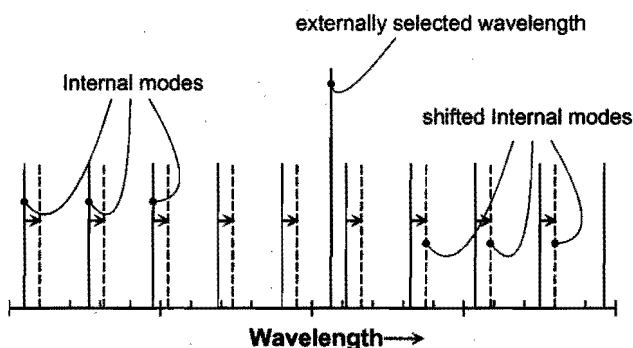
Figure 7.1 Internal longitudinal mode spectrum and externally reflected wavelength of a compound cavity laser diode with wavelength selective external optical feedback. Because of changes in the refractive index of the laser diode material, the internal mode spectrum can shift. An increase in the refractive index will cause the spectrum to shift to longer wavelengths.

As a result, changes in the longitudinal cavity mode spectrum of the laser diode will influence the behavior of the compound cavity laser diode. In Fig. 7.1 the longitudinal cavity modes spectrum of a laser diode is plotted together with the externally selected wavelength (External-cavity modes are spaced at a much smaller distance and are not shown). If, for some reason, the internal longitudinal mode wavelengths shift, the externally selected wavelength will go in and out of resonance with one of the internal longitudinal cavity modes. This will cause an increase in optical output power when the externally selected wavelength becomes closer to the nearest longitudinal mode wavelength. When the nearest longitudinal mode shifts out of resonance, the output power of the compound cavity laser diode will decrease. These effects will be more pronounced when the laser diode is operated close to threshold and small changes in the laser characteristics have a large influence on the optical output power.

The shift of the longitudinal cavity modes can be caused by a change in refractive index of the laser diode material. A change in refractive index changes the effective cavity length and therefore the longitudinal mode wavelengths.

The index of refraction depends on the carrier density of the active region [1] as well as on the device temperature [2]. The carrier density and the device temperature are related to the optical output power of the laser diode via the carrier rate-equation and the thermal conductivity of the laser diode respectively. This means that refractive index depends on the optical output power of the laser diode and vise versa.

This can cause interesting phenomena in a single external-cavity setup. In particular the carrier induced refractive index change has received considerable attention [3]–[6]. Optical bistability [2]–[5] and self-pulsation at a repetition rate determined by the external-cavity length [6] have been reported. The effects of the optical power induced thermal refractive index change, however, has not received much attention. Even in temperature stabilized laser diodes this effect will be present due to the finite thermal resistance between the laser active layer and the heatsink. The influence of the optical output power has often been neglected in the determination of the thermal properties of a laser diode [7],[8].

In a double external-cavity setup, where each cavity corresponds to one selected wavelength, modulation of the optical power at one wavelength can cause the longitudinal modes to shift. As a consequence, the optical output power at the second selected wavelength will vary. This cross-modulation can be either positive or negative, depending on the direction of the mode shift and the relative position of the second externally selected wavelength to the nearest internal longitudinal mode wavelength.

In this chapter self-pulsation at a megahertz repetition rate in a single external-cavity setup is reported. It is explained by the combined effect of carrier and temperature induced refractive index changes. With a double external-cavity setup, operating at two wavelengths, we show cross-modulation that is caused by the thermal refractive index change that results from switching the external feedback for one of the selected wavelengths. The latter setup can be used in a novel technique to measure the thermal impedance of a laser diode.

In Section 7.2 the mode-shift caused by the refractive index changes that result from variations in optical output power is analyzed. The thermal and carrier induced refractive index changes are compared. Section 7.3 describes experimental observations of self-pulsation in a single external-cavity setup, and cross-modulation in a double external-cavity setup. The results are discussed in Section 7.4 where we also relate the findings of this chapter to anomalous behavior of a laser neural network that were reported in Chapter 4. We summarize this chapter in Section 7.5.

7.2 Theory

In this section we investigate the influence of the optical output power of a laser diode on the index of refraction. In Section 7.2.1 the influence of the optical power P on the refractive index n via the carrier density N is analyzed. Section 7.2.1 is devoted to optical output power induced changes in the refractive index via the device temperature T.

The total change in refractive index caused by a change in optical power P can be written as:

$$
\begin{aligned}
\frac{dn}{dP} &= \frac{\partial n}{\partial N}\frac{\partial N}{\partial P} + \frac{\partial n}{\partial T}\frac{\partial T}{\partial P} \\
&= \left(\frac{\partial n}{\partial P}\right)_N + \left(\frac{\partial n}{\partial P}\right)_T
\end{aligned}
\tag{7.1}
$$

where $(\partial n)/(\partial P)_N$ and $(\partial n)/(\partial P)_T$ are the optical power induced changes in refractive

index via the carrier density and the device temperature respectively.

In the last part of this section the longitudinal mode shift and the resulting changes in effective mirror losses are analyzed. In a pertubation analysis it is shown that the carrier induced refractive index change can lead to instabilities.

7.2.1 Influence of the Optical Power on the Refractive Index via the Carrier Density

For a fixed injection current, changes in optical output will cause changes in carrier density according to

$$\frac{\partial N}{\partial P} = -\frac{\tau_e}{\eta_d q V} \tag{7.2}$$

with τ_e the carrier life-time, η_d the differential quantum efficiency of the laser diode (in WA^{-1}), q the elementary charge and V the volume of the active region. The value of the carrier induced refractive index change $\partial n / \partial N$ can be found in literature and lies in the range of $-(5\text{--}11) \times 10^{-21} \mathrm{cm}^3$ [1].

For the laser diode used in our experiment we estimate $\tau_e \approx 1$ ns, $\eta_d \approx 0.2 \, \mathrm{WA}^{-1}$ and $V \approx 2 \times 10^{-11} \, \mathrm{cm}^3$. This results in $(\partial n / \partial P)_N$ in the range of 8-17 W^{-1}. As we consider the influence on the spectral mode structure of the laser diode, the effective refractive index change rather then the total refractive index change should be considered. The effective refractive index change for a mode is reduced by the optical confinement factor of the laser diode as only the carrier density in the active region changes [9]. The optical confinement factor for our MQW laser diode is estimated at $\Gamma \approx 0.02$. Thus we find for the power induced refractive index change via carrier density:

$$\left(\frac{\partial n}{\partial P} \right)_{N,\mathrm{eff}} = 0.16 - 0.34 \, \mathrm{W}^{-1}. \tag{7.3}$$

Changes in the carrier number can occur on a time scale equal to or greater than the carrier life-time τ_e. This means that the carrier induced change in refractive index can occur at a time scale larger than a nanosecond.

7.2.2 Influence of the Optical Power on the Refractive Index via the Device Temperature

The temperature of the active region of a laser diode depends on the amount of electrically injected power that is dissipated in the laser. This equals the injected electrical power minus the total optical power. With reference to the equivalent circuit diagram of Fig. 7.2 we can estimate the change in active region temperature that is caused by a change in optical output power.

For typical laser diodes the thermal impedance $R_{th} = \partial T / \partial P$ is in the range of 30–140 KW^{-1} [7],[10],[11]. This means that changes in optical output power of a few miliwatts can result in a temperature change of 0.1–1 K. Note that, with a fixed electrical current through the laser, an increase in optical output power will result in a decrease of device temperature.
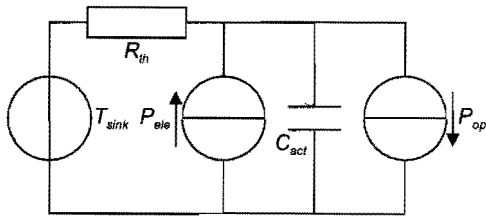
Figure 7.2 Equivalent circuit diagram describing the thermal characteristics of a laser diode with electrically injected power P_{ele} and optical output power P_{opt}. The thermal capacity of the active layer is C_{act}. The active layer is thermally connected to the heatsink at temperature T_{sink} via a thermal impedance R_{th}.

A change in temperature will result in a change in refractive index via $\partial n/\partial T$. For GaAs a value for $\partial \ln(n)/\partial T$ is reported $\sim 5.6 \times 10^{-5}$ K^{-1} [2]. Using this value and the value for $\partial T/\partial P$, a refractive index n of ~ 4 results in a value for the power induced refractive index change via temperature:

$$\left(\frac{\partial n}{\partial P}\right)_T = -(2.2 - 22) \times 10^{-3} \text{ W}^{-1} \tag{7.4}$$

A typical time constant can be associated with changes in the temperature of the active region of the laser diode. This time constant is determined by the thermal capacity of the active region and the thermal impedance between the active region and the heatsink (See Fig. 7.2). For typical laser diodes values in the order of 0.01-3 μs have been reported [8],[12],[13].

7.2.3 Stability Analysis

Comparing the results of the previous two subsections (Eqs. 7.3 and 7.4), we find that the thermal and carrier effect have an opposite sign. We also find that the carrier effect is much stronger than the thermal effect. By use of a perturbation analysis we will investigate the stability of the laser diode coupled to an external cavity. In this analysis we will neglect the thermal effect. The carrier induced refractive index change is introduced phenomenologically in the effective mirror losses α of the compound cavity via $\alpha' = \partial \alpha/\partial N = (\partial \alpha/\partial n)(\partial n/\partial N)$.

To relate changes in the effective optical losses α of an external-cavity laser diode to changes in the refractive index n of the laser diode material, we consider the compound cavity model of Fig. 7.3. The figure shows a laser diode with back facet reflectivity $R_0 = r_0^2$ and front facet reflectivity $R_{int} = r_{int}^2$. The oscillation frequency of the laser diode ω_0 is determined by the wavelength selective external optical feedback with reflectivity $R_{ext} = r_{ext}^2$.

It is obvious that the effective amplitude reflectivity of the facet facing the external mirror reaches a maximum when the internal reflection is in phase with the optical wave reflected back from the external-cavity end mirror. In other words, when a longitudinal cavity mode wavelength is equal to the externally selected wavelength. Neglecting multiple reflections in the external cavity and considering an antireflection coated laser diode
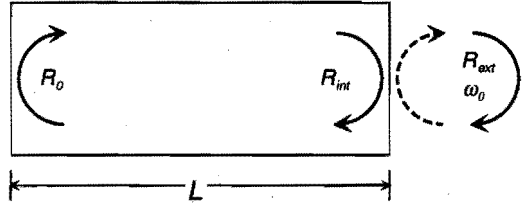
Figure 7.3 Compound cavity model of laser diode with wavelength selective external optical feedback. A laser diode with cavity length L has back facet power reflectivity R_0. The front facet with antireflection coating of reflectivity R_{int} faces an external cavity with reflectivity R_{ext} at frequency ω_0.

($R_{int} \approx 0$) this maximum can be estimated at $r_{eff} = r_{ext} + r_{int}$. Accordingly a minimum value of $r_{ext} - r_{int}$ can be calculated for the effective amplitude reflectivity of the laser diode front facet when the internally and externally reflected light is exactly 180^0 out of phase. In this case the externally selected wavelength is exactly in the middle of two longitudinal cavity wavelengths. A more rigorous approach using a parametric solution of the phase and amplitude equations of a laser diode [3] yields the same result.

The optical losses of the compound cavity corresponding to the minimum and maximum effective reflectivity of the front facet can be evaluated using

$$\alpha = \alpha_{int} - \frac{1}{L} \ln(r_0 |r_{\text{eff}}|) \tag{7.5}$$

where α_{int} represents the optical losses of the laser diode material. By use of this equation we can estimate the minimum and maximum optical losses for the laser diode that is used in our experiments. The reflectivity of the antireflection coated front facet measures $R_{int} \approx 5 \times 10^{-4}$, the internal losses for our MQW laser diode are estimated at $\alpha_{int} = 10 \text{ cm}^{-1}$ and the back facet reflectivity is typically $R_0 \approx 0.3$. The feedback efficiency of the external cavity including coupling losses is estimated at $R_{ext} \approx 0.02$. The maximum value for the optical losses using these parameters is $\sim 65 \text{ cm}^{-1}$, the minimum value is $\sim 58 \text{ cm}^{-1}$.

To change the effective optical losses from a minimum to a maximum or vise versa, a mode shift of 0.5 spectral mode distance is sufficient. The needed change in refractive index can be calculated using [14]

$$\frac{d\lambda}{\lambda} = \frac{dn}{n} \tag{7.6}$$

For our laser diode operating around 675 nm with a cavity length of 500 μm, which corresponds to a spectral mode spacing of ~ 0.1 nm, we find that the needed change in refractive index is $\Delta n \approx 3.4 \times 10^{-4}$.

Using this value of Δn, and $\Delta \alpha$ from the preceding paragraph we obtain a value of $|\partial \alpha / \partial n|$ in the order of 10^4 cm^{-1}. When the externally selected wavelength is on the short wavelength side of the nearest internal cavity mode, the effective optical losses increase as a function of n. The nearest longitudinal mode wavelength moves further away from the externally selected wavelength. Decreasing optical losses occur on the

long-wavelength side. With this value of $\partial\alpha/\partial n$ and the value for $\partial n/\partial N$ from literature [1] we can calculate $|\alpha'| = (0.5 - 1.1) \times 10^{-16}$ cm^2. Note that α' is positive on the long wavelength side whereas it is negative on the short wavelength side of an internal longitudinal mode.

Starting from the carrier and photon rate-equations, the stability of the compound cavity laser diode can be analyzed using a pertubation analysis. In these rate-equations α' is introduced to account for the change in effective mirror losses resulting from the carrier induced refractive index change. We obtain for a disturbance in the photon density ΔS (See the appendix to this chapter):

$$\Delta \dot{S} = C \left(-a_0 + \alpha'\right) \Delta S \tag{7.7}$$

with C a positive constant and a_0 the differential gain coefficient. It is easily seen from Eq. 7.7 that disturbances grow exponentially when $(-a_0 + \alpha') > 0$. Recalling that the value for α' is in the order of 10^{-16} cm^2 we find it is in the same order of magnitude as the estimated value for $a_0 \approx 4 \times 10^{-16}$ cm^2. This means that instabilities are possible when α' is positive. As discussed earlier, this occurs when the externally selected wavelength is on the long wavelength side of an internal longitudinal mode wavelength. At this side of an internal mode, disturbances can grow with a typical time constant governed by the carrier life-time as carrier density induced refractive index changes are the cause of the effect.

7.3   Experimental

In this section we present experimental observations that demonstrate the combined effect of carrier and temperature induced refractive index changes in a compound cavity laser diode. Section 7.3.1 deals with a single external-cavity laser diode that exhibits self-pulsating behavior. In Section 7.3.2 we present results of experiments using a double cavity, two-wavelength laser diode showing cross-modulation between the two wavelengths.

7.3.1   Single Cavity Setup

With the single external-cavity laser setup of Fig. 7.4 we measured the temperature dependent shift of the cavity resonance frequencies of a laser diode. The laser diode (Uniphase CQL806, $\lambda \approx 680$ nm) is antireflection coated and operates below threshold without feedback. Wavelength selective feedback is provided by use of grating G1 (2400 l/mm). The amount of optical feedback is made such that the laser is still below threshold if the (fixed) wavelength selected in the external cavity is between two internal longitudinal mode wavelengths. The temperature of the laser diode chip is controlled and measured by use of a thermo-electric temperature controller and a thermistor. A part of the laser beam is coupled out and is used to measure the optical power and the spectrum of the external-cavity laser diode output.

In Fig. 7.5 the time-averaged output power of the laser diode is plotted as a function of temperature. The figure shows two peaks that occur when an internal longitudinal mode
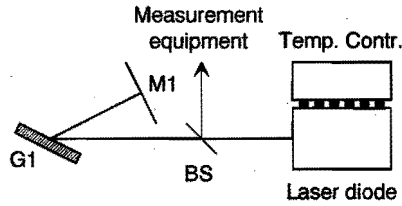
Figure 7.4 Single external-cavity laser diode setup. A temperature controlled, antire-flection coated laser diode is coupled to a wavelength selective external cavity consisting of grating G1 and mirror M1. The temperature can be controlled to shift the internal longitudinal mode spectrum of the laser diode. The output light intensity and the output wavelength are monitored.

wavelength coincides with the externally selected wavelength. In the figure circles indicate measurement points with stable, single external-cavity mode operation. Crosses indicate measurements with unstable, self-pulsating behavior. The self-pulsation occurs when the externally selected wavelength is on the long wavelength side of the nearest internal longitudinal mode wavelength. The internal longitudinal mode spacing is approximately 0.1 nm.
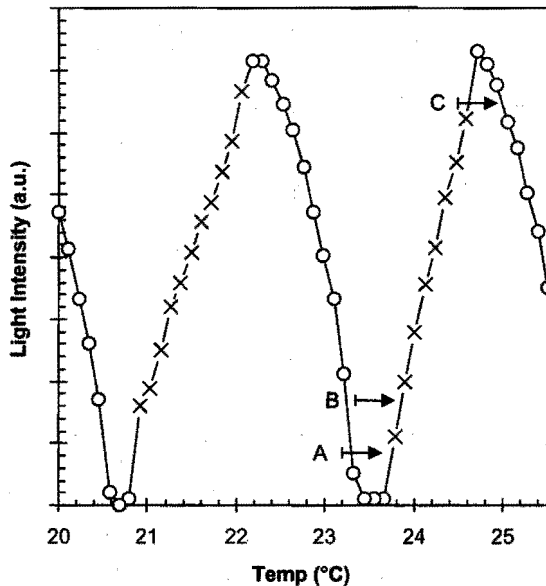
Figure 7.5 The output light intensity as a function of diode temperature. Temperature values are calculated by use of the calibration table of a thermistor equal to the one used in the measurements. Circles represent measurement points with stable operation, crosses represent measurement points with self-pulsating behavior.

Various regimes of self-pulsation are shown in Fig. 7.6. The figure shows the light intensity of the laser diode as a function of time for various levels of detuning between the external feedback frequency and the nearest internal longitudinal mode wavelength. Chaotic transitions from a lasing to a non-lasing state and back can be observed. The top graph corresponds to a small difference between the externally selected wavelength and the nearest internal longitudinal mode, a cross somewhere near a peak in Fig. 7.5. The bottom graph is measured with a large wavelength difference, near a valley in Fig. 7.5. Other graphs show measurements with intermediate wavelength differences. With increasing wavelength difference, the laser tends to stay longer in the non-lasing state.
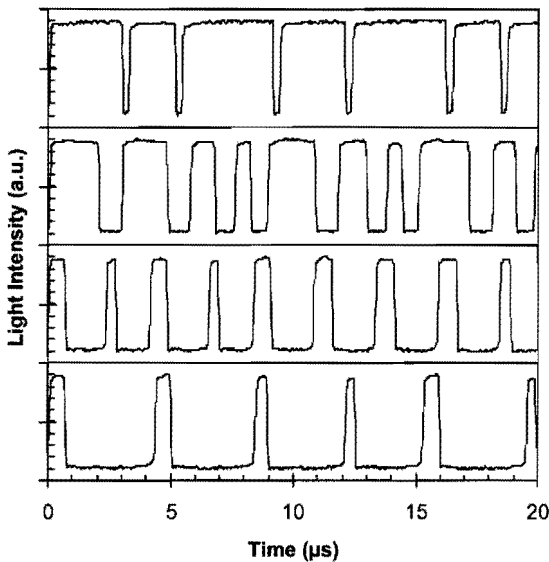
Figure 7.6 Various regimes of self-pulsation. Top curve, self-pulsation when the externally selected frequency is almost equal to an internal longitudinal mode frequency. Bottom curve, external and longitudinal mode frequencies are far apart. Other curves show measurements with intermediate frequency differences.

7.3.2   Double Cavity Setup

To demonstrate cross-modulation we have build a setup according to Fig. 7.7. The figure shows a laser diode that is coupled to two external cavities. In each external cavity a different longitudinal mode is selected by use of gratings G1 and G2, and mirrors M1 and M2. A $\lambda/2$-plate and a polarizing beam splitter enable us to direct a controllable portion of light to the two external cavities.

In one cavity an electro-optical modulator is inserted to modulate the feedback for one selected wavelength, λ_1. When the modulator is open, the laser emits at wavelength λ_1. When it is closed the laser can emit at wavelength λ_2, selected in the second external
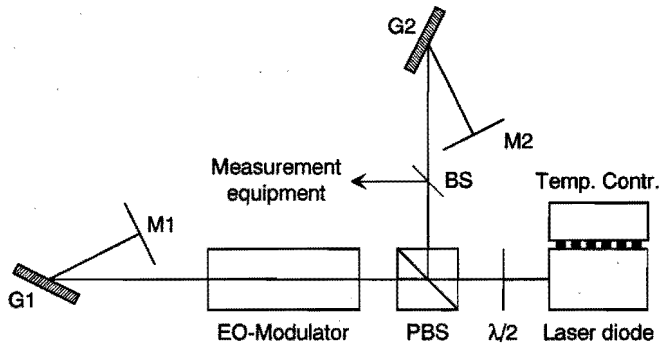
Figure 7.7 Double external-cavity setup to demonstrate cross-modulation. In each external cavity a different wavelength is selected. A polarizing beam splitter PBS and a $\lambda/2$-plate control the feedback levels for the two cavities. The feedback for one cavity is modulated with an electro-optical modulator.

cavity, if the level of feedback provided by this cavity is sufficiently high.

Part of the intra-cavity optical power is coupled out and analyzed. Detectors (Opto Electronics Inc. PD 10) and a sampling oscilloscope (Tektronix 11802 with SD-26 sampling heads) are used to monitor the optical power at the two selected wavelengths.

By tuning mirror M2 we are able to set the frequency mismatch between wavelength λ_2 and the nearest cavity resonance frequency. In a first experiment λ_2 is tuned halfway between two internal longitudinal mode wavelengths. The external optical feedback at this wavelength is controlled such that it is insufficient to make the laser lase. Now the feedback for λ_1 is modulated and consequently the laser emits at λ_1 when the modulator is open. The average output power of the laser diode measures 2.8 mW. When the modulator is closed, however, the laser starts lasing at λ_2.

The transient behavior of the light emission at λ_2 is presented in Fig. 7.8. Before $t \simeq 1\ \mu s$, the modulator is open and the laser is lasing at λ_1. Emission at λ_2 is suppressed. When the modulator closes, a sharp increase in the light intensity at λ_2 can be observed. Gradually the light intensity at λ_2 decreases to the spontaneous emission level until the modulator opens again at $t \simeq 13\ \mu s$ and lasing starts again at λ_1.

The temporal increase in light intensity at λ_2 after $t \simeq 1\ \mu s$ can be explained by the mode shift resulting from the emission of light at λ_1. The mode shift results in a decrease of effective optical losses for λ_2. The feedback for λ_1, however, is much stronger and lasing action at λ_2 is suppressed. At $t \simeq 1\ \mu s$ the emission at λ_1 stops and the internal longitudinal mode wavelengths relax to their original spectral positions.

The time scale at which the light intensity at λ_2 decreases is in the order of μs, the thermal time constant. This leads us to believe that the effect is caused by a temperature change due to the emission of optical power at λ_1 before $t \simeq 1\ \mu s$. To estimate the temperature change, the feedback path for λ_1 is blocked and the temperature of the laser diode is actively decreased by use of the temperature controller until the light intensity at λ_2 reaches the maximum level of Fig. 7.8. The temperature change amounts ~ 0.5 K.

The temperature trajectory corresponding to the measurement of Fig. 7.8 is indicated
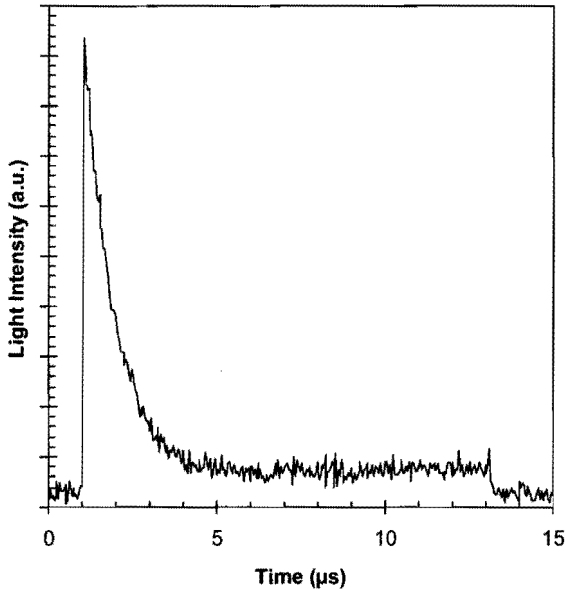
Figure 7.8 Time dependent light intensity at wavelength λ_2 showing cross-modulation. At $t \simeq 1$ ms the modulator closes and the lasers stops lasing at λ_1. From this point the laser emits at λ_2 due to the decreased temperature. As the temperature increases to a steady state, the optical output power at λ_2 slowly decreases. The laser is in a stable state during the temperature relaxation. The corresponding temperature trajectory is indicated by arrow A in Fig. 7.5.

with arrow A in Fig. 7.5. Arrow A has a length corresponding to 0.5 K. The laser operates in a stable regime and the difference between the selected wavelength and the nearest chip mode wavelength increases as a function of time.

By rotating mirror M2 the wavelength difference between λ_2 and the nearest internal longitudinal mode wavelength is changed. With the same output power at λ_1 as in the measurements of Fig. 7.8, the results of Figs. 7.9 and 7.10 were obtained. The corresponding temperature trajectories are indicated with arrows B and C in Fig. 7.5.

Figure 7.9 shows an initially stable operation that turns into an unstable operation at $t \approx 3$ μs. After this point the light intensity at λ_2 is similar to that of the bottom graph of Fig. 7.6 which is measured with an ordinary oscilloscope. The seemingly damped sinusoidal oscillation in Fig. 7.9 is an artefact of the measurement resulting from the random phase of the chaotic pulsation and the averaging mechanism of the sampling scope. A number of waveforms like the one of the bottom graph of Fig. 7.6 are averaged by the sampling scope. Due to the random phase of the chaotic pulsation, the pulsation averages out as a function of time.

In Fig. 7.10 laser operation at λ_2 starts in an unstable region near the resonance peak, within a few microseconds the temperature relaxes to a steady state and the laser operates in a stable regime from this point.
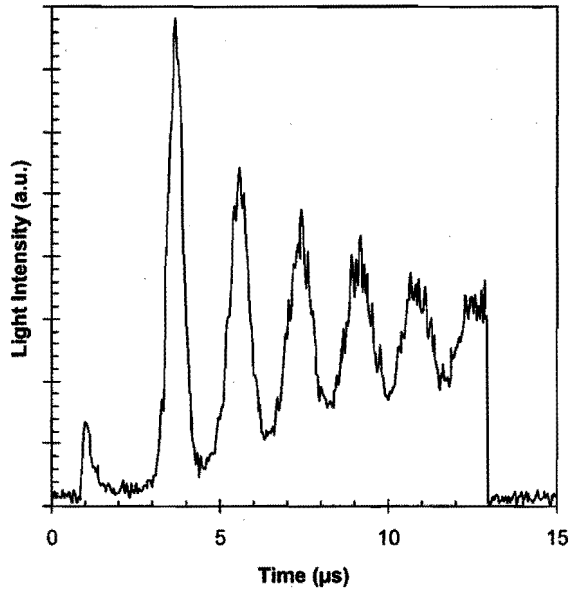
Figure 7.9 Same as Fig. 7.8 but the laser goes from a stable to an unstable state. Temperature trajectory is indicated by arrow B in Fig. 7.5.
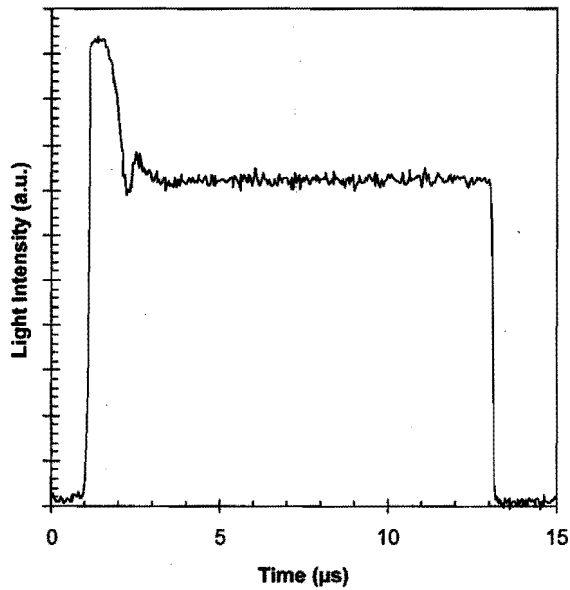
Figure 7.10 Same as Fig. 7.8 but the laser goes from an unstable (1 μs $< t <$2 μs) to a stable ($t >$3 μs) state. Temperature trajectory is indicated by arrow C in Fig. 7.5.

7.4 Discussion

7.4.1 Self-Pulsation

The results of Section 7.3 showed self-pulsation when the externally selected wavelength is on the long wavelength side of the nearest internal longitudinal mode. The self-pulsations can be explained by the instabilities resulting from the carrier induced refractive index change in this wavelength region, that were discussed in Section 7.2.3.

If the externally selected wavelength is on the long wavelength side of an internal longitudinal mode, any disturbance will cause the chip mode spectrum to shift until a stable region is reached. Depending on the sign of the disturbance this can result either in a lasing or a non-lasing state.

The time the system needs to reach a stable state will depend on the rate at which initial disturbances grow and the way these disturbances affect the effective optical losses of the compound cavity. As disturbances will grow with a time constant in the order of the carrier life-time (See Section 7.2.1) the results of Fig. 7.6, where a steady state is reached at a time-scale of ~ 0.1 μs, are in reasonable agreement with these considerations.

When the stable state is reached the temperature of the active region will change as the output power of the laser diode is altered. Because the temperature induced refractive index change has an effect opposite to that of the carrier induced change, it will cause the chip mode spectrum to shift back towards the unstable region. As discussed in Section 7.2.2, the temperature induced effect is much slower with a typical time scale in the order of microseconds.

The temperature of the active layer will oscillate around some average temperature as the laser switches on and off during the self-pulsation. This average temperature depends on the average optical output power of the laser diode and the heatsink temperature (See the equivalent circuit diagram of Fig. 7.2). At a given externally selected wavelength, the effective optical losses and thus the optical output power are related to the active layer temperature. This means that the average optical output power is a function of the heatsink temperature.

From the preceding we can conclude that the laser diode switches on and off with a switch-on and switch-off time determined by the carrier effect. The repetition rate of the pulsation is governed by the thermal time constant of the laser. The average output power, and thus the duty-cycle of the pulses, depends on the heatsink temperature at a given externally selected wavelength.

7.4.2 Cross-Modulation

The fact that the temperature induced change in refractive index plays a role in the behavior of the laser diode on a μs time-scale can also be seen from the results of Section 7.3.2. This is in agreement with our explanation of the self-pulsation effect. Also the time scale at which the thermal effects influence our experimental results agrees with the explanation of the self-pulsation effect as well as with values of the characteristic thermal time constant reported in literature [8],[12],[13].

The results of Section 7.3.2 show thermal cross-modulation. The optical output power

at wavelength λ_2 is (temporarily) changed by the emission of optical power at λ_1. The decrease in temperature resulting from the emission at λ_1 causes the internal longitudinal modes to shift. When λ_2 is on the long wavelength side of the nearest internal longitudinal mode, the shift caused by the decreased temperature will be towards λ_2. On the other side of an internal mode the shift will be away from λ_2.

This means that the thermal cross-modulation effect between λ_1 and λ_2 is either positive or negative depending on the position of λ_2 relative to an internal longitudinal mode. Thus the effect shows resemblance with asymmetric nonlinear gain [15], that is caused by the beating of two wavelengths in the active region, and also exhibits a wavelength asymmetry. The asymmetric nonlinear gain however only plays a role when the two wavelengths are less than a few internal longitudinal modes apart. The cross-modulation reported in this chapter occurs throughout the whole spectrum of the laser diode.

The cross-modulation effect will be visible only if the light at one of the wavelengths exhibits pulsation. When it doesn't, the internal modes might be shifted but lasing action at the non-lasing wavelength will be suppressed by mode competition. Note that the carrier induced refractive index change is much larger than the thermal induced change and hence one would expect that this effect would play a dominant role in the cross-modulation. This, however, is not the case in our external-cavity setup as the cavity round-trip time ($\sim$10 ns) is much larger than the carrier life-time. Therefore changes in refractive index caused by variations in carrier density have disappeared before they have an effect on the optical output power.

In our laser neural network (LNN), that operates by applying controlled optical feedback for a number of wavelengths, anomalous behavior has been reported in Chapter 4, that can be explained by the cross-modulation as described in this chapter. When increasing the level of optical feedback for one wavelength, the time averaged optical output power for a second wavelength also increased (See Fig. 4.16 around $\overline{W_0 I}$ =0.5). This increase can be due to a shift in the internal mode spectrum that results from the increase in optical output power (P_0 in Fig. 4.16) of the first wavelength. Although we did not measure the time development of the light intensity in the LNN, it is very well possible that self-pulsation occurred in the LNN as the setup of the LNN essentially is equal to that of Fig. 7.4.

7.4.3 Determination of Thermal Parameters

The measurements of Section 7.3 can be used to determine some of the thermal parameters of our laser diode. The temperature change needed to shift the longitudinal mode spectrum one mode spacing can be used to calculate $\partial n / \partial T$. With a mode spacing of $\sim$0.1 nm and a corresponding temperature change of 2.4 K (See Fig. 7.5 we obtain $\partial \lambda / \partial T$ = 0.042 nmK^{-1}. The relative change in wavelength $d\lambda / \lambda$ is equal to the relative change in optical cavity length $d(nL)/(nL)$. Thus we can write:

$$\frac{\partial (nL)}{\partial T} = \frac{\partial \lambda}{\partial T} \frac{nL}{\lambda} \tag{7.8}$$

This leads to a normalized temperature induced effective optical cavity length change, $\partial \ln(nL)/\partial T$, of 6.2×10^{-5} K^{-1}. The cavity length also depends on the temperature with $\partial \ln(L)/\partial T = 5.7 \times 10^{-6}$ K^{-1} [2]. This results in a temperature derivative of the refractive

index of $\partial \ln(n)/\partial T = 5.6 \times 10^{-5}$ K^{-1} which is in good agreement with the value for GaAs of 5.4–5.8×10^{-5} K^{-1} reported in literature [2].

The thermal impedance R_{th} can be calculated using the measurements of Section 7.3.2. We measured a time averaged optical output power of 2.8 mW. The duty cycle of the optical modulator was 50%. Thus the optical output power at λ_1 in the open state of the modulator was $\sim$5.6 mW. A change in active layer temperature of $\sim$0.5 K was needed in a null method to adjust the optical power at λ_2 (See Section 7.3.2). These values of dP and dT yield a thermal impedance R_{th} of 90 KW^{-1}. This value for R_{th} is within the range reported in literature [7],[10],[11].

Compared to other methods to measure the thermal impedance of a laser diode the method proposed here uses the optical power instead of the electrical power [7],[10],[11]. These other methods measure the thermal impedance from the area where the electrical power is dissipated, to the heatsink. The method presented above can be used to measure the thermal impedance from the area where the optical power is generated, to the heatsink. The area where the electrical power is dissipated is in general extended beyond this region.

7.5 Conclusions

We have analyzed the influence of the optical output power on the refractive index induced shift of the internal mode spectrum of a compound-cavity laser diode. The thermal and carrier induced changes in refractive index have been examined. The thermal induced refractive index changes are expected to be of the order of 10^2 smaller than the carrier induced refractive index changes and have an opposite sign. The time scale of the temperature effect is in the order of μs. The carrier induced refractive index changes will occur on the time scale of the carrier life-time which is $\sim$1 ns.

In a single wavelength external-cavity setup self-pulsing behavior is observed. The self-pulsation is shown to be caused by the combined effect of the carrier and temperature induced changes in refractive index. The carrier induced refractive index causes unstable regions to occur in the tuning curve of the external-cavity laser. This effect determines the switch-on and switch-off time of the self-pulsation. The thermal refractive index change causes reentrance in the unstable area and determines the repetition rate.

In a double wavelength external-cavity setup cross-modulation is observed that is caused by the temperature induced refractive index change. The effect will only be visible when the laser output power is modulated. In the experiments presented in this chapter this modulation is caused by switching the optical feedback for one wavelength. In our laser neural network experiments the self-pulsation effect can be responsible for the cross-modulation, that was reported as an anomalous effect in the laser neural network experiments (see Chapter 4).

The measurements are used to determine the thermal impedance and the temperature induced change in refractive index. The thermal impedance is obtained using a novel technique that uses the optical output power of the laser diode. The results are in agreement with values found in literature.

Appendix

In this appendix we derive an expression to examine the stability of a compound-cavity laser diode with effective optical losses that depend on the carrier density via carrier induced refractive index variations. Let us consider the rate-equations for the carrier density N and photon density S of a single mode laser diode:

$$\dot{N} = \frac{I}{qV} - \gamma_e N - GS \tag{7.9}$$
$$\dot{S} = GS - \gamma_p S$$

where I is the electrical driving current, $\gamma_e = 1/\tau_e$ is the carrier decay rate. G is the optical gain equal to $G = \Gamma v_g a_0 (N - N_t)$ with v_g the group velocity in the active region, N_t the carrier density at transparency and a_0 the differential gain constant. The photon decay rate, γ_p, is equal to $v_g \alpha$, with α the effective optical losses of the compound cavity laser diode.

Using a perturbation analysis and introducing $\alpha = \alpha_0 + \Gamma \alpha' \Delta N$, with $\alpha' = \partial \alpha / \partial N$ we can write:

$$\Delta \dot{N} = -\Gamma v_g a_0 (S_0 \Delta N + N_0 \Delta S) - \gamma_e \Delta N \tag{7.10}$$
$$\Delta \dot{S} = \Gamma v_g a_0 (S_0 \Delta N + N_0 \Delta S) - v_g \alpha_0 \Delta S - \Gamma v_g \alpha' \Delta N S_0$$

with S_0 and N_0 the steady state solutions of Eqs. 7.9.

Considering changes in the carrier density to be slow compared to changes in the photon density we can set $\Delta \dot{N} = 0$ resulting in

$$\Delta \dot{S} = \Gamma v_g \left(-a_0 + \alpha' \right) \frac{\Gamma v_g a_0 N_0 S_0}{\Gamma v_g a_0 S_0 + \gamma_e} \Delta S \tag{7.11}$$

With $C = \left(\Gamma v_g a_0 N_0 S_0 \right) / \left(\Gamma v_g a_0 S_0 + \gamma_e \right)$, a positive constant, we obtain Eq. 7.7.

References

[1]   P. R. Selway, G. H. B. Thomson, G. D. Henshall and J. E. A. Whiteaway, "Measurement of the effect of injected carriers on the p-n refractive-index step in single heterostructure diode lasers," *Electron. Lett.* **10**, 453–455, 1974.

[2]   Y. Tsay, B. Bendow, and S. S. Mitra, "Theory of the temperature derivative of the refractive index in transparent crystals," *Phys. Rev. B* **8**, 2688–2696, 1973.

[3]   P. Zorabedian, W. R. Trutna, and L. S. Cutler, "Bistability in grating-tuned external-cavity semiconductor lasers," *IEEE J. Quantum Electron.* **23**, 1855–1860, 1987.

[4]   V. Y. Bazhenov, A. P. Bogatov, P. G. Eliseev, O. G. Okhotnikov, G. T. Pak, M. P. Rakhvalsky, M. S. Soskin, V. B. Taranenko, and K. A. Khairetdinov, "Bistable operation and spectral tuning of injection laser with external dispersive cavity," *IEE Proc. I* **129**, 77–82, 1982.

[5] P. Glas and R. Müller, "Bistable operation of a GaAs-AlGaAs diode laser coupled to an external resonator of narrow spectral bandwidth," *Opt. Quantum Electron.* **14**, 375–389, 1982.

[6] R. Müller and P. Glas, "Bistability, regular self-pulsing, and chaos in lasers with external feedback," *J. Opt. Soc. Am. B* **2**, 184–192 1985.

[7] J. S. Manning, "Thermal impedance of diode lasers: comparison of experimental method and a theoretical model," *J. Appl. Phys.* **52**, 3179–3184, 1981.

[8] W. Freude, "Measurement of the thermal impedance of injection lasers," *Archiv fur Elektronik und Übertragungstechnik* **31**, 478–480, 1977.

[9] I. I. Vinogradov, O. V. Danilina, A. E. Kosykh, and A. S. Logginov, "Determination of the dependence of the refractive index of the active region of an injection laser on the carrier density," *Sov. J. Quantum Electron.* **21**, 1195–1196, 1991.

[10] T. S. Paoli, "A new technique for measuring the thermal impedance of junction lasers," *IEEE J. Quantum Electron.* **11**, 498–503, 1975.

[11] S. Y. Huang, "Accurate thermal impedance measurement for semiconductor lasers by the double modes of fibre grating lasers," in *1996 Proceedings 46th Electronic Components and Technology Conference*, (Orlando, FL, 1996), pp. 635–639.

[12] H. I. Abdelkader, H. H. Hausien, and J. D. Martin, "Temperature rise and temperature rise-time measurements of a semiconductor laser diode," *Rev. Sci. Instrum.* **63**, 2004–2007, 1992.

[13] M. Suyama, N. Ogasawara, and R. Ito, "Transient temperature variation of injection lasers," *Jap. J. Appl. Phys.* **20**, L395–L398, 1981.

[16] J. S. Manning and R. Olshansky, "Carrier-induced index change in AlGaAs double-heterostructure lasers," *Electron. Lett.* **17**, 506–507, 1981.

[15] J. Manning, R. Olshansky, D. M. Fye, and W. Powazinik, "Strong influence of non-linear gain on spectral and dynamic characteristics of InGaAsP lasers," *Electron. Lett.* **21**, 496–497, 1985.

[16] E. C. Mos, J. J. H. B. Schleipen, H. de Waardt, and G. D. Khoe, "Loop-mirror laser neural network using a fast liquid-crystal display," *Appl. Opt.* **38**, 4359–4368, 1999.

8

Conclusions and Further Research

In the final chapter of this thesis general conclusions are drawn. We discuss capabilities and limitations of the proposed optical neural network. We relate these capabilities and limitations to the possibilities for using the optical neural network in optical telecommunication systems. Recommendations are made for improvement of the optical neural network and future research topics are indicated.

8.1   Conclusions

With the work presented in this thesis we investigated the operation, optimization and application of an all-optical neural network that uses the longitudinal modes of a laser diode as neurons. The main conclusions of this research are listed below.

- It is possible to use the longitudinal modes of a laser diode as the neurons of a neural network. This is done by actively controlling the optical feedback provided to a laser diode. The optical feedback for each longitudinal mode of the laser diode is made proportional to a weighted sum of input signals. The outputs of the network are the optical powers contained in the modes, the inputs are applied in the optical transmission domain. As the optical feedback can only be positive, input signals can only have excitatory influence on the weighted sum. The resulting all-optical laser neural network is a single-layer *winner-take-all* neural network.

- This laser neural network can perform functions that are applicable in optical tele-communication systems. We have successfully demonstrated training of simple and more complicated computational tasks. A data bit belonging to an input vector was routed according to an input address, also contained in the input vector.

- The operation speed of the experimental LNN is at present not sufficient for the application area of optical telecommunications. A theoretical and experimental analysis of the mode-switching behavior of an external-cavity laser diode showed that a number of speed limitations exist. A first limitation is due to the round-trip time of the external cavity. If the total optical power of the laser diode before and after the transient is not the same, a second limitation will result from the fact that the charge carrier density needs to change. A third, more fundamental limitation arises from the switch-on time of an initially non-lasing longitudinal mode.

- It is possible to use optical power as input signals in an alternative optical neuron. By injecting light into an external-cavity laser diode we are able to demonstrate neural operation. Both inputs and outputs of the resulting injection seeding neuron are represented in the optical power domain. An additional advantage of this approach is the possibility to obtain excitatory as well as inhibitory input signals.

- A wavelength selective external-cavity laser diode, such as used in the laser neural network, can exhibited self-pulsating behavior and cross-modulation. The self-pulsation is shown to be caused by the combined effect of carrier and thermal induced refractive index changes. The cross-modulation is visible on the time scale of the thermal refractive index changes. It is believed that the carrier and thermal induced refractive index changes are responsible for observed anomalous shapes of the neural response function of the laser neural network.

8.2   Recommendations

Research on the use of longitudinal modes of a laser diode as neurons will be continued and therefore this thesis marks a starting point for further investigations. Below sugges-

tions are made for future research topics.

- For a general neural network it would be beneficial if the input signals could also have an inhibitory influence on the weighted sum of inputs. For the laser neural network this means that it would be necessary for an input signal to have a positive as well as a negative influence on the amount of optical feedback. This could be achieved in optics by using the phase of the light wave that is reflected back into the laser. Rays of light corresponding to an excitatory input should have a 180^0 phase difference with those corresponding to an inhibitory input signal. Excitatory and inhibitory input signals would then interfere destructively.

- To overcome limitations caused by the *winner-take-all* behavior of the laser neural network, alternative laser types should be considered. With these lasers it should be possible to have multiple lasing modes at the same time. Examples of such lasers are glass lasers that exhibit a type of inhomogeneous line broadening, which is essential to obtain multi-frequency operation.

- The number of neurons in the laser neural network is currently limited to 32 by the experimental setup. This number can be enlarged by using more longitudinal modes of the laser diode. With the currently used laser diode we can estimate the number of neurons to be higher than 100. This number is only limited by the gain bandwidth of the used laser and the spectral distance between the neural wavelengths. Therefore a much larger number of neurons can be achieved with a proper choice of laser gain bandwidth and a lower spectral distance between the neural wavelengths.

- The number of inputs that can be used in the experimental laser neural network presented in this thesis was $\sim$12. With the optical feedback more evenly distributed over the input signals, the number of inputs is estimated at $\sim$27. A larger number of inputs can be achieved by increasing the level of controlled optical feedback.

- Two different types of supervised learning algorithms were used in this thesis to train the neural network. A stochastic learning algorithm was used in an initial experiment to train simple tasks to the network. A modified δ-rule algorithm, that anticipates on the *winner-take-all* behavior of the laser neural network, was used in a more advanced experiment. Although the tasks trained with the δ-rule learning algorithm were more complex than the simple tasks trained with the stochastic learning algorithm, less iteration steps were needed. Further optimization of the learning algorithm is possible by incorporating more knowledge of the optical neural network in the algorithm.

- Two of the speed limitations of the laser neural network can be overcome by miniaturizing the experimental setup and ensuring an equal optical output power in each state of the neural network. A third limitation, that results from the relaxation oscillations of a laser diode, cannot be avoided in this way. Although a more efficient optical feedback or a higher optical gain will somewhat alleviate the speed limitations, it remains questionable if the optical neural network will be usable in applications that require a transient time lower than $\sim$1 ns.

- Applications of the optical neural network are envisioned in the area of optical telecommunication systems. In typical telecommunication a bit-error-rate (BER) as small as $\sim 10^{-9}$ is required. In our experimental optical neural network we were able to demonstrate a BER of $< 10^{-5}$. Although this figure is an upper limit of the actual BER, further investigations of the error behavior of the optical neural network are in order.

- To be more compatible to the field of optical telecommunications, the possibilities of building a fiber-optics based optical neural network should be investigated. As a free space optical setup is abandoned in this way, the ease of implementing a vector-matrix multiplier no longer applies. Such a fiber-optic neural network should operate at wavelengths that are currently being used in telecommunication systems.

- For the proposed packet-switched router some fundamental building blocks are still missing. An important building block is the optical memory that will be needed to store the destination address during the time a packet passes the router. Ideas are being developed in this direction at the Eindhoven University of Technology. They will play an important research role in the realization of an all-optical packet router.

- For optical telecommunication applications, and for other possible application areas where data is represented in the optical domain, it is preferable to apply inputs to the optical neural network in the optical power domain. As the inputs of the optical neural networks are currently represented in the optical transmission domain, optically controlled modulators, such as multiple-quantum-well modulators, should be introduced in the neural network setup. Research on these devices will be necessary.

- As an alternative to using optically controlled optical modulators, an injection seeding neuron is proposed. The feasibility of the injection seeding neuron remains a topic for future research. Problems can arise in connecting a number of injection seeding neurons as this will require a stable oscillation wavelength for each laser diode.

Summary

In this thesis we describe an optical neural network that uses the longitudinal modes of a laser diode as neurons. The threshold that is needed for neural operation originates from the nonlinear response of a laser diode to external optical feedback. The optical power contained in each longitudinal mode of the laser diode exhibits a threshold as a function of the level of optical feedback for that mode. Thus the longitudinal modes can be used to define neurons by controlling the amount of optical feedback as a function of neural inputs and weights. All key neural functions are implemented in the optical domain.

In Chapter 1 we provide an introduction to neural networks. We introduce the basic requirements and features of neural networks and discuss the classical reasons for implementing neural networks by means of optics. An additional reason to build an optical neural network, being the possibility to use neural networks in optical telecommunication systems in this way, is introduced. For this application area it is important that the threshold is in the optical domain. In most of the optical neural networks that are presented in literature to date the threshold is implemented in the opto-electronic domain.

We analyze the operation principle of the all optical neural network that is proposed in this thesis in Chapter 2. The way laser diode physics provides threshold operation is clarified by use of a rate-equation model of a multimode laser diode with controlled optical feedback. It is explained that the resulting neural network will be of the *winner-take-all* type, in which only one neuron will be active for each input. The experimental concepts that are used throughout the thesis to implement neural inputs and weights are introduced.

In Chapter 3 we describe experiments that demonstrate the operation principles of the all-optical neural network. The experimental setup is presented that consists of an antireflection coated laser diode coupled to a linear cavity. In the cavity a set of gratings, a number of lenses and a standard liquid-crystal-display are placed. With the liquid-crystal-display the feedback for each longitudinal mode is controlled separately to provide inputs and weights. The liquid-crystal-display is controlled by a computer on which a simple stochastic learning algorithm is implemented. Learning of a number of functions with up to three inputs and up to five outputs is demonstrated. One of these functions is the NOR-XOR-AND function that can only be trained to our single layer neural network by virtue of its *winner-take-all* nature.

More advanced experiments are presented in Chapter 4. A loop-mirror is introduced in the experimental setup and a more sophisticated liquid-crystal-display is used. The display enables us to speed up the learning phase by allowing us to feed more input patterns

to the network per unit of time. The number of inputs and neurons is enhanced in this setup to about 12 and 32 respectively. By use of an improved learning algorithm we trained the experimental optical neural network some functions toward the application area of optical telecommunications. With these experiments we demonstrate the functional capabilities of the laser neural network.

To examine whether the operation speed of the optical neural network is sufficient for optical telecommunication applications, we examined the transient behavior of longitudinal mode switching in a dual external-cavity laser diode. Simulations and experiments are presented in Chapter 5. Three speed limitations are indicated. One is the number of cavity round-trip times needed to switch from one longitudinal mode to another. A second limitation arises from the change in carrier number that is due to a change in total optical feedback. These limitations can be avoided by reducing the size of the setup and constraining the input vectors of the network respectively. A third speed limitation, that originates from the switch-on time of an originally nonlasing longitudinal mode, cannot be easily avoided. It remains to be seen whether this third limitation will prevent the optical neural network from being applicable in optical telecommunication systems.

In the optical neural network discussed in Chapters 2–5 the inputs are implemented in the optical transmission domain by use of a liquid-crystal-display . For applications in all-optical systems it is preferable to have the inputs implemented in the optical transmission domain. A possible solution is presented in Chapter 6. We use a laser diode that is provided with controlled optical feedback thus forcing it to lase at one of two selected longitudinal modes. The inputs are implemented via the injection of light. When the amount of injected light at the wavelength of one of the two longitudinal modes reaches threshold, the laser will start to lase in this mode. The shape of the resulting threshold function can be controlled by changing the amount of optical feedback for the two longitudinal modes. The operating principle is verified theoretically by use of a rate-equation model of a multi-mode laser diode with controlled external optical feedback and light injection. We demonstrate basic neural operation experimentally.

During the measurements on the operation speed, presented in Chapter 5, anomalous behavior was observed. This anomalous behavior is the subject of Chapter 7, in which we present and analyze experimental results. We show observations of self-pulsating behavior in a single wavelength external-cavity laser diode. We show that the self-pulsation is caused by the combined effect of carrier and thermal induced refractive index changes in the laser diode. These refractive index changes cause a shift in the longitudinal mode spectrum. It is believed that the carrier induced effect causes unstable regions to occur in the tuning curve as any initial disturbance will grow exponentially. As the temperature and carrier induced changes have an opposite effect on the wavelength shift, the thermal refractive index change can result in a reentrance in the unstable region. Thus the switch-on and switch-off times of the self-pulsation are determined by the carrier effect and the repetition time by the thermal effect as is observed in the experiments. In a two wavelength double external-cavity setup in which the feedback for one wavelength is actively modulated we observe cross-modulation effects at the other selected wavelength. The cross-modulation is explained by the thermal refractive index change and is used in a novel method to determine some of the thermal characteristics of the laser diode.

Samenvatting

Dit proefschrift behandelt een neuraal netwerk dat is opgebouwd met behulp van een laser-diode. Om de lezer enig idee te geven waar dit proefschrift over gaat is in dit hoofdstuk een en ander samengevat.

Zenuwcellen, Computers en Licht

Kunstmatige neurale netwerken zijn afgekeken van het neurale netwerk van de mens, dat beter bekend is als ons zenuwstelsel. Deze netwerken bestaan uit een (liefst groot) aantal neuronen die met elkaar verbonden zijn. Net als de zenuwcellen in ons zenuwstelsel ontvangen de neuronen in een neuraal netwerk prikkels uit hun omgeving. Als de sterkte van de som van alle signalen die een neuron ontvangt boven een bepaalde drempel komt, gaat het neuron zelf ook signalen sturen naar de neuronen waarmee het verbonden is. Deze drempelfunctie stelt de neuronen in staat simpele beslissingen te nemen en geeft zo het neurale netwerk zijn rekenkracht.

Het interessante van neurale netwerken is dat ze van huis uit goed zijn in het doen van parallelle berekeningen. Doordat veel neuronen met elkaar verbonden zijn, gebeuren veel berekeningen gelijktijdig ofwel parallel. Een voorbeeld hiervan is het herkennen van een gezicht door ons zenuwstelsel. Alle beeldpuntjes die samen het beeld vormen van een gezicht worden tegelijk ontvangen als prikkels op het netvlies van ons oog. Deze prikkels worden parallel verwerkt en het resultaat van de berekening in dit voorbeeld is het wel of niet herkennen van het gezicht.

De berekening die een neuraal netwerk uitvoert hangt af van de sterkte van de verbindingen tussen de neuronen. Hoe sterker een verbinding, of wegingsfactor, des te meer beïnvloedt een signaal dat via deze verbinding bij een neuron aankomt de activiteit van het neuron. In feite vormen de wegingsfactoren het geheugen van het neurale netwerk.

Net als de mens kan een neuraal netwerk leren van voorbeelden. Hiertoe is een leeralgoritme nodig dat de wegingsfactoren instelt. In zo'n leeralgoritme worden voorbeelden van invoerpatronen en uitvoerpatronen aan het neurale netwerk aangeboden en worden de wegingsfactoren net zo lang veranderd totdat het neurale netwerk het juiste uitvoerpatroon geeft bij ieder invoerpatroon. Het neurale netwerk heeft dan geleerd welke uitvoer bij welke invoer hoort.

De meeste huidige kunstmatige neurale netwerken bestaan in de vorm van een computerprogramma. Als een neuraal netwerk op deze manier wordt gerealiseerd, voert de computer de berekeningen van elk van de neuronen in het netwerk één voor één uit. Het

kan allemaal veel sneller als de berekeningen van de neuronen door aparte rekeneenheden, en dus echt tegelijkertijd, uitgevoerd worden. Er zijn tegenwoordig neurale netwerken die bestaan uit geïntegreerde elektronische circuits. Op deze chips zijn de neuronen verwezenlijkt met behulp van transistoren en de verbindingen bestaan uit elektrische contacten.

Wanneer verbindingen in een neuraal netwerk elkaar kruisen, moeten op een chip de draden over elkaar heen gelegd worden om kortsluiting te voorkomen. In een neuraal netwerk dat gebruik maakt van licht is dit niet nodig. De verbindingen in zo'n optisch neuraal netwerk bestaan uit lichtstralen die elkaar zonder problemen kruisen.

Om deze reden zijn er dan ook vele beschrijvingen van optische neurale netwerken te vinden in de literatuur. De drempelfunctie in deze optische neurale netwerken wordt vrijwel altijd verwezenlijkt in elektronica. In toepassingen waarin de invoer en de uitvoer bestaan uit licht zou het beter zijn als ook de drempelfunctie in het optische domein zou plaatsvinden. Een dergelijke toepassing is glasvezeltelecommunicatie waarbij informatie wordt verstuurd door het verzenden van lichtpulsjes door een glasvezel. Meer over neurale netwerken en de voordelen van een realisatie met licht kunt u vinden in Hoofdstuk 1 van dit proefschrift.

Prikkels en Kleuren

In dit proefschrift wordt een optisch neuraal netwerk beschreven waarbij ook de drempelberekening in het optische domein plaatsvindt. Hiertoe gebruiken we een laser-diode. Dit is een elektronische component die licht uitzendt met een zeer zuivere kleur. De laserdiode die wij gebruiken is een multimode laser-diode; een laser-diode die licht van verschillende kleuren kan uitzenden. Het licht dat uit de laser-diode komt wordt bewerkt en vervolgens teruggekaatst in de laser-diode. Als de hoeveelheid weerkaatst licht voor één van de kleuren die de laser uitzendt boven een bepaalde waarde komt, gaat de laser licht van die kleur uitzenden. Op deze manier ontstaat er een drempelfunctie voor iedere kleur van de laser-diode. Overigens zien die kleuren er voor de mens allemaal hetzelfde uit: zij liggen in het kleurenspectrum ongeveer duizend keer dichter bij elkaar dan rood en blauw in de kleuren van de regenboog.

Iedere kleur van de laser-diode, dus ieder neuron, ontvangt invoergegevens via de hoeveelheid teruggekaatst licht van die kleur. Hoe sterker een invoersignaal, des te meer licht wordt weerkaatst naar de laser-diode. Door voor iedere invoer het teruggekaatste licht gecontroleerd te verzwakken maken we de wegingsfactoren voor ieder neuron. Door de drempelfunctie bij iedere kleur ontstaat op deze manier een laser neuraal netwerk waarvan het uitvoerpatroon gelijk is aan het kleurenspectrum van de laser-diode. Een typische multimode laser kan meer dan 100 kleuren licht uitzenden; het is dus in principe mogelijk met een laser-diode een neuraal netwerk te realiseren met meer dan 100 neuronen.

Theorie en Experiment

In Hoofdstuk 2 beschrijven we de werking van een laser neuraal netwerk met behulp van een wiskundig model voor de laser-diode. In dit model is er voor de hoeveelheid licht van iedere kleur van de laser-diode een vergelijking. Samen met een vergelijking voor het aantal ladingdragers (elektronen en gaten) in de laser-diode kunnen we een oplossing

vinden voor het kleurenspectrum van de laser-diode. Het blijkt dat er een drempelfunctie is voor iedere kleur van de laser-diode en dat de laser-diode slechts één kleur tegelijk zal uitzenden.

Met een experimentele opstelling die bestaat uit een laser-diode en een aantal standaard optische componenten (bijvoorbeeld spiegels, lenzen en rasters) is voor het eerst de werking van een laser neuraal netwerk aangetoond. In deze experimentele opstelling worden eerst de diverse kleuren van de laser-diode van elkaar gescheiden in de ruimte. Vervolgens wordt de hoeveelheid licht van iedere kleur afzonderlijk op een gecontroleerde manier verzwakt. Uiteindelijk voeren we, door middel van een spiegel, het licht weer via dezelfde weg terug in de laser-diode.

We brengen invoerpatronen aan in het experimentele neurale netwerk door middel van een vloeibaar kristal display. Met dit display verzwakken we de hoeveelheid teruggekaatst licht voor iedere kleur van de laser afzonderlijk. Deze verzwakking is een produkt van de invoer en de wegingsfactoren. Om de uitvoer van het neurale netwerk te bepalen, meten we het kleurenspectrum van de laser-diode.

Met een computer die in staat is de wegingsfactoren te sturen, de invoer aan te bieden en de uitvoer te lezen, hebben we het experimentele neurale netwerk een aantal functies geleerd. Met het gebruikte leeralgoritme worden in iedere stap de wegingsfactoren willekeurig veranderd. Lijken de uitvoerpatronen hierdoor meer op de voorbeelden, dan worden de nieuwe wegingsfactoren onthouden in de volgende stap. Is het resultaat slechter, dan gebruiken we de vorige wegingsfactoren. Zo wordt doorgegaan totdat het laser neuraal netwerk de gewenste functie correct heeft geleerd.

Op deze manier zijn functies met ten hoogste drie invoerelementen en ten hoogste vijf uitvoerelementen geleerd aan het netwerk om het werkingsprincipe ervan aan te tonen. In Hoofdstuk 3 kunt u een gedetailleerde beschrijving vinden van deze experimenten.

Een meer geavanceerde opstelling wordt beschreven in Hoofdstuk 4. In deze opstelling gebruiken we een experimenteel display dat gevuld is met een speciaal type vloeibaar kristal. Met dit display zijn we in staat veel meer veranderingen van de wegingsfactoren te realiseren per tijdseenheid. Ook kunnen we grotere invoerpatronen aan het laser neuraal netwerk aanbieden en zijn we in staat om maximaal 32 neuronen te definiëren.

Om de hoeveelheid weerkaatst licht te vergroten, en daarmee het aantal invoerelementen te optimaliseren, hebben we in dit experiment gebruik gemaakt van een speciale ringopstelling. In de ring kan het licht maar één kant op en door dit eenrichtingsverkeer wordt het vloeibaar kristal display slechts één maal gepasseerd. Hierdoor gaat minder licht verloren en wordt er dus meer licht teruggekaatst in de laser-diode.

Met een verbeterd leeralgoritme heeft het neurale netwerk functies geleerd in het toepassingsgebied van glasvezelcommunicatie. We hebben daarmee aangetoond dat het laser neuraal netwerk in staat is om niet alleen triviale maar ook zinnige functies te leren.

Snelheid

In huidige telecommunicatiesystemen gaan meer dan een miljard bits per seconde door een glasvezel. Voor dit toepassingsgebied is het dan ook van belang dat de berekeningen door het laser neuraal netwerk uitgevoerd worden met een voldoende hoge snelheid.

Om te onderzoeken of het laser neuraal netwerk snel genoeg is voor deze toepassing hebben we het schakelgedrag onderzocht van een laser-diode met veranderende licht-weerkaatsing. Deze verandering moet er voor zorgen dat de laser-diode van één kleur naar een andere schakelt.

Met behulp van een wiskundig model voor de laser-diode en zijn kleuren, hebben we dit gedrag gesimuleerd. Met een experimentele opstelling, waarbij licht van twee kleuren door een spiegel wordt teruggekaatst in de laser-diode, hebben we het schakelgedrag ook gemeten. In deze experimentele opstelling wordt de hoeveelheid licht voor één kleur veranderd terwijl die voor een ander kleur hetzelfde blijft.

Uit zowel de simulaties als de experimenten blijkt dat het licht een aantal keren heen en weer gekaatst moet worden tussen de laser-diode en de spiegel alvorens de laser van kleur wisselt. Het aantal keren hangt af van het verschil in de hoeveelheid teruggezonden licht voor de twee kleuren.

Door experimenten uit te voeren met verschillende afstanden tussen de spiegel en de laser-diode, en vervolgens de meetresultaten te extrapoleren naar een oneindig kleine af-stand, kunnen we een schatting maken van de schakelsnelheid voor een geminiaturiseerd neuraal netwerk. Het blijkt dat er een schakelvertraging optreedt van enkele nanoseconden. Deze vertraging wordt deels veroorzaakt doordat het aantal ladingdragers tijdens het schakelen verandert. Uit simulaties blijkt dat een andere oorzaak van deze vertraging niet gemakkelijk voorkomen kan worden. Het is dan ook nog niet zeker of de snelheid van het laser neurale netwerk voldoende zal zijn voor de beoogde toepassing in optische telecommunicatie.

Het onderzoek naar de schakelsnelheid van het laser neurale netwerk wordt beschreven in Hoofdstuk 5.

Een Alternatief Optisch Neuron

In het laser neuraal netwerk zoals dat in de Hoofdstukken 1 t/m 5 van dit proefschrift wordt beschreven, is de invoer geïmplementeerd door de hoeveelheid weerkaatst licht te regelen. Dit betekent dat de informatieoverdracht niet plaatsvindt via een hoeveelheid licht maar via een hoeveelheid lichtverzwakking. Om dit optische neurale netwerk bruik-baar te maken in toepassingen waar informatie gerepresenteerd wordt door een hoeveel-heid licht, zal er een conversie nodig zijn van een hoeveelheid licht naar een hoeveelheid lichtverzwakking.

Als een alternatief op deze werkwijze presenteren we in Hoofdstuk 6 een geheel optisch neuron waarbij de hoeveelheid licht de invoer vertegenwoordigt. Weer maken we gebruik van een laser-diode. Deze is, door toevoeging van gecontroleerde optische terugkoppe-ling, zó ingesteld dat hij slechts licht kan uitzenden van twee kleuren.

Wanneer de laser licht uitzendt van de ene kleur kan hij door het instralen van licht met een andere kleur gedwongen worden om deze kleur uit te gaan zenden. Daartoe moet de hoeveelheid ingestraald licht boven een bepaalde drempel komen. De laser zal dan geen licht meer uitzenden van zijn oorspronkelijke kleur. Deze drempelfunctie kan gebruikt worden om een neuron te definiëren door één van de kleuren te kiezen als de uitvoer van het neuron.

Dit principe is theoretisch geverifieerd door een model van de laser-diode te gebruiken. In een experimentele opstelling is de werking van dit geheel optische neuron voor het eerst aangetoond.

Zelf Pulserend Gedrag en Kleur Overspraak

Tijdens het meten van de snelheid van het laser neurale netwerk zijn enkele interessante fenomenen waargenomen. Een van deze fenomenen is het vanzelf aan- en uitgaan van de laser-diode dat we zelf pulserend gedrag noemen. Op willekeurige tijdstippen stopt de laser met het uitzenden van licht om na enige microseconden, wederom willekeurig, weer te beginnen.

We verklaren dit merkwaardige gedrag door een subtiel samenspel van temperatuur-schommelingen en veranderingen in de hoeveelheid ladingdragers. Deze schommelingen hebben tot gevolg dat de brekingsindex van het laser-diode materiaal varieert. Dit heeft weer tot gevolg dat de kleuren waarop de laser kan uitzenden veranderen. Als het terug-gekaatste licht slechts één kleur bevat kan het gebeuren dat de laser-diode instabiel wordt en er zelf pulserend gedrag optreedt.

Het andere waargenomen fenomeen is hier nauw mee verbonden. In een opstelling waarin een laser-diode twee kleuren kan uitzenden waarvan er één aan- en uitgeschakeld wordt, treedt overspraak op tussen de twee kleuren. Als de laser-diode gedwongen wordt te stoppen met het uitzenden van de ene kleur, verandert zijn temperatuur. Dit heeft tot gevolg dat de kleuren die de laser kan uitzenden verschuiven in het kleurenspectrum. Op deze manier wordt ook de hoeveelheid licht van de andere kleur die de laser kan uitzenden beïnvloed.

De waargenomen fenomenen worden beschreven en verklaard in Hoofdstuk 7. Het proefschrift wordt afgesloten in Hoofdstuk 8 waarin de conclusies van het onderzoek samengevat worden en we suggesties aandragen voor verder onderzoek.

Curriculum Vitae

Op 9 december 1968 ben ik geboren in Arnhem. Daar ben ik in het geboorteregister bijgeschreven als Everhardus Cornelis Mos. Men noemt mij Evert. Van 1981 tot 1987 heb ik het VWO gevolgd aan het Liemers College te Zevenaar. Tot 1987 heb ik bij mijn ouders in Duiven gewoond. Hierna ben ik naar Eindhoven verhuisd om daar Elektrotechniek te gaan studeren aan de Technische Universiteit Eindhoven.

Tijdens deze studie heb ik onder andere stage gelopen in de cleanroom van de vakgroep *Elektronische Bouwstenen* aan de TU Eindhoven en bij *Telefones de Lisboa e Porto* in Portugal. De studie elektrotechniek heb ik in 1994 afgerond bij de vakgroep *Elektronische Schakelingen* met het afstudeerproject "Een laser neuraal netwerk". Tijdens dit project werd ik begeleid door dr.ir. J. A. Hegt van de vakgroep *Elektronische Schakelingen* en dr. J. J. H. B. Schleipen en dr. S. B. Colak van het Philips Natuurkundig Laboratorium, alwaar ik het afstudeerproject heb uitgevoerd. Op 30 juni 1994 heb ik mijn ingenieursdiploma in ontvangst genomen.

Vervolgens ben ik op 1 januari 1995 bij de vakgroep *Telecommunicatie Technologie en Elektromagnetisme* begonnen aan mijn promotieonderzoek. Onder auspiciën van promotor prof.ir. G. D. Khoe en dr.ir. H. de Waardt heb ik bij de leerstoel *Optische Telecommunicatie* gewerkt aan het onderzoek waarvan u in deze dissertatie de vruchten kunt lezen. Het onderzoek is uitgevoerd op het Philips Natuurkundig Laboratorium onder begeleiding van dr. J. J. H. B. Schleipen. De resultaten van het onderzoek zijn gepubliceerd op internationale conferenties en in wetenschappelijke tijdschriften. Gedurende het promotieonderzoek heb ik meegewerkt aan het verzorgen van colleges en tentamens van de vakgroep en heb ik twee studenten begeleid bij hun afstudeerproject.

List of Publications

Journal Articles

- E. C. Mos, J. J. H. B. Schleipen, and H. de Waardt, "Optical mode neural network by use of the nonlinear response of a laser diode to external optical feedback," *Appl. Opt.* **36**, 6654–6663, 1997.

- E. C. Mos, J. J. H. B. Schleipen, H. de Waardt, and G. D. Khoe, "Loop-mirror laser neural network using a fast liquid-crystal display," *Appl. Opt.* **38**, 4359–4368, 1999.

- E. C. Mos, J. J. H. B. Schleipen, H. de Waardt, and G. D. Khoe, "Longitudinal mode switching dynamics in a dual external-cavity laser diode," Submitted for publication in *IEEE J. Quantum Electron.*

- E. C. Mos, J. J. L. Hoppenbrouwers, M. T. Hill, M. W. Blüm , J. J. H. B. Schleipen, and H. de Waardt, "Optical neuron by use of a laser diode with injection seeding and external optical feedback," Submitted for publication in *IEEE Trans. Neural Networks*.

- E. C. Mos, G. W. 't Hooft, J. J. H. B. Schleipen, and H. de Waardt, "Chaotic self-pulsation and cross-modulation in a wavelength selective external-cavity laser diode," To be published.

Other Publications

- J. J. H. B. Schleipen, S. B. Colak, E. C. Mos and C. T. H. Liedenbaum, "An injection laser neural network," in *Proceedings of the fourth int. conf. on microelectronics for neural networks and fuzzy systems*, (IEEE Computer Society Press, Los Alamitos, Calif., 1994), pp. 8–12.

- E. C. Mos, J. J. H. B. Schleipen, and H. de Waardt, "An optical neural network using a diode laser with external feedback," in *Proceedings 1996 IEEE/LEOS symposium Benelux Chapter*, A. Driessen and R. M. De Ridder Eds., (IEEE/LEOS Benelux Chapter, The Netherlands, 1996), pp. 168–170.

- E. C. Mos, J. J. H. B. Schleipen, and H. de Waardt, "Laser neural network promises improved pattern recognition," *Laser Focus World*, March, 131–133, 1998.

129

- E. C. Mos, J. J. H. B. Schleipen, and H. de Waardt, "Neural network experiment demonstrating all-optical data switching," in *Applications of photonic technology III*, G. A. Lampropoulos and R. A. Lessard Eds., SPIE vol. 3491, 67–70, 1998.

- E. C. Mos, J. J. H. B. Schleipen, and H. de Waardt, "Laser neural network demonstrates data switching functions," in *Proc. of the 8th int. conf. on artificial neural networks*, (Springer-Verlag, Berlin, 1998), pp. 1165–1170.

- E. C. Mos and J. J. H. B. Schleipen, "Een laser neuraal netwerk," *Nederlands Tijdschrift voor Fotonica* 3, 7–16, 1999

Stellingen

behorende bij het proefschrift

Optical Neural Network based on Laser Diode Longitudinal Modes

door Evert C. Mos

1. Het is mogelijk om met behulp van één laserdiode een optisch neuraal netwerk te construeren met meerdere neuronen.

   Dit proefschrift

2. Op een laserdiode kun je rekenen.

   Dit proefschrift.

3. Door het combineren van *injection seeding* en optische terugkoppeling is het mogelijk een geheel optisch neuron te construeren waarbij zowel de invoer- als de uitvoersignalen in het optische vermogensdomein gedefinieerd zijn.

   Dit proefschrift, hoofdstuk 6.

4. Met de verwachting dat het verwezenlijken van neurale netwerken met behulp van optische methoden pas tot toepassingen zal leiden bij 1000 of meer verbindingen per neuron wordt voorbijgegaan aan toepassingsgebieden als optische telecommunicatie waarin de te bewerken signalen in het optische domein worden aangeboden.

   S. Jutamulia en F.T.S. Yu, "Overview of hybrid optical neural networks," Optics and Laser Technology, Vol. 28, pp. 59–72, 1996

5. Golflengte selectieve optische terugkoppeling bij een laserdiode kan tot merkwaardig gedrag aanleiding geven.

   Dit proefschrift, hoofdstuk 7.

6. hOewElhEtmEnsEliJkbReInaLsnEuraAlnEtweRkoVerhEtaLgemEenvo ORtReFfelIjkiNstAatispAtronENzoaLswOoRdeNenzInNenteherKenne nluKtdiTeensTukmAKkelIjkeRalsJeHetNietTeZeerTegenwerkt.

7. Aangezien de meeste platenspelers al lang verdreven zijn door de CD-speler mag het merkwaardig heten dat "grammofoonnaald" wel en "laserdiode" niet in het woordenboek voorkomt.

   Van Dale groot woordenboek der Nederlandse taal, 12ᵉ editie.

8. Het ongegeneerd gebruiken van ontwerpen uit vroeger tijden, ook wel *retro-design* genoemd, spreekt niet erg voor de fantasie van de ontwerpers in kwestie maar verfraait over het algemeen wel het straatbeeld.

   Zie bijvoorbeeld de wijk Dierdonk in Helmond of de Rover 75.

9. Met de recentelijke hausse in plannen voor woonwijken om het water en (recreatie) meren en plassen in landbouwgebieden is de uitpoldering van Nederland begonnen.

10. Goede architectuur lekt.

    Zie bijvoorbeeld het Rietveld-Schröder huis, het Groninger Museum of de nieuwe Reichstag.

11. Een beetje stelling haalt het NRC.

12. Omdat gravel niet groeit is het interessanter om naar een tenniswedstrijd op gras te kijken.